POLITECNICO DI MILANO

Facoltà di Ingegneria dell'Informazione

Corso di Laurea Specialistica in Ingegneria dell'Automazione

Vibroacoustic modelling of orthotropic plates

Relatore: Prof. Roberto CORRADI
Correlatore: Ing. Giacomo SQUICCIARINI

Tesi di Laurea di:
Jordi VILLAR VENINI
Matr. n. 748639

Anno Accademico 2010/2011

Contents

List of Figures

List of Tables

Abstract

The main objective of the work here presented is to extend the calculation of the radiation efficiency to plates whose characteristics differ form the simply supported isotropic rectangular plates. In this work the radiation efficiency is calculated by using the modal summation approach based on the far field sound intensity. The plate is considered isotropic or orthotropic. The orthotropy is introduced by the characteristics of the material or by the presence of ribs parallel to an edge. Different combinations of free, simply and clamped supported boundary conditions are considered for the isotropic plate, while the orthotropic plate is always considered simply supported. Free vibration of isotropic plates are calculated by using the classical Kirchoff-plates theory. The results obtained for the radiation efficiency are compared with a BEM model and show the influence of the constraints in the edges. Results show that the clamped supported plate is the the configuration for which the radiation efficiency is higher, while the freely supported configuration is the one with lower radiation efficiency. The difference between different boundary conditions is also summarized in terms of third octave bands. In this manner it has been shown that the difference between a clamped plate and a simply supported plate in the mid-frequency range in terms of radiation efficiency is not 3 dB as stated in literature by Leppington, but is variable and can reach up to 10 dB.

The orthotropy has been introduced. First, a plate made of an orthotropic material is considered. Free vibration have been calculated analytically and have been compared with with a FE model, making the results a good agreement. The radiation efficiency has been calculated using the same formulae as the isotropic plate. Then the orthotropy is considered by the introduction of ribs. An analytical-numerical method is used to calculate the free vibration of a ribbed plate. Results have been compared with a FE model and make a good agreement. The radiation efficiency of a ribbed plate is calculated by modifying slightly the formulation presented for the calculation of the radiation efficiency of an isotropic plate.

The formulation adopted for the radiation efficiency allows to investigate the effect of the modal damping ratio, the influence of the boundary conditions and the effect of the ratio of the stiffness along perpendicular directions.

Sommario della tesi in lingua italiana

Nella progettazione e nella produzione di svariati tipi di veicoli e macchinari si fa largo uso di piastre rettangolari sottili, che sono spesso messe in vibrazione quando questi sono in funzione. È ben noto che una piastra vibrante produce rumore, il cui livello di intensità dipende dalla velocità di vibrazione superficiale e può essere amplificato in corrispondenza dei modi naturali della struttura.

Spesso le applicazioni richiedono sistemi di piastre rigidi e allo stesso tempo leggeri. Aumentando lo spessore si può ottenere un forte incremento nella rigidità della struttura, a prezzo però di un incremento anche nella massa. La soluzione di irrigidire la piastra tramite l'aggiunta di travi vincolate alla superficie è un buon compromesso per ottenere la rigidezza richiesta senza appesantire troppo la struttura.

Strutture formate da piastre sottili irrigidite da un insieme di travi sono usate comunemente e formano una classe di elementi strutturali di importanza pratica in svariate applicazioni ingegneristiche: aerei (in Figura 1.1)[1], scafi di navi e sottomarini (in Figura 1.2)[2] e parti di treni come il pavimento delle carrozze. Poichè i veicoli spaziali, marini e terrestri sono soggetti a carichi dinamici, è essenziale prevedere in modo affidabile le frequenze proprie di un componente strutturale per evitare livelli eccessivi di vibrazione, che possono provocare rottura a fatica o livelli di rumore molto alti. Travi di rinforzo sono adottate anche nella produzione di tavole armoniche per strumenti musicali. È il caso della tavola armonica del pianoforte a coda mostrata in Figura 1.3, dove una piastra di legno è rinforzata da un insieme di travi i cui assi sono perpendicolari alla direzione di venatura del legno.

Figure 1: Fusoliera di un aereo.

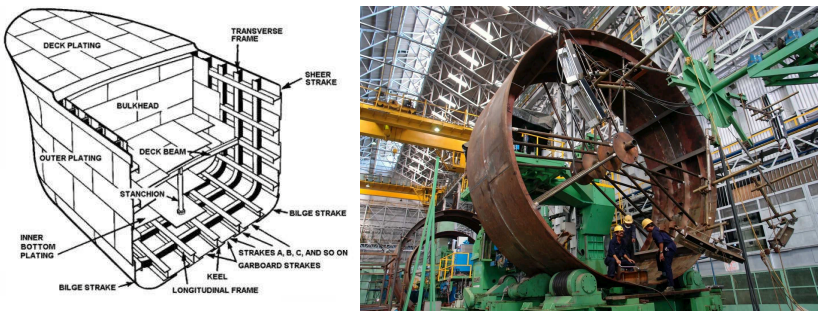

(a) *Scafo nave.* (b) *Scafo sottomarino.*

Figure 2: Scafi di un sottomarino e di una nave.

In tutti questi esempi vi è sempre una ragione per cui è importante mantenere la massa della piastra la più contenuta possibile. Qualunque veicolo, particolarmente se gli è richiesto di muoversi velocemente in un fluido, deve essere leggero ma allo stesso tempo i requisiti di resistenza strutturale devono essere soddisfatti. Le tavole armoniche invece devono essere leggere in modo da incrementare la loro mobilità meccanica, definita come il rapporto complesso tra velocità d'uscita e forza d'ingresso, e massimizzare

[1] Immagine estratta da $http://www.911research.dsl.pipex.com/ggua175/structural$.
[2] Immagini estratte da $http://ajaishukla.blogspot.com/2010_08_01_archive.html$.

Figure 3: Tavola armonica di pianoforte a coda, per gentile concessione di Fazioli Pianoforti.

quindi il suono generato, ma la resistenza meccanica deve essere sufficiente per sostenere il carico verticale dovuto alle corde tese, che nei pianoforti a coda può raggiungere i 300 kg. Il compromesso tra una struttura leggera con però alta resistenza è realizzato adottando trave irrigidenti, saldate o incollate sulla tavola.

Le travi modificano la rigidezza della piastra lungo la direzione parallela ai loro assi: strutture i cui parametri di rigidezza dipendono dalla direzione del sistema di coordinate adottato si dice mostrino comportamento ortotropo. Irrigidire la piastra non è l'unica maniera per ottenere ortotropia, infatti vi sono materiali caratterizzati naturalmente da un comportamento ortotropo, come il legno, la cui rigidezza nella direzione della venatura può risultare fino a 40 volte più grande che nella direzione perpendicolare. Il caso della tavola armonica è in effetti una particolare applicazione dove l'ortotropia è introdotta sia dal materiale, sia dalle travi.

Per caratterizzare le proprietà acustiche di una piastra, possono essere adottati differenti parametri come la potenza sonora, la velocità volumetrica o la pressione acustica. La quantità che descrive al meglio la relazione tra il suono irradiato e la velocità normale alla struttura, coniugando così l'acustica e la meccanica, è l'efficenza acustica σ, nota anche come efficienza di radiazione. È definita come:

$$\sigma(\omega) = \frac{W_{rad}(\omega)}{\rho c S \langle \overline{v^2}(\omega) \rangle} = \frac{R_{rad}}{\rho c S} \tag{1}$$

dove $W_{rad}(\omega)$ rappresenta la potenza acustica irradiata dalla struttura normalizzata per la superficie vibrante S, la densità dell'aria ρ, la velocità del suono c e la velocità quadratica media di vibrazione mediata nello spazio $\langle \overline{v^2}(\omega) \rangle$. La medesima quantità può essere anche espressa in termini di resistenza all'irraggiamento R_{rad} definita come rapporto tra la potenza acustica e la velocità quadratica media. Il denominatore dell'equazione (1) rappresenta la potenza acustica generata da un pistone rigido con la stessa area della piastra e vibrante armonicamente con velocità pari alla velocità media della piastra mediata rispetto allo spazio. L'efficienza di radiazione fornisce una un'utile relazione tra le vibrazioni strutturali e la potenza sonora associata. Se sono noti valori o relazioni per i rapporti di radiazione, la stima dell'irraggiamento sonoro, e conseguentemente il controllo del rumore, risultano facilitati. Per esempio, la potenza sonora irradiata può essere stimata direttamente dalle vibrazioni della superficie, ottenute teoricamente o sperimentalmente. È chiaro che, a seconda dell'applicazione, si può desiderare che l'efficienza di radiazione sia bassa o alta.

Con l'obiettivo di chiarificare il concetto di efficienza di radiazione, sono presentati nel seguito gli esempi di due possibili applicazioni.

Valutazione del rumore per treno in corsa

[3]

Il livello di rumore nei moderni treni diesel è spesso fortemente influenzato dalla presenza del motore diesel, che è montato direttamente sotto il pavimento della carrozza, come in Figura 1.4. Il motore è collegato a due travi longitudinali che corrono lungo il veicolo per mezzo di montanti a resilienza. Il rumore generato dal motore raggiunge l'interno del veicolo attraverso due percorsi principali: l'aria e la struttura.

[3] Questa sezione si riferisce a una lezione del *Noise Control Course* del MsC in *Sound and Vibration Studies* tenuto presso l'Università del Southampton, per gentile concessione del Prof. D.J. Thompson.

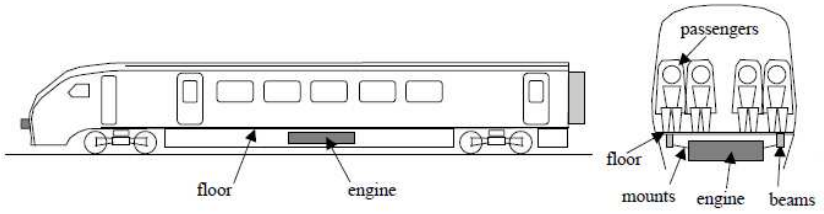

Figure 4: Schema del veicolo ferroviario, per gentile concessione di D.J. Thompson.

Concentrandoci sulla struttura, si possono proporre svariati modelli per calcolare la potenza immessa nel pavimento dal motore, e stimare di conseguenza i livelli di velocità normale del pavimento, ossia la quantità definita come $\langle \overline{v^2}(\omega) \rangle$ nell'equazione (1). Poichè il pavimento è composto da un sistema piastre-travi, conoscendo l'efficienza di radiazione la potenza acustica può essere prontamente calcolata, assieme a una stima dell'intensità sonora.

Una volta che sono note le intensità sonore all'interno del veicolo, si possono scegliere differenti soluzioni per ridurle. Tra le possibili soluzioni, a seconda del caso, vi sono per esempio: inscatolamento del motore, modifica dei montanti dei motori, incremento dello smorzamento o dello spessore del pavimento, aggiunta di travi irrigidenti, pavimento flottante. Ciascuna di queste soluzioni ha i suoi pregi e i suoi difetti in termini di emissione acustica e costi.

La tavola armonica del pianoforte a coda

Nei pianoforti la produzione del suono è ottenuta amplificando attraverso la tavola armonica la vibrazione dovuta a corde percosse. Il processo tramite cui una corda del piano è eccitata dal martelletto è piuttosto complesso e al di fuori degli scopi di questo studio. È invece importante sottolineare che dopo l'impatto la corda inizia a vibrare liberamente secondo i suoi modi propri. Con l'obiettivo di stimare il suono irradiato, si possono proporre differenti modelli per calcolare la forza trasmessa alla tavola armonica dalla corda, attraverso il ponticello. Nota la forza d'ingresso, la velocità della superficie della tavola armonica può essere stimata tramite opportuni modelli strutturali. Anche qui la conoscenza dell'efficienza di radiazione consente di dare una stima di primo tentativo della potenza sonora prodotta. In aggiunta, l'efficienza di radiazione può essere utilizzata per valutare l'effetto di modifiche strutturali sulla radiazione acustica. Confrontando le curve di efficienza di radiazione per differenti soluzioni si può trovare la configurazione più efficiente.

Si ricorda che la potenza sonora dipende sia dall'efficienza d'irradiazione sia dalla velocità della superficie, il che significa che la piastra più efficiente non è necessariamente quella con la maggiore potenza sonora: va trovato un buon compromesso tra l'efficienza di radiazione e la velocità della superficie.

Struttura di questa tesi

Il principale scopo di questo lavoro è caratterizzare l'efficienza acustica di piastre rettangolare sottili adottando un approcio modale. La parte strutturale, validata con dei modelli ad elementi finiti, è presa da letteratura ed è stesa per poter calcolare le frequenze proprie ed i modi di vibrare per diverse configurazioni della piastra. I risultati ottenuti per il calcolo dell'efficenza acustica sono stati confrontati con i risultati di un modello BEM e mostrano un alto grado di concordanza.

Questa tesi parte dal calcolo dell'efficienza acustica di una piastra fatta di un materiale isotropo per diverse condizioni al contorno. I risultati ottenuti rivelano che una piastra completamente incastrata ha l'efficienza più alta, mentre che la stessa piastra completamente libera ha l'efficenza più bassa. Si sono quantificate in termini di terzi di ottava le differenze tra due travi avendo la stessa geometria e fatte dallo stesso materiale ma con diverse condizioni al contorno. In particolare si è trovato che la differenza tra una trave completamente incastrata e una trave semplicemente appoggiata a frequenze intermedie non è di 3 dB come detto in letteratura per Leppington [1], ma è variabile ed arriva fino ai 10 dB.

Nella seconda parte di questa tesi si considera una pastra ortotropa. L'ortotropia è introdotta in due modi diversi: direttamente considerando la piastra fatta di un materiale ortotropo oppure introducendo delle travi parallele a un lato. La piastra è considerata sempre semplicemente appoggiata, e si è calcolata

l'efficenza acustica per diversi rapporti di rigidezza. I risultati ottenuti mostrano che l'efficenza acustica di una piastra rinforzata è sempre maggiore della stessa pistra senza i rinforzi, e che la differenza tra di loro aumenta all'aumentare del rapporto di rigidezza. Nello stesso modo, si è trovata la piastra ortotropa equivalente alla piastra rinforzata sia mantenendo solamente il rapporto di rigidezza, sia mantenendo il rapporto di rigidezza e la massa complessiva. I risultati mostrano che a basse frequenze la differenza tra di loro è bassa, costante, e diminuisce all'aumentare del rapporto di rigidezza. Infine, utilizzando i modelli presentati in questa tesi, si mostra un modello semplice della tavola armonica del pianoforte e si calcola la sua efficenza acustica.

Chapter 1

Introduction

1.1 Motivation for the research

Thin rectangular plates are widely used in the design and production of any type of vehicles and machineries and during the exercise are often set into vibration. It is well known that a vibrating plate produces noise/sound whose levels depend on the surface vibration velocity and can be amplified because of the natural modes of the structure.

Often the application requires the plates system to be rigid and light. By increasing the thickness one can obtain a large increase on the stiffness but at the same time the mass so does. The solution of stiffening the plate by attaching several ribs on it is a good compromise between having the required stiffness and keeping the structure as light as possible.

Structures consisting of thin plates stiffened by a set of ribs are commonly used and form a class of structural elements of practical importance in various engineering applications, such as aircrafts (see Figure 1.1)[1], ships and submarine hulls (see Figure 1.2)[2] and components of trains such as the coach floor. Since aerospace, marine and ground vehicles are subjected to dynamic loads, confident prediction of natural frequencies of a structural component is essential in preventing excessive vibration levels, which may result in fatigue failure or very high noise levels. Reinforcing ribs are also adopted in the production of soundboards for musical instruments. It is for example the case of the grand piano soundboard shown in Figure 1.3 where a wood plate is reinforced by a set of ribs whose axes are perpendicular to the grain direction of the plate. In these examples there are always reason why one has to keep the plate's mass as low as possible: any vehicle, in particular when it is expected to move fast in a fluid, has to be light but, at the same time, the resistance requirements must be satisfied. Soundboards are required to be light in order to have their mechanical mobility (i.e. the complex ratio between the output velocity and the input force) increased to maximize the sound generated, but the mechanical resistance has to be enough to sustain the vertical load due to the tensioned strings (in grand pianos it can reach up to 300 kg). The balance between having a light structure with high resistance is achieved by adopting stiffening ribs, welded or glued on the plates.

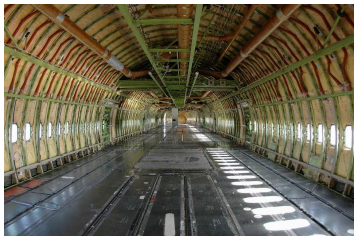

Figure 1.1: Aircraft structure.

[1] Image extracted from $http://www.911research.dsl.pipex.com/ggua175/structural$.
[2] Image extracted from $http://ajaishukla.blogspot.com/2010_08_01_archive.html$.

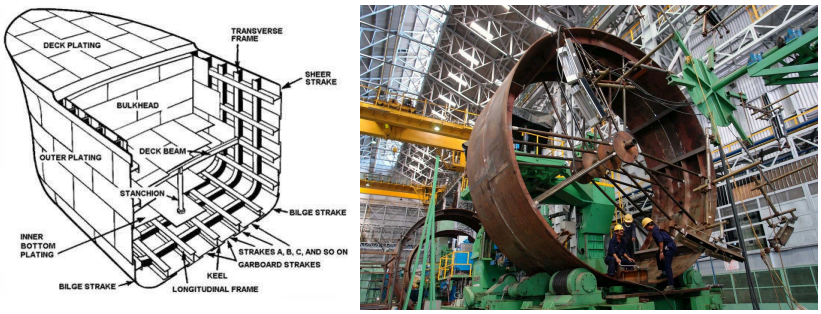

(a) *Ship hull.* (b) *Submarine hull.*

Figure 1.2: Ship and submarine hulls.

Figure 1.3: Grand piano soundboard, courtesy of Fazioli Pianoforti.

Stiffening ribs modify the plate's stiffness along the direction parallel to their axes; structures whose stiffness parameters depend on the direction of the adopted coordinate system are defined as having an orthotropic behaviour. Stiffening the plate is not the only procedure that generates orthotropy in a structure, in fact there are materials characterized by a natural orthotropic behaviour, such as the wood, whose stiffness along the grain direction can be up to 40 times greater than that in the perpendicular one. The case of the soundboard is in fact a particular application where orthotropy is introduced by both the material and the ribs.

In order to characterize the acoustic properties of the plate, several parameters can be adopted such as the sound power, the volume velocity or the field pressures. The quantity that describes better the relation between the sound radiated and the structure's normal velocity, putting thus together the acoustics and the mechanics, is the radiation ratio (also known as radiation efficiency) σ. It is defined as:

$$\sigma(\omega) = \frac{W_{rad}(\omega)}{\rho c S \left\langle \overline{v^2}(\omega) \right\rangle} = \frac{R_{rad}}{\rho c S} \tag{1.1}$$

where $W_{rad}(\omega)$ is the sound power radiated from the structure and it is normalized by the vibrating area S, the air density ρ, the speed of sound c and the space-average mean square vibration velocity $\langle \overline{v^2}(\omega) \rangle$.The same quantity can also be expressed in terms of radiation resistance R_{rad} being the ratio between acoustic power and the averaged mean square velocity. The denominator of equation (1.1) is representative for the acoustic power generated by a rigid piston having the same area of the plate and vibrating harmonically with a velocity equal to the space averaged mean square velocity of the plate. Radiation efficiency provides a powerful relationship between the structural vibrations and the associated radiated sound power. If values or relationships for radiation ratios of a structure are known, then the estimation of the noise radiation and any subsequent noise control is a relatively easy process. For example, radiated sound power can be estimated directly from surface vibrations levels which can be obtained either theoretically or experimentally. It is clear that, depending on the application, the radiation efficiency is wished to be low or high.

With the aim of clarifying the concept of radiation efficiency, two examples of possible applications are presented hereafter.

Assessment of noise in a running train

[3] The noise level in modern diesel-powered trains is often strongly affected by the presence of the diesel engine, which is mounted directly under the carriage floor, see Figure 1.4. For example the engine is usually mounted underneath the floor and it is attached to two longitudinal ribs running along the vehicle, through resilient mounts. The noise generated by the engine reaches the inside of the vehicle through two main paths: the airborne and the structure borne one.

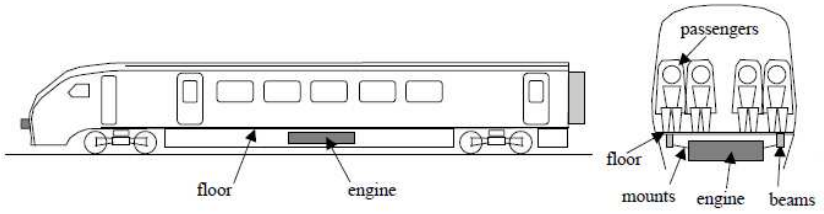

Figure 1.4: Overview of railway vehicle, courtesy of D. J. Thompson.

Concentrating on the structure-borne part, several models can be proposed to calculate the vibrational power injected to the floor by the engine and consequently estimate the floor normal velocity levels, i.e. the quantity defined as $\langle \overline{v^2}(\omega) \rangle$ in equation 1.1. Since the floor is made of a plates-ribs system, if one knows its radiation efficiency, the acoustic power can be readily calculated and the level of the sound noise can be evaluated.

Once the noise levels are known inside the vehicle, different solutions can be taken to reduce them. Possible solutions could be, for example, and depending on the case, to enclosure the engine, to modify the engine mounts, to increase the damping or the thickness of the floor, to add extra transverse stiffening ribs or to make a floating floor. Every solution has its advantages and disadvantages in terms of acoustic emission and costs.

The grand piano soundboard

In the pianos the production of sound is generated by amplifying the vibration of struck strings by the usage of a soundboard. The process by which a piano string is excited by the hammer is rather complex and it is not the purpose of this work to investigate it. What is important to underline is that, after the impact the string starts to freely vibrate according to its normal modes. With the aim of estimating the sound radiated several models can be proposed to calculate the force transmitted to the soundboard by the string through the bridge. Once the input force is known, the surface velocity of the soundboard can be estimated adopting proper structural models. Again the knowledge of the radiation efficiency allows one to give a first rough estimation of the sound power produced. Moreover the radiation efficiency can be used to evaluate the effect on the acoustic radiation of structural modifications. By comparing the radiation efficiency curves for different solutions, the most efficient configuration can be found.

Remind that the acoustic power depends on both the radiation efficiency and the surface velocity, which means that the most efficient plate is not always the one having the highest sound power: a good compromise between the radiation efficiency and the surface velocity to has to be obtained.

1.2 Structure of the thesis

The main purpose of this work is to characterize the radiation efficiency of rectangular, flat, thin plates. Plates made of an isotropic and orthotropic material are considered. The orthotropy is also given by

[3] This section refers to an example class of the Noise Control course of the MsC in Sound and Vibration Studies at the University of Southampton. Courtesy of prof. D. J. Thompson.

the introduction in an isotropic plate of equidistant ribs parallel to an edge. In the following chapters, for each plate configuration analyzed, the formulation for the free vibrations problem is first proposed, then, by adopting the modal summation approach, the radiation efficiency is calculated.

The first chapter is devoted to the analytical solution for the vibrations of homogeneous plates for several combinations of the simply supported, clamped and free boundary conditions. Results are compared with Finite Element Model (FEM).

The radiation efficiency of homogeneous plates is calculated in chapter two; the formulation adopted for the radiation efficiency has allowed to investigate the effect of the modal damping ratio and the influence of the boundary conditions. Results are compared with BEM.

Chapter three is devoted to the analytical solution for the vibrations of plates made of an orthotropic material considering the plate simply supported.

In chapter four the solution for the vibrations of ribbed plates is presented. The effect of the introduction of ribs is investigated in terms of stiffness, natural frequencies and mode shapes. Results are obtained by a combined analytical-numerical method.

The part dedicated to homogeneous plates can be considered as an introduction of the consequent models presented for orthotropic plates. The ortotropy has been considered both due to the material orthotropic behaviour and to stiffening ribs parallel to one edge.

1.3 State of the art

The topic of sound radiation from plates is of great practical importance and has been deeply investigated in the literature during the last century. The most famous work in this sense was presented by Rayleigh in his "The Theory of sound"[2], a book first published in 1877 which can still be considered actual for the ideas and formulation proposed. In fact his solution for the sound radiation from flat plates known as "'Rayleigh integral"' is largely used in nowadays publications and its solution is often numerically computed. Since then many authors dealt with this topic mainly because of the needing for a simple formulation aimed at giving reference results for people interested in noise control.

Considering the radiation efficiency, from the 1960s several authors proposed different methodologies and approximate formulae for calculating this parameter. Some of them focused on the single mode radiation efficiency (the radiation efficiency of a single mode of the plate), others on the total radiation efficiency. In the most cases the plate is considered to be simply supported at the four edges.

A classical modal method is to write the plate solution as a product of the rib solutions with the same boundary conditions, which yields the approximate natural frequencies and mode shapes of the plate. This implies that the boundary conditions should be uniform along each edge of the plate. In reference [3], Maidanik in analysing the response of panel and reinforced panels via ribs systems, noted that the mass law behaviour cannot be used to predict the radiation efficiency when the structure differs than the flat plate configuration. Accounting for the high modal density of the structures he first proposed some simplified formulation to calculate the modal radiation resistance for simple plates and for ribbed plates. When considering a plate fully simply-supported, it was shown by Wallace [4] and Xie [5] that the problem can be in part analytically solved, giving, for the radiation efficiency, a rather simple formula which can be easily numerically integrated. If the plate is not fully simply-supported, in order to get precise results, a complete numerical solution is required and, if one wants to consider low damping values, a high frequency resolution is necessary, which means high computational power. In [4], Wallace also presented integral expressions for the modal radiation efficiency of rectangular plates at arbitrary frequencies based on far-field acoustic intensity. Approximate expressions of radiation efficiencies for frequencies well below the critical frequency were also presented. The effects on radiation efficiency of the inter-nodal areas and their aspect ratios were also investigated and the characteristics of the radiation from a baffled rectangular plate were clearly shown. Gomperts [6, 7] investigated the modal radiation of a rectangular plate under general boundary conditions. He calculated the radiation efficiency of baffled rectangular plates carrying one-dimensional or two-dimensional vibration patterns for a variety of boundary conditions. The results presented taking the one-dimensional vibration pattern cannot be considered quantitatively reliable due to the approximations adopted. On the other hand the results presented taking the two-dimensional pattern made a good agreement with the results presented by Wallace and some other boundary conditions were considered. Another set of results for different boundary conditions is found in Berry's work [8], in which the radiation of sound is analysed in the

far field, and it is calculated from one-dimensional Fourier transforms. It turned out from Gompert's work that a low force impedance at the edge (free supported cases) significantly decreases the radiation efficiency. This affirmation is confirmed in [9], in which is found that the modal response is strongly regulated by the energy dissipation at the edges, which determines the amplitude of the spatially vibration response and the radiated sound power. Leppington [1] later introduced several asymptotic formulae to calculate the modal radiation efficiency for large acoustic wave numbers, especially in the range close to the critical frequency. The plate critical frequency has been identified as an important parameter. Sound with frequencies above critical is radiated efficiently and depends largely on the area and the space-averaged square of surface velocity. Sound with frequencies below critical is radiated less efficiently and depends largely on the spatial distribution of vibration near structural discontinuities such as the plate perimeter or stiffeners, and neighbouring structures which baffle the plate. Leppington re-investigated the problem of average radiation efficiency and revised some of Maidanik's work, using the assumption of high modal densities for the plate. It was found in Leppington's study that Maidanik overestimated the radiation resistance at coincidence, particularly for a plate with a very large aspect ratio. In particular, the difference in terms of radiation efficiency between a fully simply supported and fully clamped supported plate was found to be around 3dB in average sense. Leppington also gave an equivalent formula to Maidanik's for large acoustic wave numbers. However, in the works of both Maidanik and Leppington, the radiation resistance was considered without including the cross-mode contributions. Snyder and Tanaka [10] introduced the contribution of the cross-modal couplings to calculate the total acoustic power at low frequency using modal radiation efficiencies. It was demonstrated that the contributions of the cross-mode are only nonzero for pairs of modes that are either both odd or both even in a given direction.

Although rib-stiffening has been widely used in many applications for sound and vibration control, its effects on sound radiation has not been fully studied theoretically. During the recent years the interest for this topic is growing since ribbed plates are often present in structures. In [3] Maidanik stated that the introduction of ribs in a fully simply-supported plate makes the radiation resistance of the plate increase by a simple factor that depends on the perimeter of the ribs, as equation(1.2)shows:

$$\frac{\left(P_r^{ribs} + P_r^0\right)}{P_r^0} \tag{1.2}$$

in which P_r^{ribs} is twice the total length of the ribs and P_r^0 is the perimeter of the original plate, where the conditions on the size of the plate, with respect to the acoustic wavelength are to be applied to each of the subpanels and not to the entire dimensions of the system. By studying the acceleration spectrum, and its relation to the sound power, he showed that the discontinuities of the plate at the rib's location will, in general, increase the coupling between the structure and the surrounding acoustic medium. Maidanik also derived approximate expressions for the radiation efficiency of the rib-plate system as a function of frequency, by employing a statistical method, which led to the development of a then new technique later called Statistical Energy Analysis.

Some studies about this topic do not take in account the modal behaviour of the rib. This is considered by Heckl [11], where a plate infinite in one dimension and finite in the other dimension, with attached ribs across the finite dimension is studied. Expressions for the transmission and reflection coefficients are presented, in order to discuss the wave propagation along the complex system. A number of publications are concerned with the sound radiation by periodically stiffened infinite plates. Analytical solutions for the vibration and the radiated sound pressure in the far-field is given for the case where the structure is excited by harmonic pressure and by point or line forces. However, in many practical situations, such as panels in automotive structures, the excitation is much more complicated than simple point or line forces.

In recent years, some researchers have focused on the numerical optimisation of the acoustic design of a structure, by taking advantage of the increasing capabilities of microprocessors. The proposed methods use optimisation algorithms, such as genetic algorithms, and numerical methods such as the finite element method and/or the boundary element method, to optimise the position and properties of a rib attached onto a plate. Although, the acoustic optimisation techniques are very powerful for dealing with problems where the parameters are specific and they are known a priori, they are unable to shed light on the physical phenomena of sound radiation by rib-stiffened plates and hence to give general guidelines for designing such structures. In Rousounelos [12], in order to excite the structure with an equal amount

of energy at all frequencies, the vibration field of a finite simply supported plate with attached stiffeners is considered by assuming a propagating wave in the plate, in the direction perpendicular to the rib, and the scattering caused by the ribs along with an infinite number of reflections from the boundaries. In this way, in the direction of the rib, the vibration field is considered to be one of the mode shapes of the simply supported plate. From the numerical evaluation of the above model, the first observation was that the resonance frequency of the plate are shifted depending upon whether they are above or below the resonance frequency of the rib. When the resonance frequency of the plate is below the resonance frequency of the rib, the stiffener behaves as an added stiffness hence it shifts the resonant frequency higher. The opposite effect is observed when the resonance of the plate is higher than that of the rib. Then the rib behaves as an added mass hence it shifts the resonant frequency lower. The shift of resonant frequencies has an effect upon the radiation efficiency as modes with lower resonance frequency have lower radiation efficiency and modes with higher resonance frequency have higher radiation efficiency.

Chapter 2

Plates made of an isotropic material

2.1 Introduction

Consider a thin, flat rectangular plate of isotropic and linearly elastic material with modulus of elasticity E, poisson ratio ν and density ρ, having uniform thickness h and occuping the region in the *(x,y)*-plane $\Omega(x, Y) : 0 \leq x \leq a, 0 \leq y \leq b$. The strain-stress relationship is known and it is given by:

$$\begin{bmatrix} \epsilon_x \\ \epsilon_y \\ \gamma_{xy} \end{bmatrix} = \begin{bmatrix} 1/E & -\nu/E & 0 \\ -\nu/E & 1/E & 0 \\ 0 & 0 & 1/G \end{bmatrix} \begin{bmatrix} \sigma_x \\ \sigma_y \\ \tau_{xy} \end{bmatrix} \tag{2.1}$$

and the inverse of equation (2.1) gives:

$$\begin{bmatrix} \sigma_x \\ \sigma_y \\ \tau_{xy} \end{bmatrix} = \begin{bmatrix} \frac{E}{1-\nu^2} & \frac{E}{\nu(1-\nu^2)} & 0 \\ \frac{E}{\nu(1-\nu^2)} & \frac{E}{1-\nu^2} & 0 \\ 0 & 0 & G \end{bmatrix} \begin{bmatrix} \epsilon_x \\ \epsilon_y \\ \gamma xy \end{bmatrix} \tag{2.2}$$

Consider now the possible boundary conditions along its edges: simply supported, clamped supported and freely supported. For an edge, for example $x = 0$, they can be expressed as follows:

- Simply supported edge:
$$w|_{x=0} = 0 \qquad \frac{\partial^2 w}{\partial x^2}|_{x=0} \tag{2.3}$$
- Clamped supported edge:
$$w|_{x=0} = 0 \qquad M|_{x=0} \tag{2.4}$$
- Free supported edge:
$$M|_{x=0} \qquad M_{xy}|_{x=0} = 0 \qquad T_x|_{x=0} = 0 \tag{2.5}$$

where w is the vertical displacement. A formulation for calculating the natural frequencies and modal shapes of a previously considered plate will be presented for different boundary conditions.

2.2 Free vibration of a thin isotropic rectangular plate

According to the *Kirchoff classical plate theory*, the equation for free vibrations, valid for small plate vertical displacement $w = w(x, y, t)$ is:

$$D\left(\frac{\partial^4 w}{\partial x^4} + 2\frac{\partial^4 w}{\partial x^2 \partial y^2} + \frac{\partial^4 w}{\partial y^4}\right) + \rho_s h \frac{\partial^2 w}{\partial t^2} = 0 \tag{2.6}$$

where ρ_s is the material density and D is the bending stiffness of the plate. Considering a time harmonic vibration and adopting the so called *assumed modes solution* (see [13]), the displacement w is expressed in the form:

$$w(x,y,t) = \sum_{m=1}^{M}\sum_{n=1}^{N} s_{mn}(x,y)\eta_{nm}(t) = \sum_{m=1}^{M}\sum_{n=1}^{N} s_{mn}(x,y)w_{mn}e^{jwt} \tag{2.7}$$

According to the classical modal solution, the mode shape function s_{mn} can be expressed as the product of the modes shape of the ribs having the same boundary conditions.

$$s_{mn} = \phi_m(x)\psi_n(y) \tag{2.8}$$

Imposing the time harmonic solution to the rib equation motion one obtains

$$\phi_m(x) = C_{1m}\sin(\lambda_m x) + C_{2m}\cos(\lambda_m x) + C_{3m}\sinh(\lambda_m x) + C_{4m}\cosh(\lambda_m x) \tag{2.9}$$

where $C_{1m}, C_{2m}, C_{3m}, C_{4m}$ and λ_m are obtained imposing the considered boundary conditions. The function $\psi_n(y)$ can be obtained from equation (2.9) by replacing m by n, x by y and λ_m by λ_n.

2.2.1 Mode shapes

The six possible distinct sets of boundary conditions along edges $x = 0$ and $x = a$ are satisfied by the following mode shapes (see Leissa [14]):

Simply supported boundary condition at two opposite edges (SS-SS)

$$\phi_m(x) = \sin\frac{(m-1)\pi x}{a} \qquad (m = 2,3,4...) \tag{2.10}$$

Clamped boundary condition at two opposite edges (C-C)

$$\phi_m(x) = \cos\gamma_1\left(\frac{x}{a}-\frac{1}{2}\right) + \frac{\sin(\gamma_1/2)}{\sinh(\gamma_1/2)}\cosh\gamma_1\left(\frac{x}{a}-\frac{1}{2}\right) \qquad (m = 2,4,6,...) \tag{2.11}$$

where the values of γ_1 are obtained as the roots of

$$\tan(\gamma_1/2) + \tanh(\gamma_1/2) = 0 \tag{2.12}$$

and

$$\phi_m(x) = \sin\gamma_2\left(\frac{x}{a}-\frac{1}{2}\right) - \frac{\sin(\gamma_2/2)}{\sinh(\gamma_2/2)}\sinh\gamma_2\left(\frac{x}{a}-\frac{1}{2}\right) \qquad (m = 3,5,7,...) \tag{2.13}$$

where the values of γ_2 are obtained as the roots of

$$\tan(\gamma_2/2) - \tanh(\gamma_2/2) = 0 \tag{2.14}$$

Clamped at x = 0 and simply supported at x = a (C-SS)

$$\phi_m(x) = \sin\gamma_2\left(\frac{x}{2a}-\frac{1}{2}\right) - \frac{\sin(\gamma_2/2)}{\sinh(\gamma_2/2)}\sinh\gamma_2\left(\frac{x}{2a}-\frac{1}{2}\right) \qquad (m = 2,3,4,...) \tag{2.15}$$

with γ_2 as defined in equation (2.14).

Free boundary condition at two opposite edges (F-F)

$$\phi_m(x) = 1 \qquad (m=0) \tag{2.16}$$

$$\phi_m(x) = 1 - \frac{2x}{a} \qquad (m=1) \tag{2.17}$$

$$\phi_m(x) = cos\gamma_1 \left(\frac{x}{a} - \frac{1}{2}\right) - \frac{\sin(\gamma_1/2)}{\sinh(\gamma_1/2)} \cosh\gamma_1 \left(\frac{x}{a} - \frac{1}{2}\right) \qquad (m=2,4,6,...) \tag{2.18}$$

$$\phi_m(x) = \sin\gamma_2 \left(\frac{x}{a} - \frac{1}{2}\right) + \frac{\sin(\gamma_2/2)}{\sinh(\gamma_2/2)} \sinh\gamma_2 \left(\frac{x}{a} - \frac{1}{2}\right) \qquad (m=3,5,7,...) \tag{2.19}$$

with γ_1 and γ_2 as defined in equations (2.12) and (2.14).

Clamped at x = 0 and free at x = a (C-F)

$$\phi_m(x) = \cos\frac{\gamma_3 x}{a} - \cosh\frac{\gamma_3 x}{a} + \left(\frac{\sin\gamma_3 - \sinh\gamma_3}{\cos\gamma_3 - \cosh\gamma_3}\right)\left(\sin\frac{\gamma_3 x}{a} - \sinh\frac{\gamma_3 x}{a}\right) \qquad (m=1,2,3,...) \tag{2.20}$$

where

$$\cos\gamma_3 \cosh\gamma_3 = -1 \tag{2.21}$$

Free at x = 0 and simply supported at x = a (F-SS)

$$\phi_m(x) = 1 - \frac{x}{a} \qquad (m=1) \tag{2.22}$$

$$\phi_m(x) = \sin\gamma_2 \left(\frac{x}{2a} - \frac{1}{2}\right) + \frac{\sin(\gamma_2/2)}{\sinh(\gamma_2/2)} \sinh\gamma_2 \left(\frac{x}{2a} - \frac{1}{2}\right) \qquad (m=2,3,4,...) \tag{2.23}$$

The solution of equations (2.12), (2.14) and (2.21) can be numerically computed or, if a small error on the natural frequency calculation of the first mode is accepted, an approximate solution is readily given by:

$$\gamma_1 = 2\pi\left(\frac{3}{4} + \frac{m-1}{2}\right) \qquad (m=2,3,4,...) \tag{2.24}$$

$$\gamma_2 = 2\pi\left(\frac{5}{4} + \frac{m-2}{2}\right) \qquad (m=3,5,7,...) \tag{2.25}$$

$$\gamma_3 = 2\pi\left(\frac{3}{4} + \frac{m-2}{2}\right) \qquad (m=2,3,4,...) \tag{2.26}$$

In Figure 2.1 the approximate solution for equations (2.12), (2.14) and (2.21) is represented and it is super-imposed to the complete graphical solution. It can be noticed that above the first mode the two solutions coincide while the error for the first mode is of 1.6%.

The functions $\psi(y)$ are similarly chosen by the conditions at $y = 0$ and $y = b$ by replacing x by y, a by b, and m by n in equations (2.9)-(2.26). The indicators n and m are seen to be the number of nodal lines lying in the x and y direction, respectively, including the boundaries nodal lines, except when the boundary is free.

2.2.2 Natural frequencies

The natural frequencies of the plates are found to be expressed as:

$$\omega^2 = \frac{\pi^4 D}{a^4 \rho}\left[G_x^4 + G_y^4\left(\frac{a}{b}\right)^4 + 2\left(\frac{a}{b}\right)^2 \left[\nu H_x H_y + (1-\nu) J_x J_y\right]\right] \tag{2.27}$$

Boundary conditions at	m	Gx	Hx	Jx
SS (x=0) SS (x=a)	$2, 3, 4, \ldots$	$m-1$	$(m-1)^2$	$(m-1)^2$
C (x=0)	2	1.506	1.248	1.248
C (x=a)	$3, 4, 5, \ldots$	$m-\frac{1}{2}$	$\left(m-\frac{1}{2}\right)^2\left[1-\frac{2}{\left(m-\frac{1}{2}\right)^2\pi}\right]$	$\left(m-\frac{1}{2}\right)^2\left[1-\frac{2}{\left(m-\frac{1}{2}\right)^2\pi}\right]$
F (x=0)	0	0	0	0
	1	0	0	$12/\pi^2$
F (x=a)	2	1.506	1.248	5.017
	$3, 4, 5, \ldots$	$m-\frac{1}{2}$	$\left(m-\frac{1}{2}\right)^2\left[1-\frac{2}{\left(m-\frac{1}{2}\right)^2\pi}\right]$	$\left(m-\frac{1}{2}\right)^2\left[1+\frac{6}{\left(m-\frac{1}{2}\right)^2\pi}\right]$
C (x=0) SS (x=a)	$2, 3, 4, \ldots$	$m-\frac{3}{4}$	$\left(m-\frac{3}{4}\right)^2\left[1-\frac{1}{\left(m-\frac{3}{4}\right)^2\pi}\right]$	$\left(m-\frac{3}{4}\right)^2\left[1-\frac{1}{\left(m-\frac{3}{4}\right)^2\pi}\right]$
F (x=0)	1	0	0	$3/\pi^2$
SS (x=a)	$2, 3, 4, \ldots$	$m-\frac{3}{4}$	$\left(m-\frac{3}{4}\right)^2\left[1-\frac{1}{\left(m-\frac{3}{4}\right)^2\pi}\right]$	$\left(m-\frac{3}{4}\right)^2\left[1+\frac{3}{\left(m-\frac{3}{4}\right)^2\pi}\right]$
C (x=0)	1	0.597	-0.0870	0.471
F (x=a)	2	1.494	1.347	3.284
	$3, 4, 5, \ldots$	$m-\frac{1}{2}$	$\left(m-\frac{1}{2}\right)^2\left[1-\frac{2}{\left(m-\frac{1}{2}\right)^2\pi}\right]$	$\left(m-\frac{1}{2}\right)^2\left[1+\frac{2}{\left(m-\frac{1}{2}\right)^2\pi}\right]$

Table 2.1: Coefficients for equation (2.27).

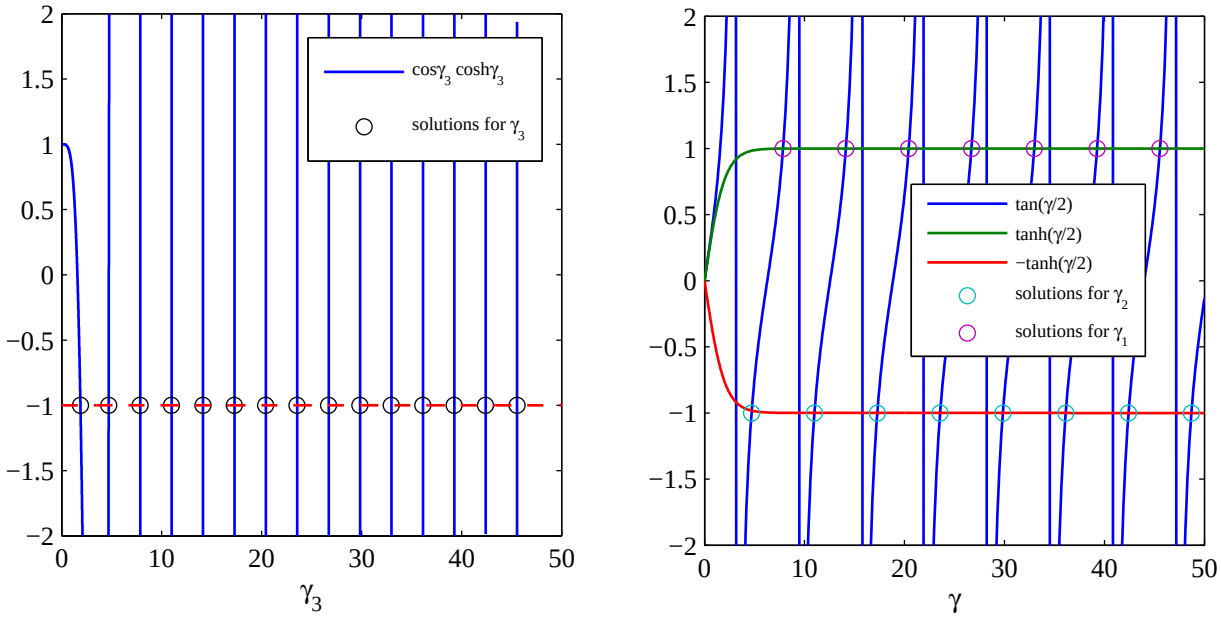

(a) *Solutions for a CF rib.*

(b) *Solutions for a CC rib.*

Figure 2.1: Solutions for equations (2.12),(2.14) and (2.21).

where G_x, G_y, H_x, H_y, J_x and J_y are functions of the mode number mn and depend on the boundary conditions, they are given in Table 2.1.

Once the natural frequencies and the mode shape are obtained the modal mass of the plate can be computed as:

$$M_{mn} = \int_0^a \int_0^b \rho h s_{mn}^2 \, dxdy \tag{2.28}$$

2.3 Results

A MATLAB code has been written for the purpose of calculating the free-vibrations and mode shapes of an isotropic plate for different boundary conditions using the formulation given above. In parallel, a Finite Element Model (FEM) of the plate has also been created in Abaqus in order to compare the numerical results with the analytical results. The geometry of the plate is shown in Figure 2.2. It is considered that the plate is made of aluminium ($\rho = 2700\ kg/m^3,\ \nu = 0.3,\ E = 7.1e10\ MPa$).

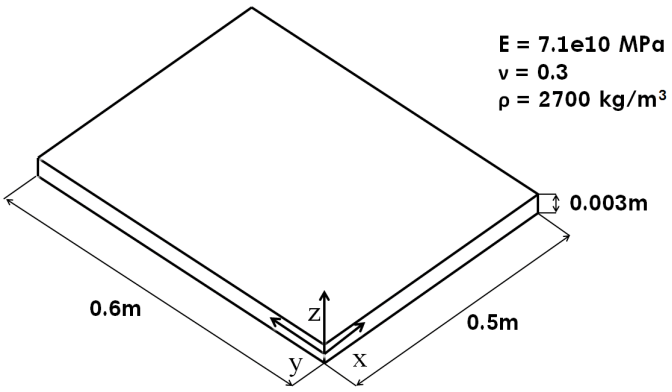

Figure 2.2: Geometry of the plate.

In the numerical model the plate is composed of 0.01m shell elements with 6 degrees of freedom (DOF) per node. For each element, the approximate global size is 0.01m . The final structure is formed of 3000 elements and 3111 nodes. Figure 2.3 shows the final mesh.

After setting the mesh, the boundary conditions must be defined. Taking into account that every node has 6 DOF, which consist in three displacements (parallel to the axis) and three rotations (respect to the axis), the constraints imposed to the external nodes appertaining to an element which forms part of an edge are:

- if the node appertains to an edge which is simply supported, both three displacements are prevented.
- if the node appertains to an edge which is clamped supported, all displacements and rotations are prevented.
- if the node appertains to an edge which is freely supported, no constrain is defined. That is, elements can displace and rotate in all directions.

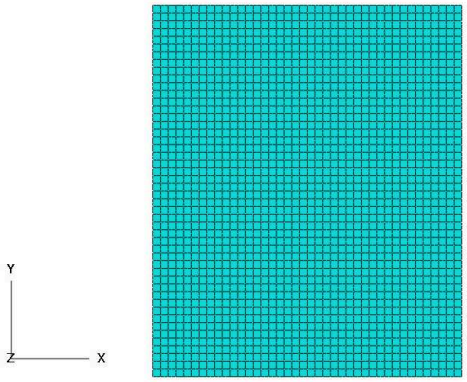

Figure 2.3: FE Model.

Finally, natural frequencies and mode shapes are calculated using a frequency step. Using the Lanczos eigensolver and defining the range of interest (until 10 KHz in case of study), Abaqus solves the eigenvalue problem. Eigenvectors can be normalized respect by displacement or by the mass.

2.3.1 Scatter plot and MAC

Analytical and numerical models can be compared by analysing their solutions and obtaining the correlation index, known as MAC (Modal Assurance Criterion) between their modal shapes. The expression of MAC is:

$$MAC(i,j) = \frac{|S_{an}^{i\ T} S_{num}^{j}|^2}{(S_{an}^{i\ T} S_{an}^{i})(S_{num}^{j\ T} S_{num}^{j})} \tag{2.29}$$

It consists in a square matrix whose elements have a value between zero and one depending on the correlation degree of the mode shape. While diagonal elements are desired to be equal to one, that is, the i-th analytical mode corresponds to the i-th numerical mode, extra-diagonal elements are desired to be equal to zero. Analytical and numerical modal frequencies are also compared using the scatterplot.

MAC and scatterplot are used to compare analytical and numerical models at low frequencies. For mid-high frequencies the comparison is made in terms of FRF (Frequency Response Function). Results for different boundary conditions are presented in Figures 2.5, 2.6, 2.7, 2.8, 2.9, 2.10 and 2.11. Letters indicate the boundary condition considered in the edges $x = 0$, $x = a$, $y = 0$ and $y = b$. (E.g SS-SS-F-F means Simply Supported in edges $x = 0$ and $x = a$, and freely supported in edges $y = 0$ and $y = b$). Figure (2.4) shows graphically the notation adopted.

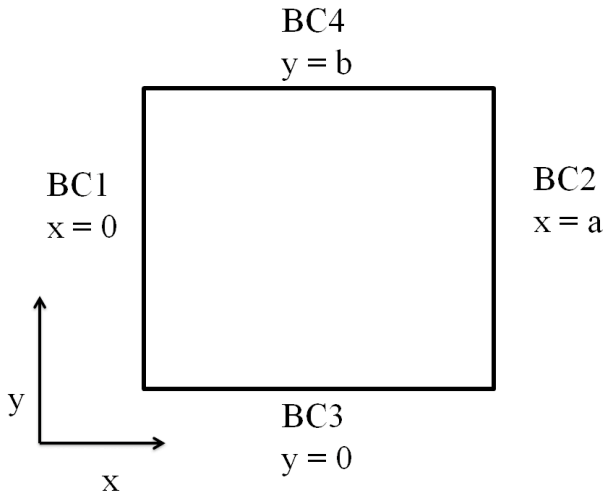

Figure 2.4: Notation adopted to define the boundary conditions.

In SS-SS-SS-SS and C-C-C-C cases (Figure 2.5) and (Figure 2.6) Mac-plot reveals that results between analytical and numerical solution make an agreement in the frequency range considered. However one can see in the scatter-plot that when the frequency considered increases, the free vibration frequency calculated by the numerical solution tends to be lower than the analytical one in the SS-SS-SS-SS case and and higher for the C-C-C-C case. Results for SS-SS-F-F and F-F-C-C are satisfactory as well. Otherwise, results for C-F-C-F and F-SS-F-SS (Figures 2.10 and 2.11) are satisfactory, but one can notice that there is a slight deviation for numerical results as the frequency increases. Indeed, the F-F-F-F case, in which static modes have not been considered in Figure 2.7 shows that fact clearly. After an analysis, one can conclude that in a plate in which there is free supported corner, that is F-F-F-F, C-F-C-F and F-SS-F-SS cases, the numerical solution and the analytical is slightly different. This results concord with Leissa [14]: the analytical solution for a fully freely-supported plate is not as accurate as the rest, giving the most poorly results respect to other boundary condition combinations. The confusion in the literature concerning the existence of modes for this problem is seen in some works, concluding that frequently certain vibration modes are not discovered in the analysis (see Leissa [15]).

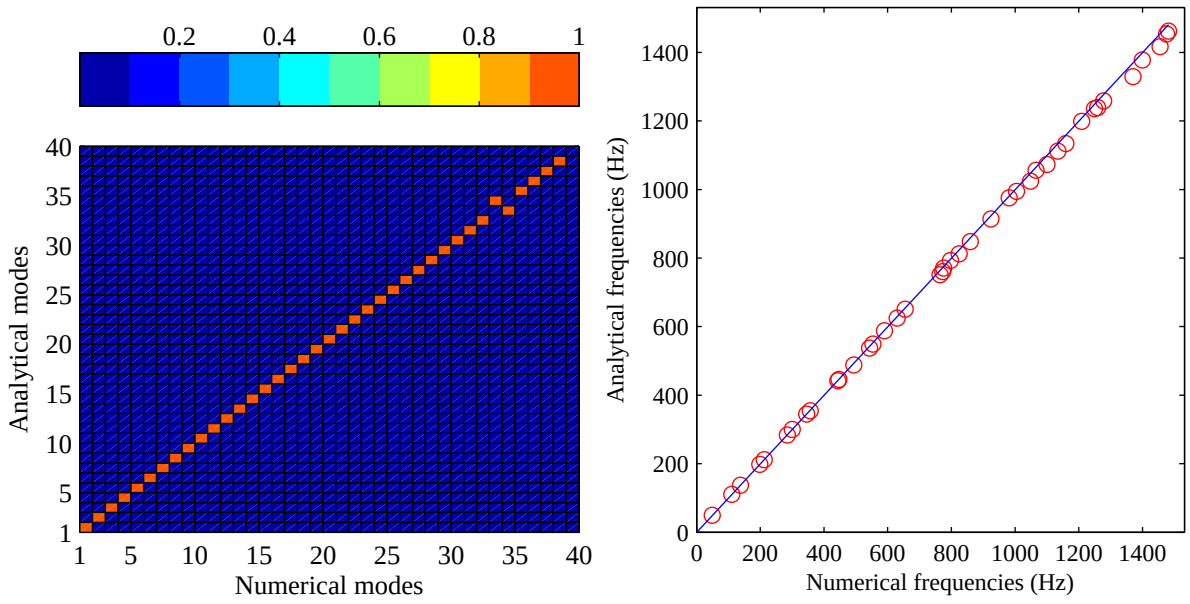

(a) *MAC* (b) *scatter plot*

Figure 2.5: MAC and scatter plot. Results for SS-SS-SS-SS.

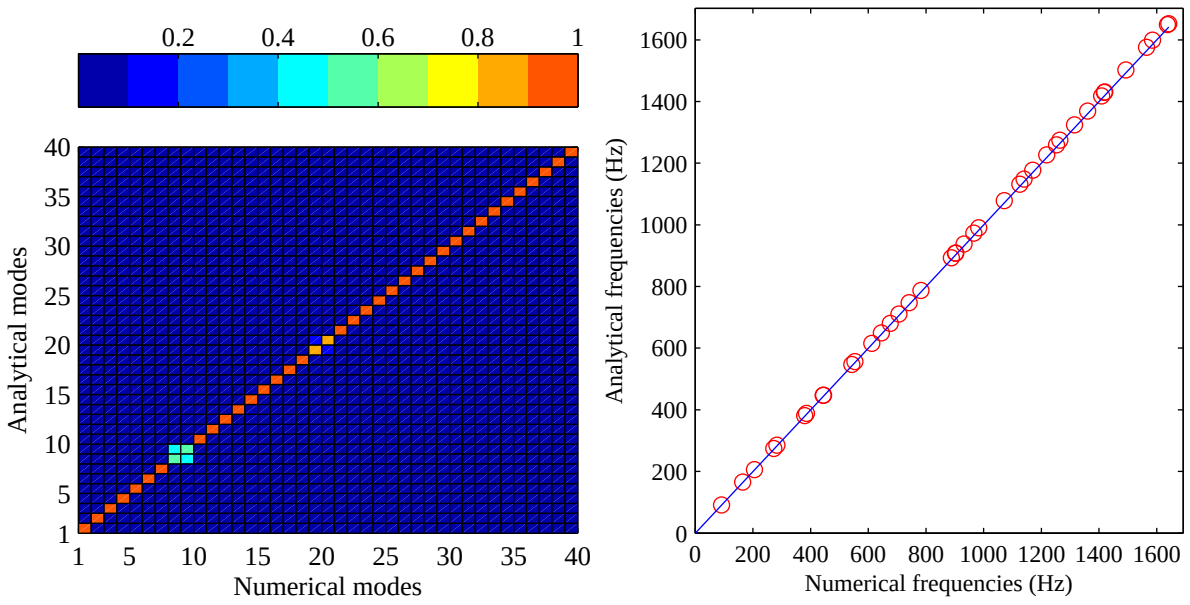

(a) *MAC* (b) *scatter plot*

Figure 2.6: MAC and scatter plot. Results for C-C-C-C.

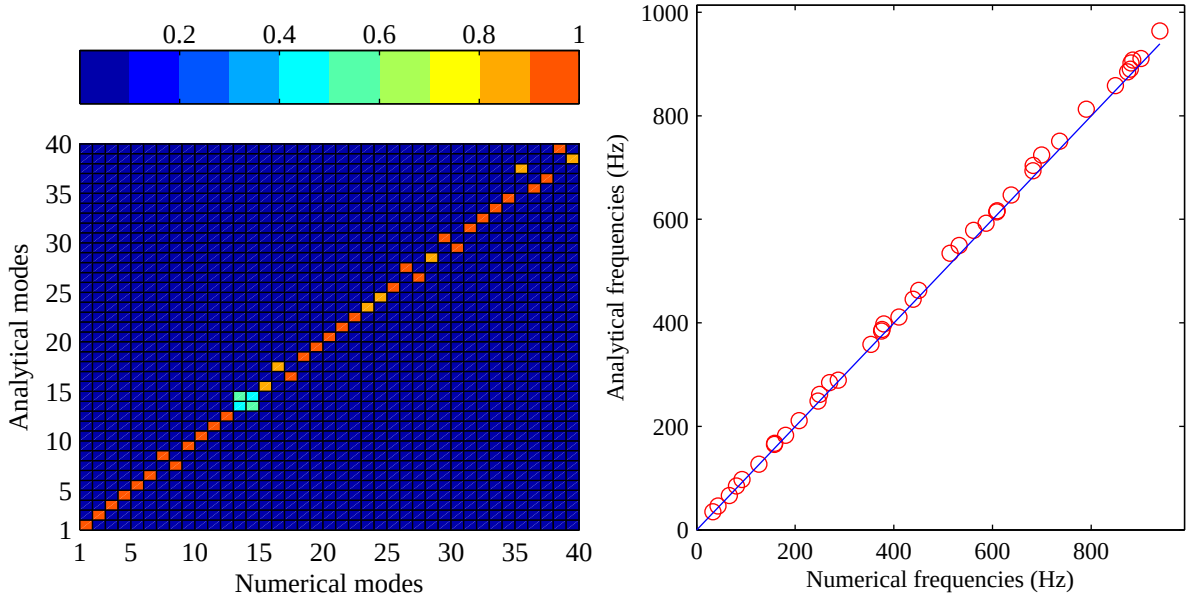

(a) *MAC* (b) *scatter plot*

Figure 2.7: MAC and scatter plot. Results for F-F-F-F.

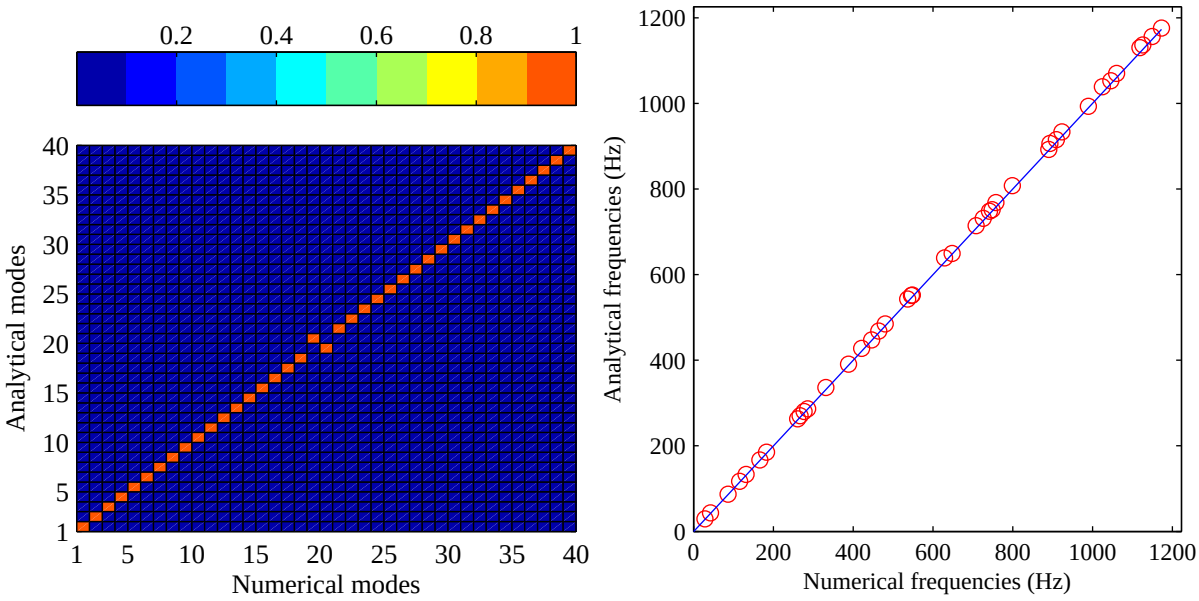

(a) *MAC* (b) *scatter plot*

Figure 2.8: MAC and scatter plot. Results for SS-SS-F-F.

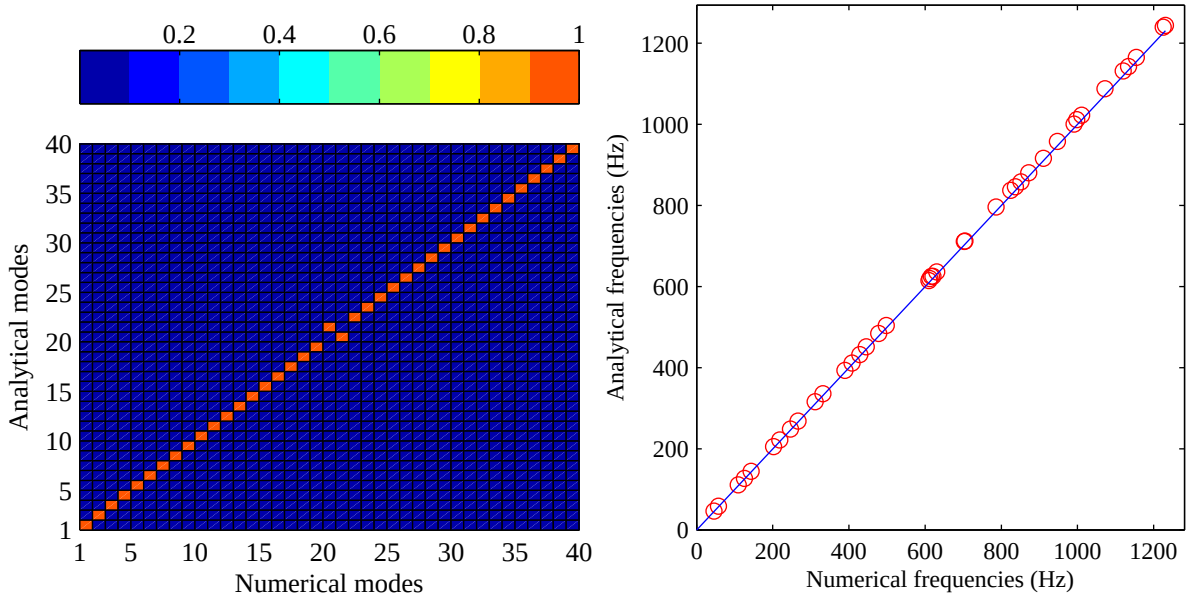

(a) *MAC* (b) *scatter plot*

Figure 2.9: MAC and scatter plot. Results for F-F-C-C.

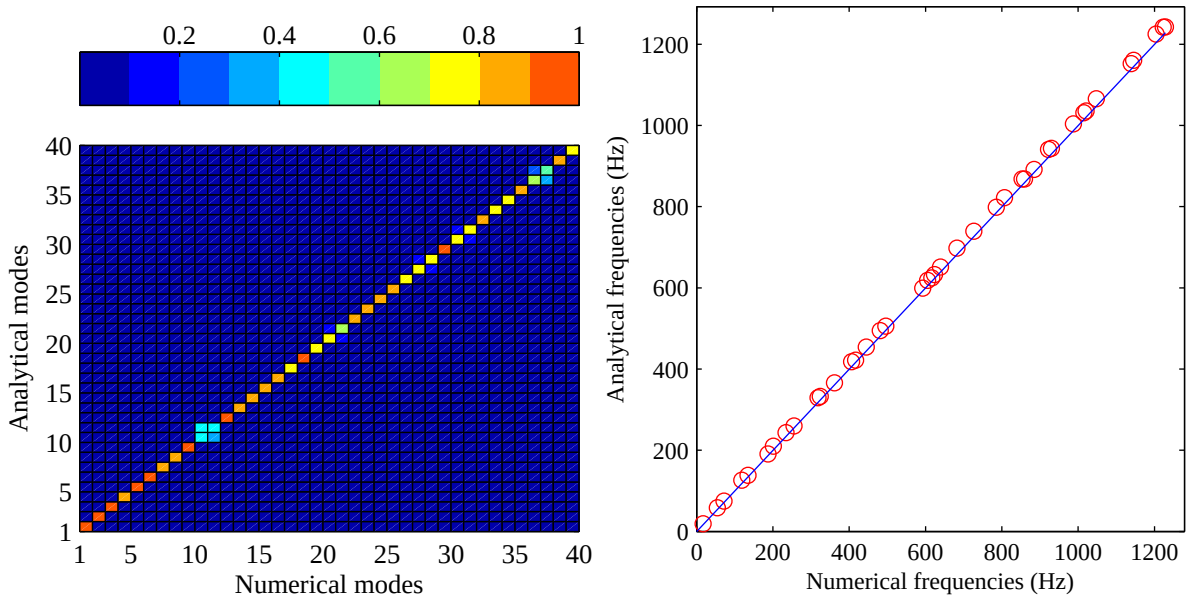

(a) *MAC* (b) *scatter plot*

Figure 2.10: MAC and scatter plot. Results for C-F-C-F.

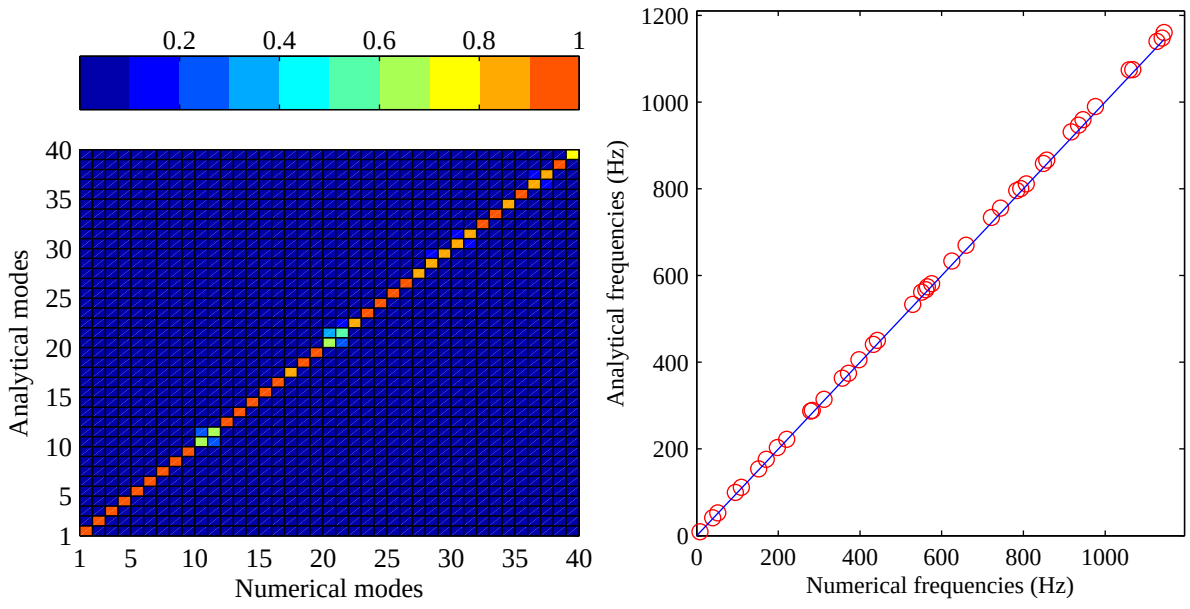

(a) *MAC* (b) *scatter plot*

Figure 2.11: MAC and scatter plot. Results for F-SS-F-SS.

2.3.2 Free vibration at low frequencies

First eight free-vibration modes for different combinations of simply supported, clamped edges and free edges are presented in Table 2.2. Given a mode number, the frequency value of the free-vibration of a plate in which there is almost a clamped edge will always be higher than the SS-SS-SS-SS case. The reason is that a clamped edge introduces a bigger stiffness than a Simply Supported one. Static modes for F-F-F-F case are considered. One can easily see the influence of a freely supported edge. For a given mode number, the fact that two opposite edges are freely supported makes the frequency value decrease considerably, as it can be seen in cases SS-SS-F-F and C-C-F-F. In cases in which there is a Freely Supported corner, this value of frequency is even lower (cases C-F-C-F and F-SS-F-SS) than two opposite edges freely supported cases.

2.3.3 Free vibration in the mid-high frequency range

When dealing with sound radiation problem the exact natural frequency of each single vibration mode is not the main problem to be solved. In fact in the mid-high frequency range the vibration response of a structure is never dominated by one single mode but it is always composed by the contribution of several. What is thus important for a simplified analytical model is to reproduce the correct average levels of the vibration response. At this purpose in Figures 2.12 and 2.13 the numerically calculated FRF is presented along with the corresponding analytical function. The boundary conditions considered are fully simply-supported and fully freely-supported. Observing Figure 2.12 it is found that at low frequencies the results correspond perfectly. As the frequency increases, the deviation between analytical and numerical results so does, but the average levels of the vibration response are similar. In case of a fully freely-supported (Figure 2.13), the fact that the value of the some natural frequencies of both models are slightly different, implies a slight difference in terms of vibration response at low frequencies. However, the analytical model is able to reproduce the the behaviour of plate in the mid-high frequency range, having an average level of vibration response similar to the numerical model.

Case	SS-SS-SS-SS	C-C-C-C	F-F-F-F	C-F-C-F	F-SS-F-SS	SS-SS-F-F	C-C-F-F
Mode	Freq (Hz)	Freq (Hz)	Freq (Hz)	Freq (Hz)	Freq (Hz)	Freq (Hz)	Freq (Hz)
1	49.56	91.51	0.00	18.66	8.76	29.25	66.34
2	110.50	165.61	0.00	58.39	41.28	43.21	75.26
3	137.32	206.04	0.00	74.56	52.78	87.16	110.85
4	198.26	274.46	35.07	126.24	99.49	117.00	182.82
5	212.07	284.93	46.07	138.40	111.35	133.17	184.49
6	283.57	381.29	66.34	190.79	154.12	166.75	195.28
7	299.82	388.36	84.83	209.85	176.07	185.16	238.87
8	344.51	446.52	97.34	243.18	203.16	263.26	300.72

Case	SS-SS-C-C	C-SS-C-SS
Mode	Freq (Hz)	Freq (Hz)
1	66.79	68.61
2	147.45	136.67
3	150.03	170.14
4	227.92	234.41
5	273.28	247.60
6	291.15	331.13
7	351.06	342.30
8	367.75	394.00

Table 2.2: First eight frequencies for different combinations of boundary conditions.

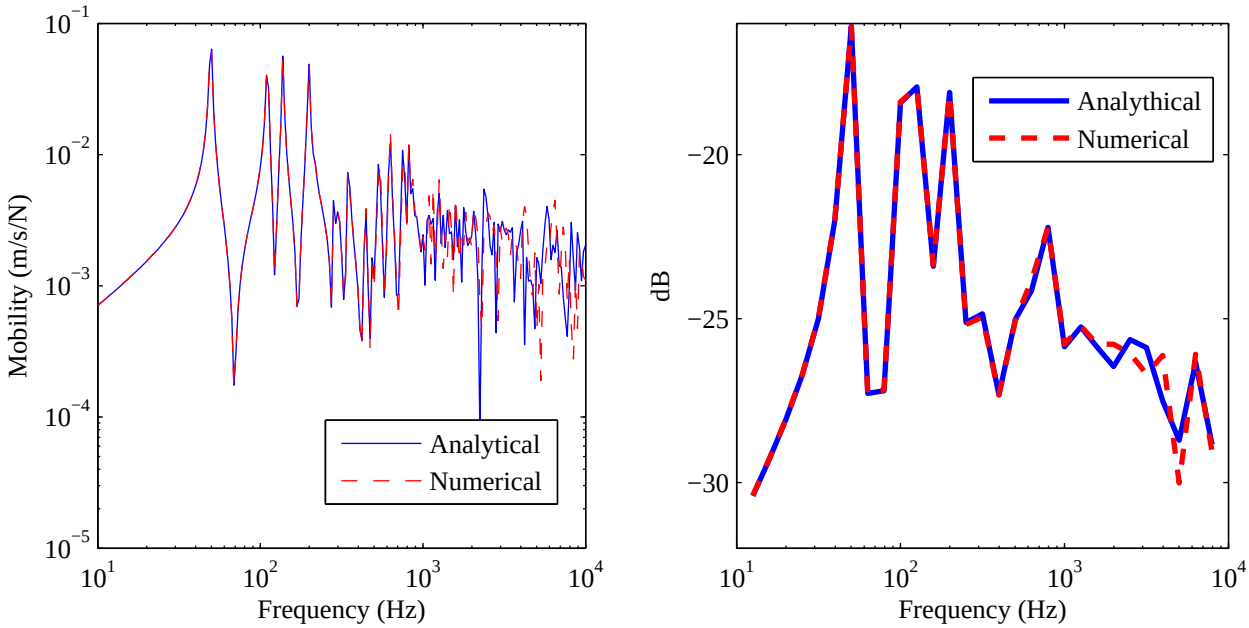

(a) *Comparison in narrow band.*

(b) *Comparison in terms of third octave band.*

Figure 2.12: Comparison between analytical and numerical model FRF of a fully simply supported plate.

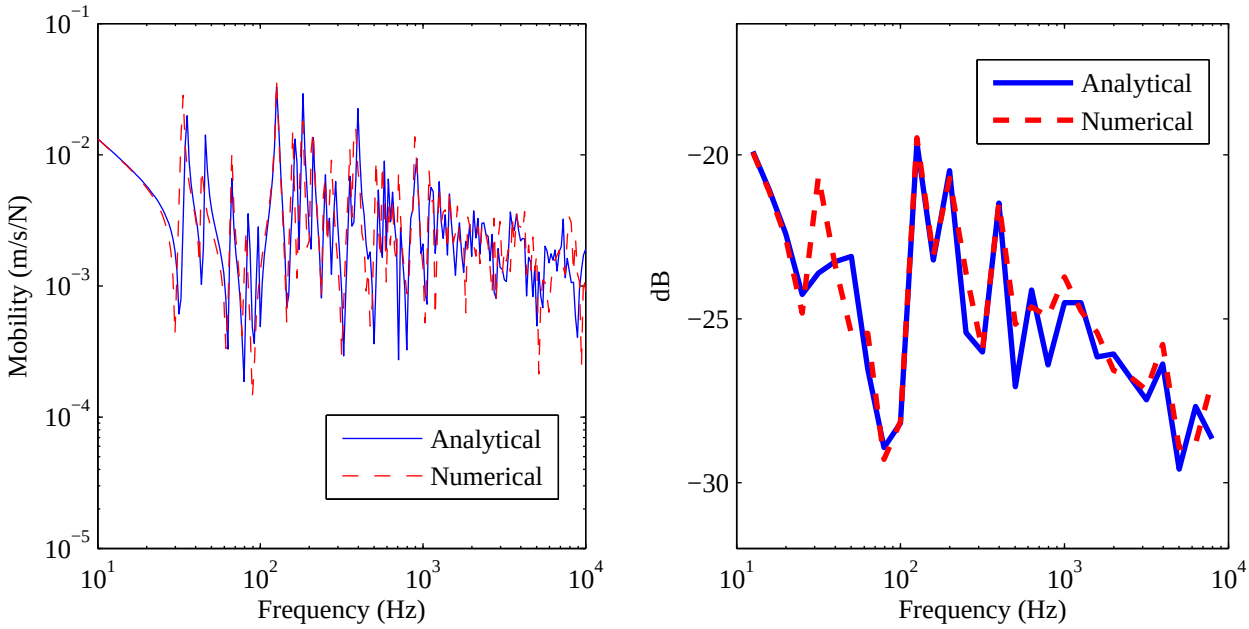

(a) *Comparison in narrow band.*

(b) *Comparison in terms of third octave band.*

Figure 2.13: Comparison between analytical and numerical model FRF of a fully freely supported plate.

Chapter 3

Radiation efficiency

According to the type of excitation and to the modal density of the structure, the parameter of interest to quantify its radiation of sound is either the single-mode radiation efficiency, known as modal radiation efficiency, or the average radiation efficiency. The modal radiation efficiency is the radiation efficiency of a single mode of the plate while the total radiation efficiency takes into account the effect of all the structural modes. In principle, the radiation efficiency of a plate can be obtained by summing the effect of all modes that contribute significantly in the frequency range under consideration. In this work the average radiation efficiency (σ) of flat plates in several boundary conditions is calculated by using the modal summation approach based on the far field sound intensity presented by Xie [5]. The radiation resistance, R_{rad}, normalized by the radiating area S, the air density ρ and the speed of sound c, gives the total radiation efficiency (equation (3.1)). The same quantity can also be expressed in terms of radiated sound power $W_{rad}(\omega)$, which is now normalized using the same terms along with the space-average mean square vibration velocity. The terms equation (3.1) have the following meaning: the numerator stands for the power radiated by the vibrating plate, while the denominator indicates the power radiated by a surface S vibrating harmonically as a rigid piston in the direction normal to the plate, its velocity amplitude being equal to the mean square velocity of the real plate averaged over its surface S.

$$\sigma = \frac{R_{rad}}{\rho c S} = \frac{W_{rad}(\omega)}{\rho c S \left\langle \overline{v^2}(\omega) \right\rangle} \tag{3.1}$$

There are two different ways used to determine the radiation efficiency, the first is to integrate the intensity on a hemisphere in the far field enclosing the plate, the latter is to integrate the acoustic intensity over the surface of the vibrating plate. Both approaches require the knowledge of the distribution of the velocity over the plate.

3.1 Derivation of average radiation efficiency using a modal summation approach

3.1.1 Radiated power in terms of plate modes

The methodology adopted for the radiation efficiency calculation is the one presented by [5]. Following their assumption the acoustic radiated power is estimated over a hemisphere in the far-field and the point force is averaged over all possible positions. Using an average over force point locations showed that the contribution in the total radiated power due to cross-modal coupling terms averages to zero and only under this assumption they can be neglected. The idea of averaging the point force leads to a results independent from the location of the forcing point. This does not mean that this argument is not important in dealing with the sound radiation from surfaces but allows to investigate the effect of other structural modification (e.g. boundary conditions, curvature, stiffening ribs, plate thickness) without the influence of the forcing point location, whose effect will be investigated separately.

Consider a rectangular plate, set in an infinite rigid baffle as shown in Figure 3.1[1]. The total acoustic

[1] Figure extracted from Xie [5]

power radiated from the plate can be obtained by integrating the far field acoustic intensity over a hemisphere of radius r to give:

$$W = \int_0^{2\pi} \int_0^{\pi/2} \frac{|p(r)|}{2\rho c} \, r^2 \sin\theta \; d\theta \; d\phi \tag{3.2}$$

where $p(r)$ is the complex acoustic pressure amplitude at a location in space expressed in spherical co-ordinates, $r = r(r, \theta, \phi)$. By using the method of images, $p(r)$ can be written in terms of the plate surface velocity using the Rayleigh integral:

$$p(r) = \frac{jk\rho c}{2\pi} \int_S v(x) \frac{e^{-jkr'}}{r'} dx \tag{3.3}$$

The same quantity can be defined considering the contribution of the structural modes

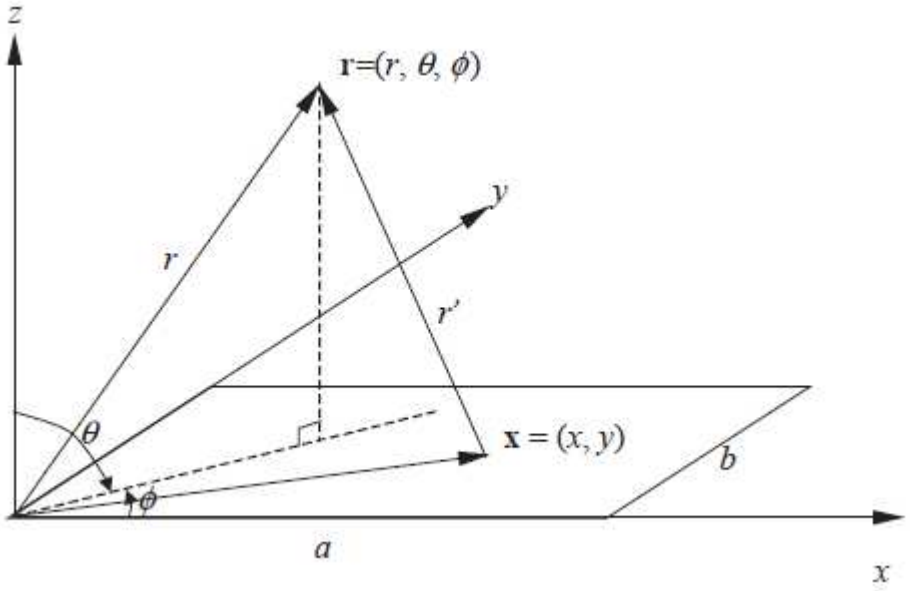

Figure 3.1: Co-ordinate system of a vibrating rectangular plate.

$$p(r) = \sum_{m=1}^{+\infty} \sum_{n=1}^{+\infty} u_{mn} A_{mn} \tag{3.4}$$

where $r = (r, \theta, \phi)$ is the the location is space expressed in spherical co-ordinates and the term A_{mn} is given by

$$A_{mn} = \frac{jk\rho c}{2\pi} \int_S s_{mn}(x) \frac{e^{-jkr'}}{r'} dx \tag{3.5}$$

where ϕ_{mn} is the (m,n)-th mode shape. From Wallace [4], the term in brackets A_{mn} is given, when the plate is fully simply-supported by:

$$A_{mn}(r) = jk\rho c \frac{e^{-jkr}}{2\pi} \frac{ab}{\pi^2 mn} \left[\frac{(-1)^m e^{j\alpha} - 1}{(\alpha/(m\pi))^2 - 1} \right] \left[\frac{(-1)^n e^{j\beta} - 1}{(\beta/(n\pi))^2 - 1} \right] \tag{3.6}$$

Substituting equation (3.5) into equation (3.2) the total radiated power of the plate can be written as:

$$W = \sum_{m=1}^{+\infty} \sum_{n=1}^{+\infty} \sum_{m'=1}^{+\infty} \sum_{n'=1}^{+\infty} \left[u_{mn} u_{mn}^* \int_0^{2\pi} \int_0^{\pi/2} \frac{A_{mn} A_{mn}^*}{2\rho c} \, r^2 \sin\theta \; d\theta \; d\phi \right] \tag{3.7}$$

3.1.2 Response to point force

Consider a point force applied on the plate at the location (x_0, y_0). The modal velocity amplitude is given by:

$$u_{mn} = \frac{j\omega F s_{mn}(x_0, y_0)}{\left[\omega_{mn}^2(1 + j\eta) - \omega^2\right] M_{mn}} \tag{3.8}$$

where F is the force amplitude, ω_{mn} is the natural frequency, η is the damping loss factor, assuming hysteretic damping, and M_{mn} is given by

$$M_{mn} = \int_0^a \int_0^b \rho h s_{mn}^2 \, dxdy \tag{3.9}$$

The modal velocity amplitude given in (3.8) is substituted in equation (3.7), obtaining the acoustic power. Thus, the velocity in mode (m,n) is given by:

$$v_{mn} = u_{mn}\phi_{mn} \tag{3.10}$$

The total velocity $v(x)$ is given by superposing the modal contributions from each structural mode of structural vibration of the plate as:

$$v(x) = \sum_{m=1}^{\infty}\sum_{n=1}^{\infty} u_{mn}\phi_{mn} = \sum_{m=1}^{\infty}\sum_{n=1}^{\infty} v_{mn}(x) \tag{3.11}$$

Finally the spatially averaged mean square velocity of the plate is given by the expression:

$$\overline{\langle v^2 \rangle} = \frac{1}{S}\int_S \overline{v^2} dx_0 dy_0 \tag{3.12}$$

where the notation $\langle v \rangle$ means the spatially averaged operation and $\overline{v}^2$ is the mean square value of the velocity. Values obtained in equations (3.7) and (3.12) are substituted in equation (3.1) in order to obtain the radiation efficiency of the structure under a force point.

3.1.3 Average over forcing points

For the purpose of obtaining a general result for the total radiated power, the average of all possible locations of the uncorrelated point forces on the plate is considered. In this case $\overline{|u_{mn}|^2}$ represents the modulus square of the modal velocity amplitude u_{mn} averaged over all positions and it is given by the expression:

$$\overline{|u_{mn}|^2} = \frac{1}{ab}\int_0^a \int_0^b u_{mn}u_{mn}^* = \frac{4\omega^2|F|^2}{M^2\left[\left(\omega_{mn}^2 - \omega\right)^2 + \eta^2\omega_{mn}^4\right]} \tag{3.13}$$

The averaged radiated power can be written as:

$$\overline{W} = \sum_{m=1}^{+\infty}\sum_{n=1}^{+\infty}\overline{W_{mn}} \tag{3.14}$$

where $\overline{W_{mn}}$ is given by:

$$\overline{W_{mn}} = \overline{|u_{mn}|^2}\int_0^{2\pi}\int_0^{\pi/2} \frac{A_{mn}(r)A_{mn}^*(r)}{2\rho c} r^2 \sin\theta \; d\theta \; d\phi \tag{3.15}$$

The spatially averaged mean square velocity in mode (m,n) averaged over all possible force positions is given by

$$\overline{\overline{\langle v_{mn}^2 \rangle}} = \frac{1}{S}\int_S \overline{\langle v_{mn}^2 \rangle} \; dx_0 \; dy_0 \tag{3.16}$$

where v_{mn} is the velocity in mode (m, n) given in equation (3.10).

The modal radiation efficiency σ_{mn} is hence given by:

$$\overline{\sigma_{mn}} = \frac{\overline{W_{mn}}}{\rho c a b \overline{\langle \overline{v_{mn}^2} \rangle}} \tag{3.17}$$

Having obtained the total radiated power in terms of summation of modal radiated power, the average radiation efficiency considering all possible point force locations is given by:

$$\overline{\sigma} = \frac{\sum_{m=1}^{+\infty} \sum_{n=1}^{+\infty} \overline{\sigma_{mn}} \overline{\langle \overline{v_{mn}^2} \rangle}}{\overline{\langle \overline{v^2} \rangle}} = \frac{\sum_{m=1}^{+\infty} \sum_{n=1}^{+\infty} \overline{W_{mn}}}{\rho c a b \overline{\langle \overline{v^2} \rangle}} \tag{3.18}$$

where $\overline{\langle \overline{v^2} \rangle}$ is the spatially averaged mean square velocity averaged over all possible force locations:

$$\overline{\langle \overline{v^2} \rangle} = \sum_{m=1}^{+\infty} \sum_{n=1}^{+\infty} \overline{\langle \overline{v_{mn}^2} \rangle} \tag{3.19}$$

3.1.4 Numerical model

A Matlab code has been developed in order to obtain the radiation efficiency of an isotropic plate under several boundary conditions. The integrals have been calculated by using a trapezoidal numerical integration method as follows: Consider a function $f(x, y)$, where $y \in [0, b]$ and $x \in [0, a]$ and the double integral

$$\int_0^a \int_0^b f(x, y) dx dy \tag{3.20}$$

Consider now the first integral $\int_0^b f(x, y) dx dy$. Taking a discretization in direction y as Figure 3.2 shows, it can be calculated as a summatory:

$$\begin{aligned} \int_0^b f(x, y) dx dy &= \sum_{j=2}^{N-1} f(x, y_j) dx \Delta y + f(x, y_1) dx \frac{\Delta y}{2} + f(x, y_N) dx \frac{\Delta y}{2} = \\ &= \frac{\Delta y}{2} \left\{ 2 \sum_{j=2}^{N-1} f(x, y_j) + f(x, y_1) + f(x, y_N) \right\} dx = g(x) dx \end{aligned} \tag{3.21}$$

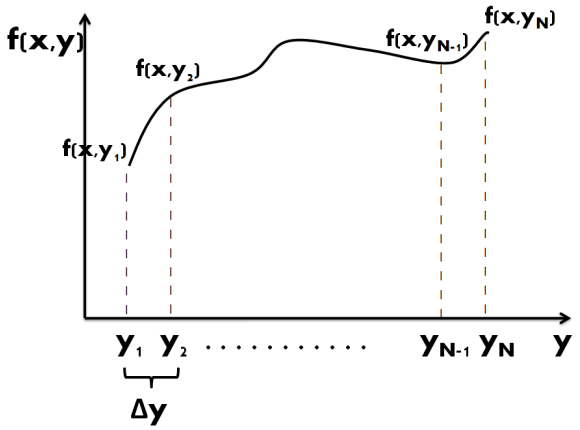

Figure 3.2: Discretization in direction y.

Consider now the second integral $\int_0^a g(x) dx$. Discretizing in direction x as Figure 3.3 shows, it can also be calculated as a summatory.

$$\int_0^a g(x)dx = \frac{\Delta x}{2}\left\{2\sum_{i=2}^{M-1} g(x_i) + g(x_1) + g(x_M)\right\} \tag{3.22}$$

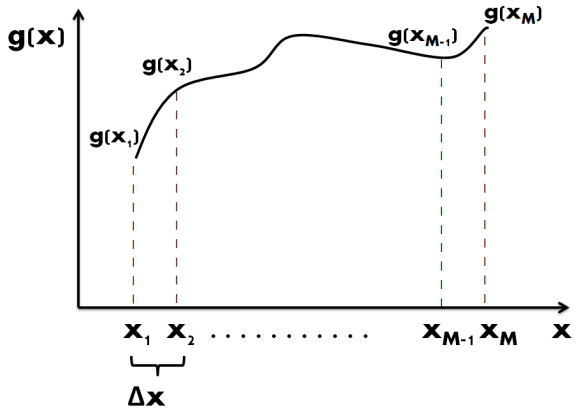

Figure 3.3: Discretization in direction x.

In conclusion, equation (3.22) gives the relation:

$$\int_0^a \int_0^b f(x,y)dxdy = \frac{\Delta x}{2}\frac{\Delta y}{2}\sum_{i=1}^{M}\sum_{j=1}^{N} a_{mn} f(x_i, y_j) \tag{3.23}$$

where a_{mn} takes the value:

$$a_{mn} = \begin{cases} 1 & if \quad i = j = 1, i = M \text{ and } j = N, i = 1 \text{ and } j = N \text{ or } i = M \text{ and } j = 1 \\ 2 & if \quad i \in [2, M-1] \text{ and } j = 1, N \text{ or } i = 1, M \text{ and } j \in [2, N-1] \\ 4 & if \quad i \in [2, M-1] \text{ and } j \in [2, N-1] \end{cases} \tag{3.24}$$

The numerical procedure adopted in Matlab is the following: two vectors containing the values of the trapezoidal coefficients have been created. Their multiplication gives the values of a_{mn}.

$$\begin{array}{ll} k = [1\ 2\ 2 \ldots 2\ 2\ 1] & size(k) = 1xM \\ v = [1\ 2\ 2 \ldots 2\ 2\ 1] & size(v) = 1xN \end{array} \tag{3.25}$$

Finally the integral is calculated as:

$$\int_0^a \int_0^b f(x,y)dxdy = \frac{1}{4}\sum_{i=1}^{M}\sum_{j=1}^{N}(v_j * f(x_i, y_j)) * k_i \ \Delta x \Delta y \tag{3.26}$$

and in matrix form:

$$\int_0^a \int_0^b f(x,y)dxdy = \underline{v}\,[f]\,\underline{k}^T \frac{\Delta x \Delta y}{4} \tag{3.27}$$

3.2 Boundary element Method

The acoustic pressure in the far-field can be calculated also using a Boundary Elements Method. Few programmes are available in market and they are frequently used in noise reduction problems. When dealing with a BEM approach to simulate an acoustic problem, one must know that the computational calculation is usually very long and that a good equipment is required. IN this work, the results of BEM are a very helpful tool in order to validate the analytical results.

3.2.1 Introduction

Over recent decades, the boundary element method (BEM) has received much attention from researchers (see [16]) and has become an important technique in the computational solution of a number of physical problems. It is essentially a method for solving partial differential equations (PDEs) and can only be employed when the physical problem can be expressed as such. As with the other methods as Finite Element Method (FEM) and Finite Difference Method (FDM), the boundary element method is a numerical method and hence it is an important subject of research amongst the numerical analysis community. The boundary element method has found application in such diverse topics as stress analysis, potential flow, fracture mechanics and acoustics (the subject of this work). An acoustic field can exist in a fluid domain such as air. The linear wave equation is an acceptable model and it is used in cases in which the air is the propagation media. BEM has received attention from engineers who are interested in applications such as the sound output of a loudspeaker, the noise from a radiating source such as an engine and the interior acoustic modes of an enclosure such as a vehicle interior. The method is equally applicable in underwater acoustics and can be used to model the scattering effect of an obstruction in the ocean or to determine the acoustic field surrounding a sonar transducer.

The Boundary Element Method is based on the following integral equation, known as Kirchoff-Helmholtz's equation:

$$p(\overline{r}) = \int_S [(p(\overline{r_0}) grad G_\omega(\overline{r}, \overline{r_0}) + j\omega\rho_0 G_w(\overline{r}, \overline{r_0})\overline{u}(\overline{r_0})) \cdot \overline{n}] dS, \qquad p(\overline{r}) = p(\overline{r}) e^{j\omega t} \tag{3.28}$$

where $p(\overline{r})$ is the sound pressure in a generic point of fluid media at a distance r, and $\overline{u}(\overline{r_0})$ is the body surface's velocity.

Kirchoff-Helmholtz's equation expresses the relation between the pressure field in the fluid media that surrounds a body and the surface's harmonic motion (with frequency ω) of the same. Due tuo the fact that in many physical situations the acoustic field is periodic, the linear wave equation has the outcome of reducing the wave equation to a sequence of Helmholtz equations by a Fourier decomposition with one Helmholtz equation for each sample frequency. In equation (3.28) this dependence on the frequency ω is also considered.

In equation (3.28), $G_w(\overline{r}, \overline{r_0})$ is known as Green's function, and represents the wave's solution in terms of Frequency Response Function (FRF) between the emitting source P and the receiver R, both punctual and at a distance r (see Figure 3.4). Green's function is the fundamental solution of the wave's equation of the sound pressure corresponding to punctual source that emits a mono-harmonic signal in an open field. Its expression is:

$$G_w(\overline{r}, \overline{r_0}) = \frac{e^{-jkr}}{4\pi r} \; r = |\overline{r} - \overline{r_0}| \tag{3.29}$$

Then, once the geometry, the surface's sound pressure $p(\overline{r_0})$ and the normal velocity in the surface of the emitting body are known, integrating along the surface S and using the Green's function $G_w(\overline{r}, \overline{r_0})$, the sound pressure $p(\overline{r})$ can be calculated in every point R of the fluid that surrounds the body.

Equation (3.28) represents then the acoustic field generated from the surface's harmonic motion of a body, as a superposition of the single acoustic fields generated from punctual sources, continuously distributed along its surface.

In real cases, the equation of reference is Kirchoff-Helmholtz's equation, and it is not possible to give an analytical solution of the problem of the acoustic field generated by the vibration of the body's surface. The fact that the acoustic field of a single source depends on the internal geometry if the body and the presence of other bodies rises up the complexity of the problem. It is necessary then a numerical procedure. BEM algorithms allow one to give a numerical solution.

3.2.2 Formulation

BEM's formulation is divided in two steps. The first step consists in considering that the receiver R is in the surface of the vibrating body. In this case, Kirchoff-Helmholtz's equation is called boundary integral equation, and expresses the relation between the sound pressure in all surface's points and the sound pressure of the point R (also in the surface). Surface's velocity is known. Once the sound pressure and the normal velocity of the surface are known, using equation (3.28), it is possible to calculate the

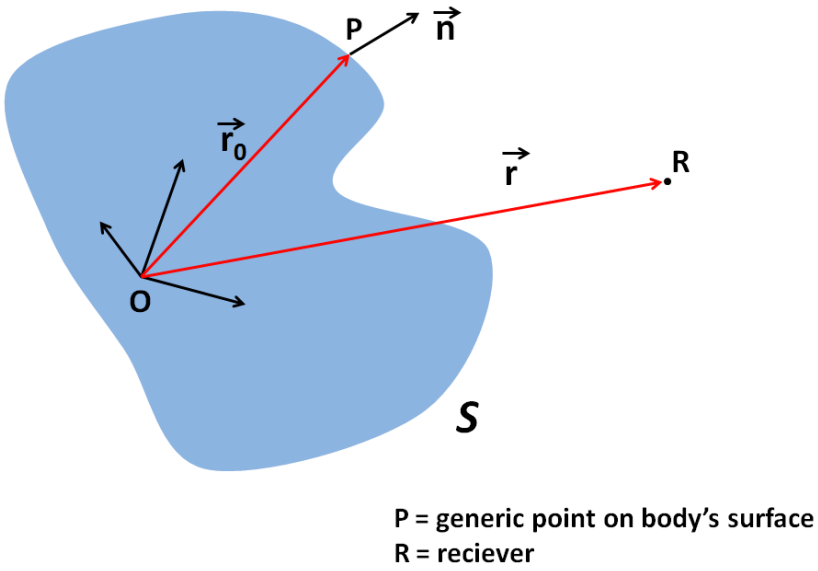

Figure 3.4: Body-space scheme.

acoustic field in every fluid media point. For the following subsections, figures will be referred to specific case of study, that is, a rectangular plate.

First step

For a generic boundary point k appertaining to the body's surface, as Figure (3.5) shows, the acoustic pressure can be calculated using the Kirchoff-Helmholtz's equation, substituting r for r_k obtaining the boundary integral equation that follows:

$$p(\overline{r_k}) = \int_S [(p(\overline{r_{xy}}) grad G_\omega(\overline{r_k}, \overline{r_{xy}}) + j\omega\rho_0 G_w(\overline{r_k}, \overline{r_{xy}})\overline{u}(\overline{r_{xy}})) \cdot \overline{n}] dS, \qquad p(\overline{r}) = p(\overline{r}) e^{j\omega t} \tag{3.30}$$

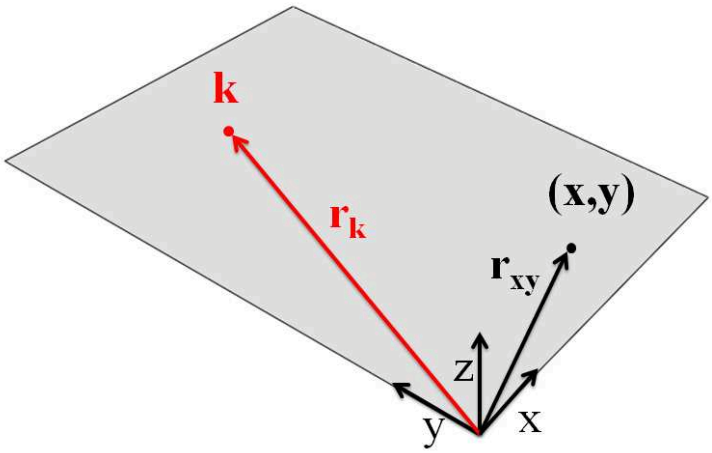

Figure 3.5: Plate's surface.

in this case, Green's expression is:

$$G_w(\overline{r_k}, \overline{r_x y}) = \frac{e^{-jkr'}}{4\pi r'} \qquad where\ r' = |\overline{r_k} - \overline{r_{xy}}| \tag{3.31}$$

After discretizing the surface into different elements N_{el}, as shown in Figure 3.6 the sound pressure p of the generic point (x, y), appertaining to the element i, can be expressed as a linear combination of the pressure on the nodes of the element i using the form functions f_i. Thus the pressure in the point (x, y) is given by the following relation:

$$p = \underline{f_i}^T \ \underline{p_i} \tag{3.32}$$

and so does the velocity

$$v_n = \underline{f_i}^T \ \underline{v_{ni}} \tag{3.33}$$

Substituting equations (3.32) and (3.33) in equation (3.30) one obtains:

$$p(\overline{r_k}) = \sum_{i=1}^{N_{el}} \underline{f_i}^T \underline{p_i} \ gradG_\omega(\overline{r_k}, \overline{r_{xy}})\Delta x_i \Delta y_i + \sum_{i=1}^{N_{el}} j\omega\rho_0 G_w(\overline{r_k}, \overline{r_{xy}}) \underline{f_i}^T \underline{v_{ni}} \Delta x_i \Delta y_i \tag{3.34}$$

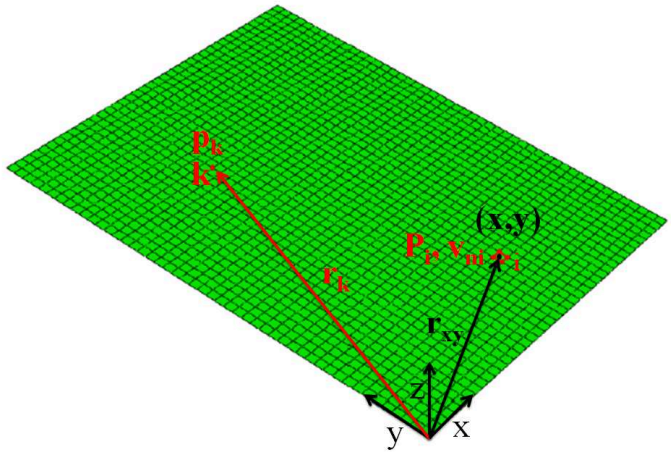

Figure 3.6: Plate's surface mesh.

Evaluating the sound pressure in a point k that coincides with a mesh point, one obtains the equation:

$$p_k = \sum_{i=1}^{N_{el}} \underline{d_i} \ \underline{p_i} + \sum_{i=1}^{N_{el}} \underline{e_i} \ \underline{v_{ni}} \tag{3.35}$$

where

$$\underline{d_i} = \underline{f_i}^T \ gradG_\omega(\overline{r_k}, \overline{r_{xy}})\Delta x_i \Delta y_i \tag{3.36}$$

$$\underline{e_i} = j\omega\rho_0 G_w(\overline{r_k}, \overline{r_{xy}}) \underline{f_i}^T \Delta x_i \Delta y_i \tag{3.37}$$

After some manipulations, equation (3.35) can be expressed as:

$$p_k = \underline{d_s}^T \underline{p_s} + \underline{e_s}^T \underline{v_{ns}} \tag{3.38}$$

where $\underline{d_s}$ and $\underline{e_s}$ are of the form:

$$\underline{d_s} = [d_1 \ d_2 \ ... \ d_{Nnode}] \tag{3.39}$$

$$\underline{e_s} = [e_1 \ e_2 \ ... \ e_{Nnode}] \tag{3.40}$$

$$\underline{p_s} = [p_1 \ p_2 \ ... \ p_{Nnode}]^T \tag{3.41}$$

$$\underline{v_{ns}} = [v_{n1} \ v_{n2} \ ... \ v_{n \ Nnode}]^T \tag{3.42}$$

Considering all nodes in the surface:

$$\underline{p_s} = [D_s]\underline{p_s} + [E_s]\underline{v_{ns}} \tag{3.43}$$

where matrix $[D_s]$ and $[E_s]$ are sparse and their dimensions are $N_{node} \ x \ N_{node}$.

The solution of equation (3.43) is:

$$\underline{p_s} = \left[([I] - [D_s])^{-1} [E_s] \right] \underline{v_{ns}} = [B]\underline{v_{ns}} \tag{3.44}$$

where

$$[B] = \left[([I] - [D_s])^{-1} [E_s] \right] \tag{3.45}$$

Equation (3.44) gives the sound pressure at the surface of the vibrating body.

Second step

As introduced before, once the sound pressure and the normal velocity at the surface are known, the sound pressure in the fluid media can be calculated using Kirchoff-Helmholtz's equation (equation (3.28)). Considering one point in the fluid media, as shown in Figure (3.7), and operating as in the first step, one arrives to the expression:

$$p_f = \underline{d_f}^T \underline{p_s} + \underline{e_f}^T \underline{v_{ns}} \tag{3.46}$$

Substituting equation(3.44) in equation(3.46) one obtains the expression of the sound pressure in the field:

$$p_f = \underline{d_f}^T [B] \underline{v_{ns}} + \underline{e_f}^T \underline{v_{ns}} = \left(\underline{d_f}^T [B] + \underline{e_f}^T \right) \underline{v_{ns}} \tag{3.47}$$

It is important to remark that the pressure p_f is calculated for a concrete frequency ω (matrix $\underline{d_f}, \underline{e_f}$ and $[B]$ depend on the Green's function).

3.2.3 Virtual Lab implementation

Virtual Lab (LMS) is a powerful program that includes a BEM acoustic part that allows one to predict and improve the sound and noise performance of a broad range of systems. With straightforward models and embedded solver technology, engineers can acquire results faster without compromising accuracy. Virtual Lab is based on the Acoustic Transfer Vector concept (ATV).

ATV is defined as an acoustic Input-Output relation. This concept is based on the fact that at the heart of classical acoustics is the hypothesis of linearity. Both the governing equation of time-domain acoustics, the wave equation, and the governing equation of frequency-domain acoustics, the Helmholtz equation, are obtained by the linearisation of the fundamental mass and momentum equations under the assumption of small pressure perturbations. Since every acoustic system can hence be considered as a linear system, one can establish a linear input-output relationship between the *input* of an acoustic system, mechanical surface vibrations that generate sound waves, and the *output* of an acoustic system, the sound pressure at a number of locations in space. If the vibrating surfaces are subdivided into a finite number of discrete vibration panels, this relationship can be expressed in the form of the following matrix equation:

$$p_f = [ATV(\omega)]^T \ \underline{v_{ns}}(\omega) \tag{3.48}$$

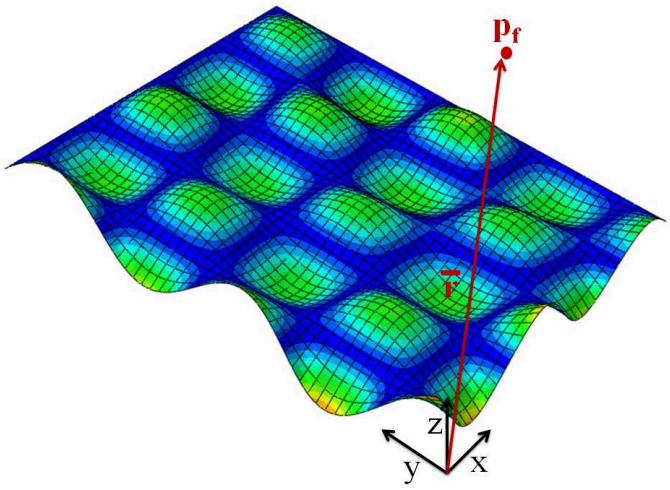

Figure 3.7: Field point pressure calculation.

where p_f is a column vector containing the sound pressures at the different locations, v_{ns} is a column vector containing the structural velocities of the vibrating panels and $[ATV]$ is the system matrix relating input and outputs.

Therefore, the Acoustic Transfer Vector concept (abbreviated to ATV) is nothing else than an ensemble of Acoustic Transfer Functions relating the normal vibration velocities of a number of discrete panels to the sound pressure at a single microphone location.

An Acoustic Transfer Vector is completely determined by the characteristics of the acoustic system under consideration and therefore only depends on the following system parameters:

- Geometry of the vibrating surfaces
- Acoustic treatment of the surfaces, i.e. absorption linings represented by impedance or admittance boundary conditions
- Microphone (field point) location
- Frequency
- Physical properties of the acoustic medium (speed of sound and density)

This immediately points to a fundamental ATV property: independence of operational structural response. The acoustic response is found simply as the matrix product of the ATVs with the operational structural response, which allows the same set of ATVs to be re-used to compute and compare acoustic performance for many different situations:

- Effect of structural modifications without changes to the actual surface geometry (e.g. adding internal stiffening ribs).
- Performance for different sets of operational conditions.

If one compares equation (3.48) with equation (3.47), finds the following relation between ATVs and BEM formulation presented before:

$$[ATV(\omega)]^T = [D_f][B] + [E_f] = [D_f]\left[([I] - [D_s])^{-1}[E_s]\right] + [E_f] \tag{3.49}$$

Virtual Lab allows one to obtain a direct input-output relation between the structural modal response vector and the field point sound pressures. In many cases, as in case of study, the structural response of a

mechanical object to a set of excitations will be computed using a modal representation. The structural displacements at a given excitation frequency are expressed as a linear combination of the structural modal vectors of the vibrating structure and so does the velocity. This relation is summarized in the following expression:

$$\underline{v_{ns}} = [\phi_m]\dot{q} = j\omega[\phi_m]q \tag{3.50}$$

where $v_{ns}(\omega)$ is the normal velocity of the surface, $[\phi_m]$ is the structural modes matrix whose columns are the structural modal vectors and q is the column vector containing the modal response vector of the structural model (modal coordinates).

Combining equations (3.50) and (3.48) one obtains:

$$p_f = [ATV(\omega)]^T \; j\omega[\phi_m]q \tag{3.51}$$

A direct input-output relation between the structural modal response vector and the field point sound pressures is found collecting terms in equation (3.51) in the following form:

$$p_f = [MATV(\omega)]^T q \tag{3.52}$$

where the Modal Acoustic Transfer Vector (abbreviated to MATV) is defined as:

$$[MATV(\omega)]^T = [ATV(\omega)]^T \; j\omega[\phi_m] \tag{3.53}$$

and can be interpreted as an ensemble of Acoustic Transfer Functions relating the contribution of the individual structural modes to the sound pressure at a single microphone location.

In equations (3.50), (3.51) and (3.52), q is a vector of the modal coordinates, whose expression depends on the treatment of the damping.

In cases in which the damping is considered proportional, the governing equations of motion (Lagrange equation) can be written in matrix form as:

$$[M]\ddot{q} + [R]\dot{q} + [K]q = F \tag{3.54}$$

and the modal coordinates can be obtained as follows:

$$q_i = \frac{[\phi]_i^T F}{-\omega^2 m_i + 2r_i\omega + k_i} \qquad (i = 1, ..., N_{modes}) \tag{3.55}$$

On the other hand, when the structural damping is considered hysteretic, the Lagrange equation is:

$$[M]\ddot{q} + [K + jD]q = F \tag{3.56}$$

and the the modal coordinates are obtained as:

$$q_i = \frac{[\phi]_i^T F}{-\omega^2 m_i + k_i + jd_i} \qquad (i = 1, ..., N_{modes}) \tag{3.57}$$

3.3 Results

3.3.1 Radiation efficiency for a flat plate under several boundary condition combination: radiation efficiency curve

Once for a given case the mode shapes have been calculated, one can proceed to calculate the radiation efficiency. A Matlab code has been written using the methodology presented in the first part of this chapter. In Figure 3.8 an example of the output of the code developed is presented. The thick black line represents the radiation efficiency calculated adding up the contribution of each mode (σ_{mn}) which is depicted by the thin grey line. The frequency range considered is 10 Hz - 10 KHz.

The typical performance of the average radiation efficiency is the next: at low frequencies the first mode determines the overall result until a frequency which is between the first and second natural frequency. This is due to the dominance of this mode in the response and its high value of σ_{mn}. Above this frequency the average result drops, only rising its maximum near from the critical frequency, whose

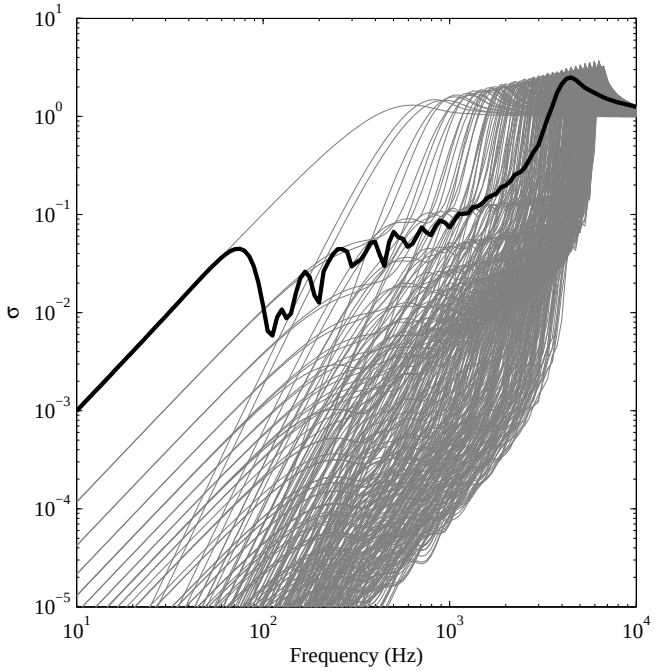

Figure 3.8: Radiation efficiency for a simply supported flat plate, the contribution of each mode is represented by the thin grey lines.

expression is given in equation (3.58) and whose value is about 4 KHz for the case of study. Above the critical frequency, after reaching its maximum value, the radiation efficiency curve tends to one. In the mid-frequency range the interaction between the modes results in several deeps and peaks.

$$f_c = \frac{c^2}{2\pi}\sqrt{\frac{\rho h}{D}} \tag{3.58}$$

where D is the bending stiffness of the plate.

A reading of the Appendix A is asked to the reader in order make easier the understanding of the next paragraph.

Taking the performance of the average radiation efficiency of a simply supported plate as an example of output, the behaviour of the average radiation efficiency can be explained as follows:

- At low frequencies, the plate behaves as a pulsating sphere (monopole) whose volume is equal to the plate's one. The modal radiation efficiency of the first mode of the plate is equivalent to the radiation efficiency of a monopole. In fact, if one considers a source consisting on a vibrating sphere whose velocity in the surface is $V_m(\omega) = Ve^{-j\omega t}$, where V is the amplitude of the velocity in the surface, the strength of the source is the product of the velocity and the surface:

$$Q = SV_m(\omega) = SVe^{-j\omega t} = 4\pi a^2 Ve^{-j\omega t} \tag{3.59}$$

  where a is the radius of the sphere. The acoustic power is given by the expression:

$$W = \frac{Q_{rms}^2 k^2 \rho c}{4\pi(1+(ka)^2)} \qquad Q_{rms}^2 = \frac{Q_p^2}{2} \tag{3.60}$$

  In equation (3.59), ρ is the air density, c is the sound speed sound in air and k is the acoustic wavenumber ($k = \frac{\omega}{c}$). Substituting equation (3.59) in equation (3.60) one obtains:

$$W = \frac{\left(4\pi a^2 V^2\right) k^2 \rho c}{8\pi(1+(ka)^2)} \tag{3.61}$$

Remembering the expression of the radiation efficiency:

$$\sigma = \frac{W}{\rho c S \left\langle \overline{v^2} \right\rangle} \qquad \left\langle \overline{v^2} \right\rangle = \frac{V^2}{2} \tag{3.62}$$

Substituting in equation (3.62) the expression of the acoustic power obtained in equation (3.61), one obtains the the expression of the radiation efficiency of a monopole:

$$\sigma = \frac{4^2\pi^2 a^2 V^2 k^2 \rho c}{8\pi 4\pi^2 a^2 \rho c \frac{V^2}{2}(1+(ka)^2)} = \frac{k^2 a^2}{1+k^2 a^2} \tag{3.63}$$

- In the mid-frequency range, also known as known as short-circuiting region, depending on the the mode, the modal radiation efficiencies behave as monopoles, dipoles or quadrupoles. A dipole source consists in two monopole sources vibrating in opposite phase separated by a distance d. On the other hand, a quadrupole source is the result of the superposition of two dipole sources or four monopoles sources forming a rectangle. The expressions of the radiation efficiency of a dipole and a quadrupole sources are given reference [17] and their expressions are found to be proportional to a power of ka. These are written in equations (3.65) and (3.65) respectively, where a is the equivalent radius of the sphere.

$$\sigma_{dipole} \propto \frac{(ka)^4}{1+(ka)^4} \tag{3.64}$$

$$\sigma_{quadrupole} \propto \frac{(ka)^6}{1+(ka)^6} \tag{3.65}$$

In this frequency range the contribution to the acoustic emission depends on the shape of the mode. In some modes only the corners of the plate contribute to the acoustic emission and are called corner modes; in some others, only the edges contribute to the acoustic emission. These latter are called edge modes. In Figures 3.9 - 3.11, some examples of modes who behave as monopoles, dipoles and quadrupoles are shown. For example in Figure 3.9 the second mde shape is shown. It corresponds to an edge edge mode and its acoustic behaviour is the same as a dipole. In Figure 3.10 the fourth mode shape is shown. It corresponds to corner mode and its acoustic behaviour is the same as a quadrupole. Another example illustrated in Figure 3.11, where the fifth mode is shown. It corresponds to an edge mode and its acoustic behaviour is the same as a monopole.

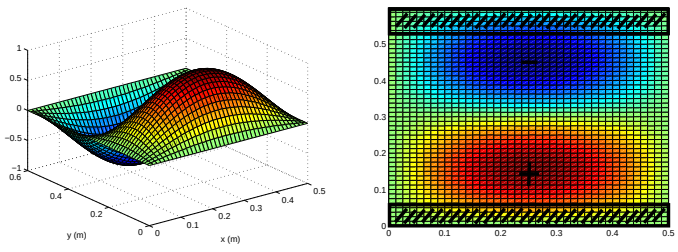

(a) (b)

Figure 3.9: Second mode shape of plate SS-SS-SS-SS.

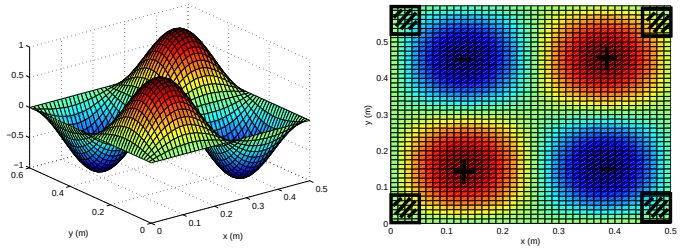

(a) (b)

Figure 3.10: Fourth mode shape of a plate SS-SS-SS-SS.

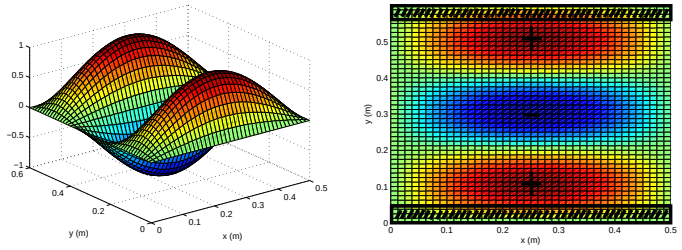

(a) (b)

Figure 3.11: Fifth mode shape of a plate SS-SS-SS-SS.

- After the critical frequency the vibration of the whole plate contributes to the acoustic emission and and modes whose frequency is inside this range are called surface modes. The estimation of the radiation efficiency above the critical frequency is given in equation (3.66).

$$\sigma = \frac{1}{\sqrt{1 - \frac{f_c}{f}}} \tag{3.66}$$

In Figure 3.12, using the expressions given in equations (3.63), (3.65) and (3.65) it is demonstrated that the modal radiation efficiency of the first mode is equivalent to the radiation efficiency of a pulsating sphere whose volume is equal to the plate's one and that the modal radiation efficiencies associated to the second and fourth modes are equivalent to a dipole and quadrupole.

Table 3.1 summarizes the behaviour of the first ten modal radiation efficiencies:

Mode (m,n)	Equivalent elementary source
1 (2,2)	monopole
2(2,3)	dipole
3(3,2)	dipole
4(3,3)	quadrupole
5(2,4)	monopole
6(4,2)	monopole
7(4,4)	dipole
8(4,3)	dipole
9(2,5)	dipole
10(3,5)	quadrupole

Table 3.1: Equivalence between a plate mode and an elementary curve.

Finally in Figure 3.13 it is shown the three different regions in which the performance of the average

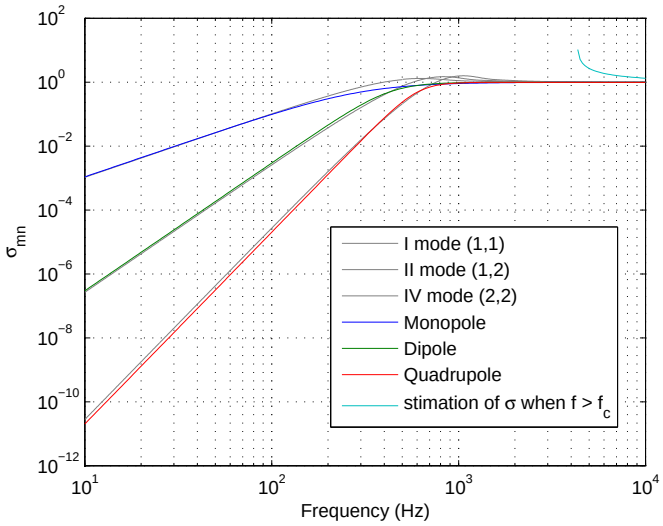

Figure 3.12: Comparison between first, second and fourth modal radiation efficiencies and elementary sources.

radiation efficiency is divided. In the first region the plate behaves as a monopole due to its dependence on the modal radiation efficiency of the first mode, whose natural frequency is f_1. In the second region, called short-circuiting region, the average radiation efficiency results in several deeps and peaks due to the interaction between the corner and edge modes. In the third region, after reaching its maximum value near from the critical frequency, the curve tends to one.

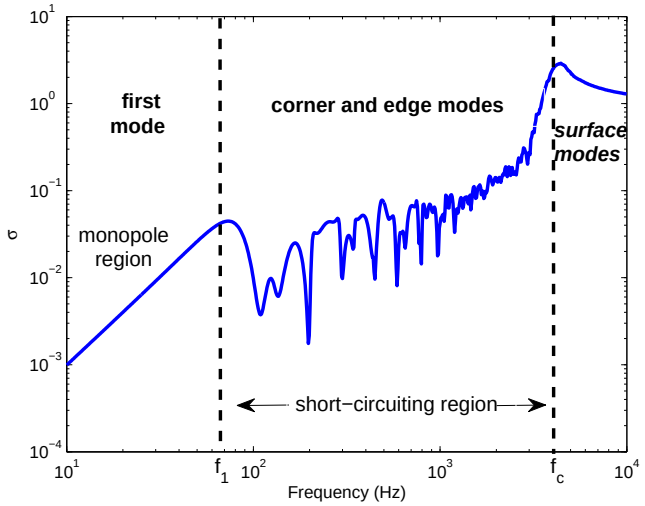

Figure 3.13: Typical radiation efficiency performance.

All the considerations presented in this part are also valid for any boundary conditions.

Frequency discretization

In order to get exactly the fluctuations in the mid-frequency range, attention must be paid in the frequency resolution. In particular it has been observed that the fluctuation amplitude increases while the damping decreases and moreover it can be observed that close to the critical frequency the curve tends to become smoother. Therefore it can be concluded that in the mid-frequency region three points per half power bandwidth should be guaranteed while in the neighbourhood of the critical frequency

the resolution should be enough to get the correct shape for the radiation efficiency curve. The number of frequency lines deeply affect the computation time but the lack of points in the frequency resolution raises doubts on the reliability of the results. In order to guarantee three points per half power bandwidth the number of points per decade can be calculated as follows:

$$\frac{\Delta f_{hp}}{f_0} = 2\eta = \frac{f_{i+1} - f_{i-1}}{f_i} = 10^{1/n_{pt}} - 10^{-1/n_{pt}} \tag{3.67}$$

where the subscripts *hp* and *pt* stand respectively for the half power bandwidth frequency spacing and for the number of points per decade.

Acoustic data

After all these considerations, acoustic data taken for different cases are written in Tables 3.2, 3.3 and 3.4.

Magnitude	air density	sound speed in air (c)
Value	1.2 (kg/m^3)	343 (m/s)

Table 3.2: Air properties.

	Number of points per decade	
Frequency range	10-100 Hz	100-10000 Hz
Value	almost 40	almost 80

Table 3.3: Number of points per decade.

	Space discretization	
Magnitude	θ	ϕ
Range	$[0, \pi/2]$	$[0, 2\pi]$
Number of points	almost 60	almost 120

Table 3.4: Space discretization.

In order to make a good estimation of radiation efficiency fluctuations in the mid-frequency range, the number of points per decade considered in this range is bigger the the first one.

Finally, the radius of the sphere, where the total acoustic power radiated is calculated, takes a constant value of 10000 m (far field) for all cases. The value of the damping loss factor η will be discussed in the following subsection.

3.3.2 Damping effect

The methodology adopted for the radiation efficiency calculation allows one to investigate the effect of damping. It is known that considering an undamped plate the radiation efficiency should be lower than in the corresponding damped ones. A damping value which guarantee the independence of the radiation efficiency from the damping contribution has been quantified. At this purpose the calculations for a flat plate are performed setting the following four damping loss factor values: 0.3, 0.1, 0.03 and 0.01. It has been observed that the difference in terms of radiation efficiency between a plate having a damping loss factor equal to 0.03 and 0.01 is very low and consequently it can be said that 0.01 is the damping loss factor value which makes the radiation efficiency independent from the damping itself. This is the reason why in the following sections the calculations are carried out considering this damping value. The calculation with variable damping were performed for a plate in two different configurations: the first case considered is the one simply supported along the four edges, the latter fully clamped. In this manner it is

possible to verify what Leppington supposed about the difference of 3 dB in terms of radiation efficiency between the two cases. The radiation efficiency is calculated according to the calculation summarized in section 2 and the results are presented in the following Figures considering also the damping effect. In Figure 3.14 the radiation efficiency of the simply supported plate is depicted considering four different damping levels. It can be noticed that between the results obtained having $\eta = 0.03$ and $\eta = 0.01$ the difference is very low. This suggests that a loss factor equal to 0.01 guarantees an independence of the radiation efficiency from the damping contribution. The vibration modes obtained for the clamped boundary conditions are used to compute the radiation efficiency of the same plate with the same four damping values. The results are summarized in Figure 3.15. The difference between the clamped and simply supported boundary condition is presented in Figure 3.16 in a third octave band resolution. The fact that the spectra obtained in this Figure for $\eta = 0.03$ and $\eta = 0.01$ are nearly coincident confirms the negligible contribution of a low damping on the radiation efficiency.

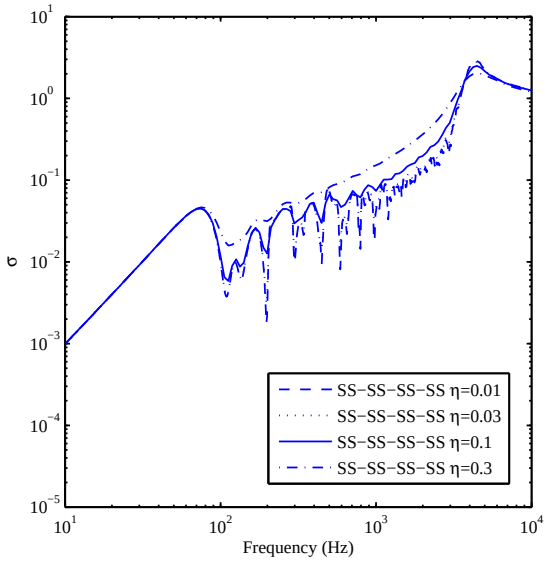

Figure 3.14: Simply supported plate; damping effect.

3.3.3 Results for different boundary condition combinations

The radiation efficiency for different boundary conditions is shown. In Figures 3.17 - 3.26, the left subfigure represents the spatially averaged mean square velocity, given in equation (3.12) and the spatially mean square velocity for each mode (equation (3.16)) for the rectangular plate with a unit force amplitude. Thus, the right subfigure represents the modal and average radiation efficiency of the above rectangular plate. The infinite number of modes are truncated to a finite number. In case of study only modes with natural frequencies below 10 KHz are included in the calculation.

The velocity Figures show the dominance of the first mode in the overall results. As explained before, the radiation efficiency of the first mode determines the overall result until a frequency which is between the first and second natural frequency. The F-F-F-F case is slightly different from the others because of the existence of three different rigid modes. In this case, even though the first rigid mode is dominant, the average radiation efficiency is slightly minor than σ_1.

The results obtained for the plate fully simply supported is made with some results in literature. Maidanik [3] produced formulae for the modal-average radiation of a lightly damped plate. These can be written as (see [18]) as in equation (3.68):

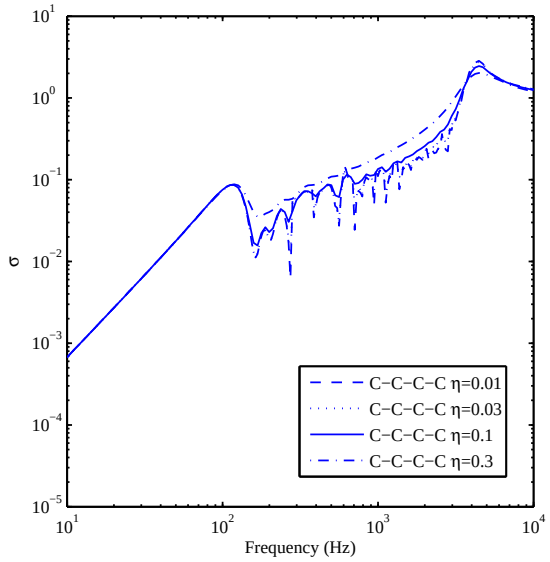

Figure 3.15: Clamped supported plate; damping effect.

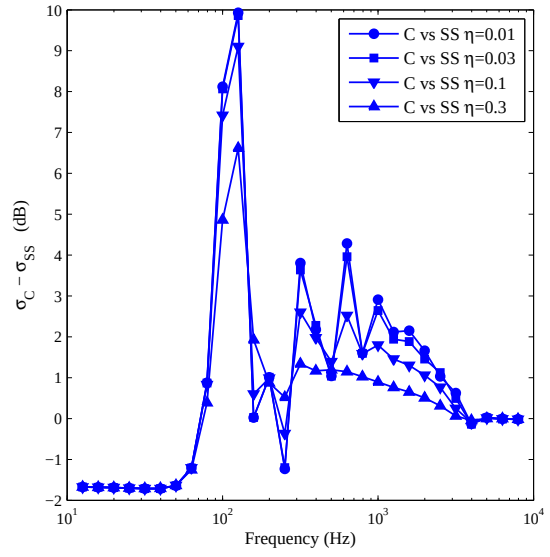

Figure 3.16: Comparison between fully clamped and fully simply supported boundary conditions in terms of third octave band; damping effect.

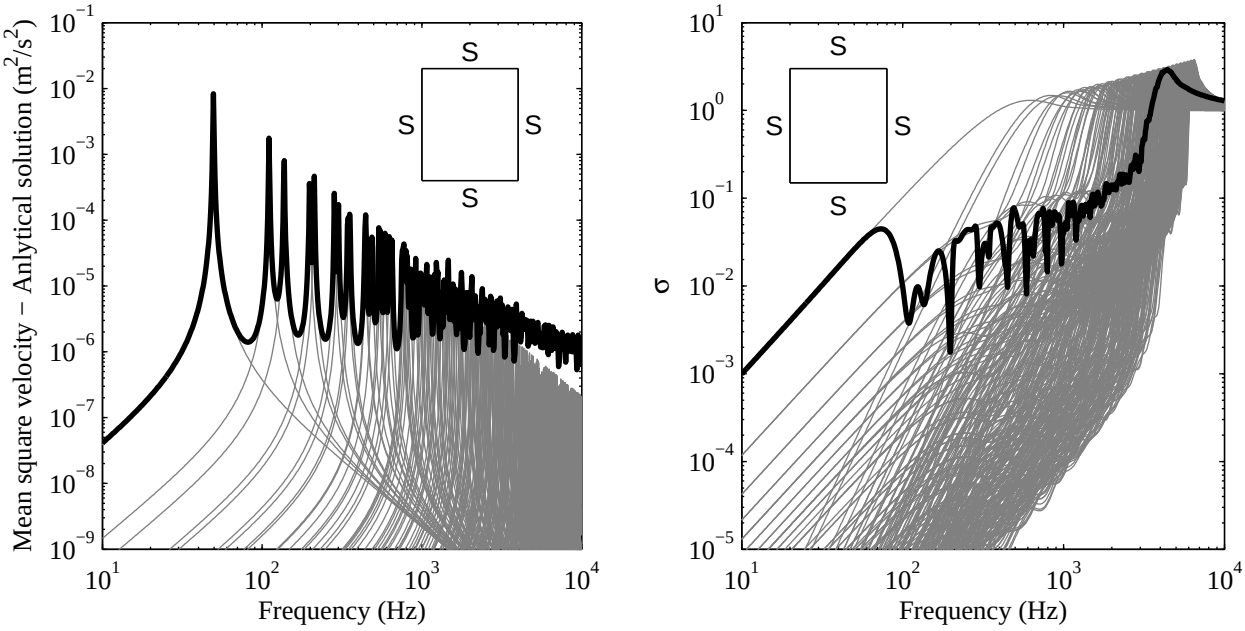

(a) *velocity* (b) *sigma*

Figure 3.17: Velocity and radiation efficiency for a plate SS-SS-SS-SS.

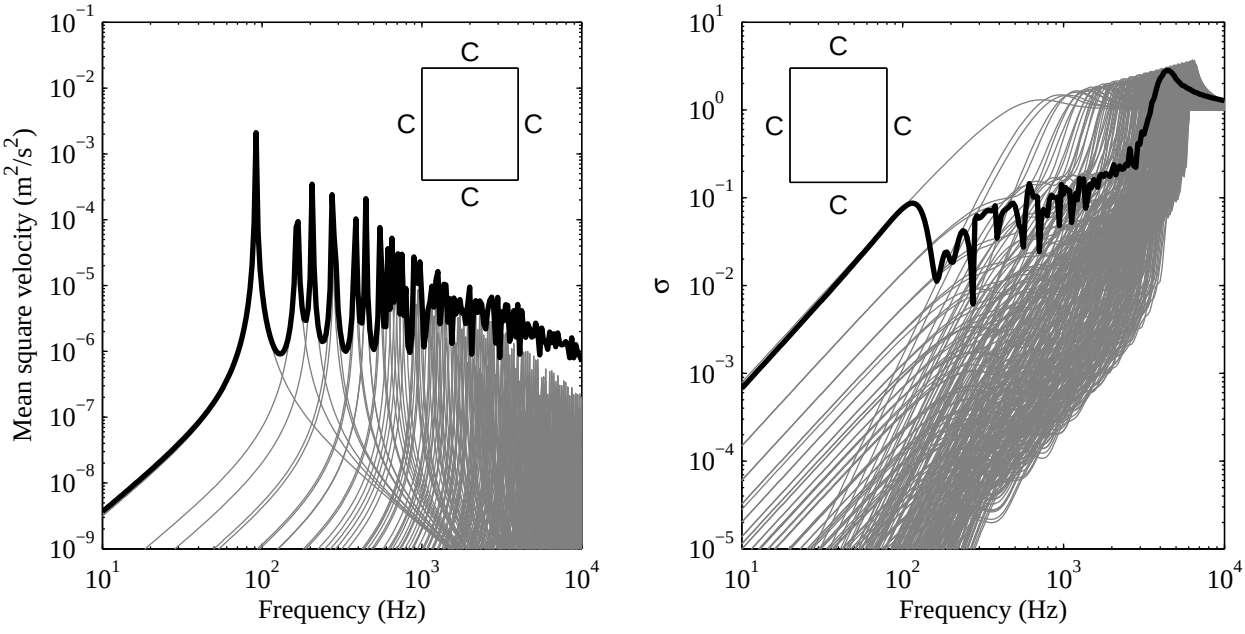

(a) *velocity* (b) *sigma*

Figure 3.18: Velocity and radiation efficiency for a plate C-C-C-C.

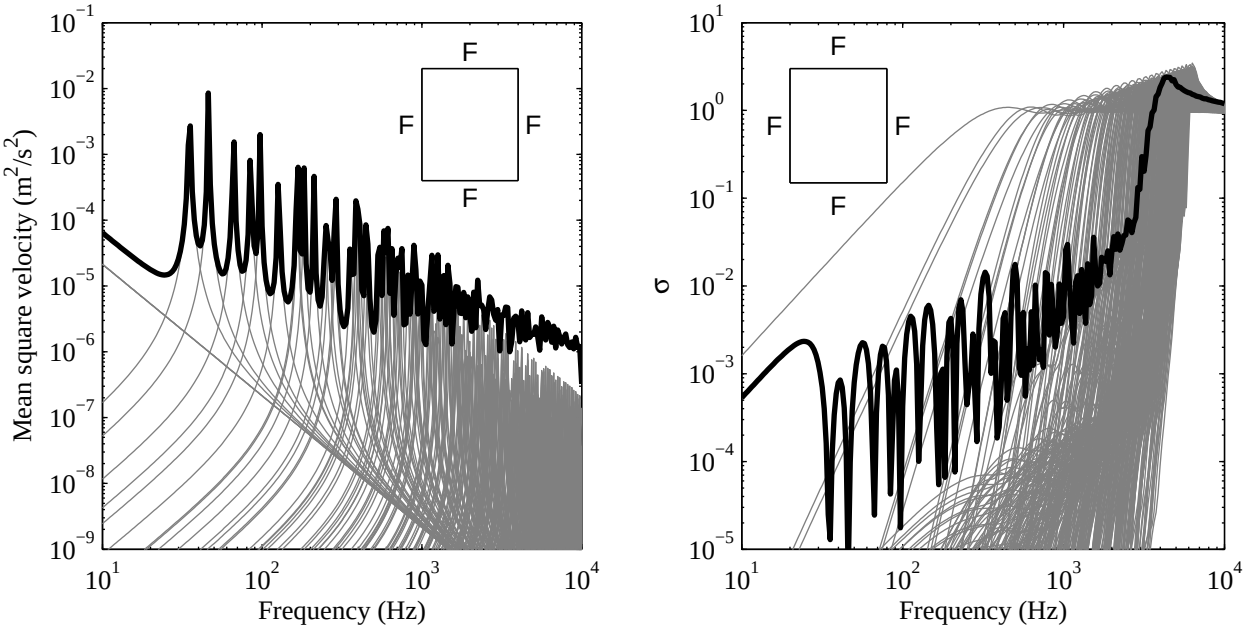

(a) *velocity* (b) *sigma*

Figure 3.19: Velocity and radiation efficiency for a plate F-F-F-F.

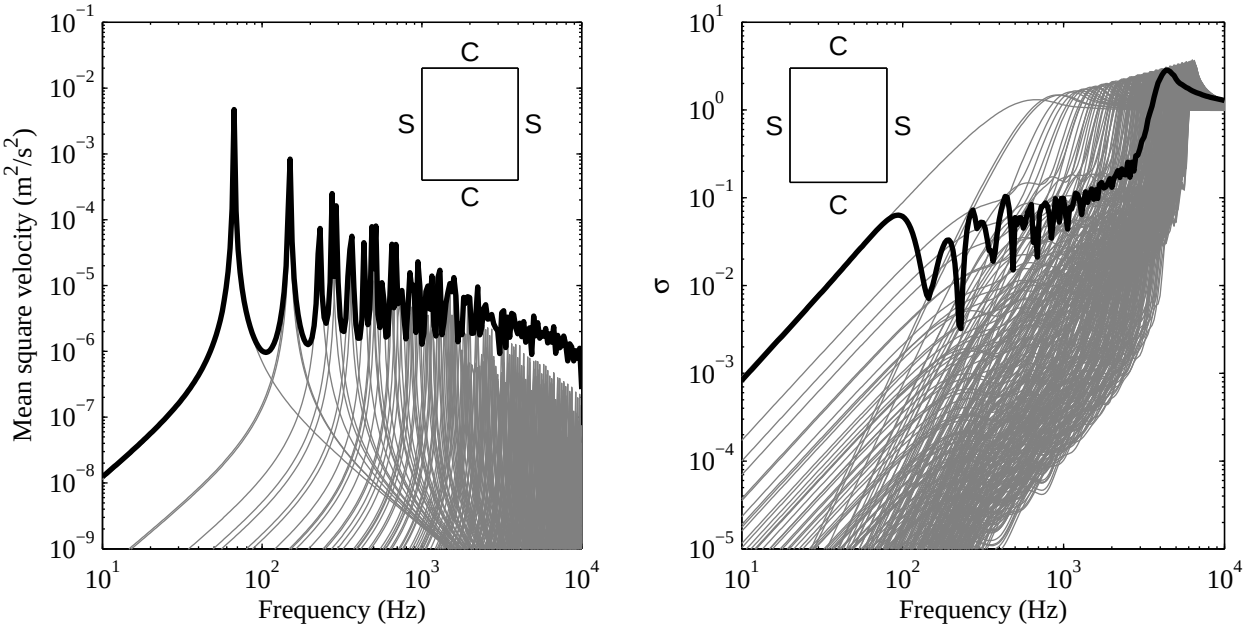

(a) *velocity* (b) *sigma*

Figure 3.20: Velocity and radiation efficiency for a plate SS-SS-C-C.

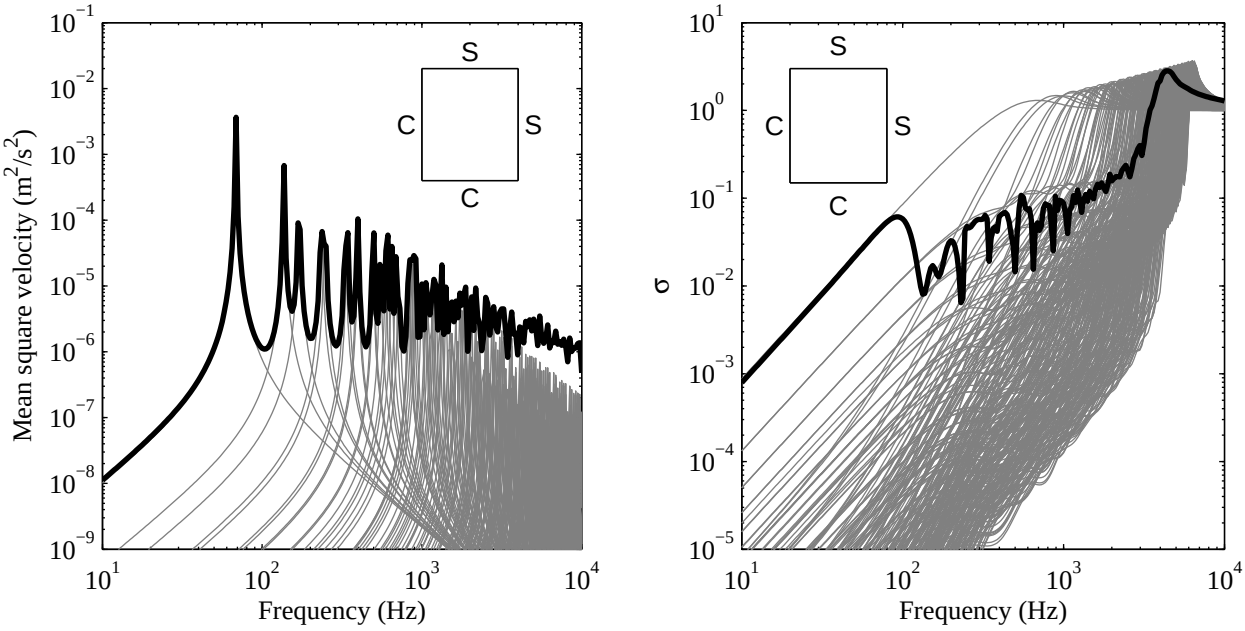

(a) *velocity* (b) *sigma*

Figure 3.21: Velocity and radiation efficiency for a plate C-SS-C-SS.

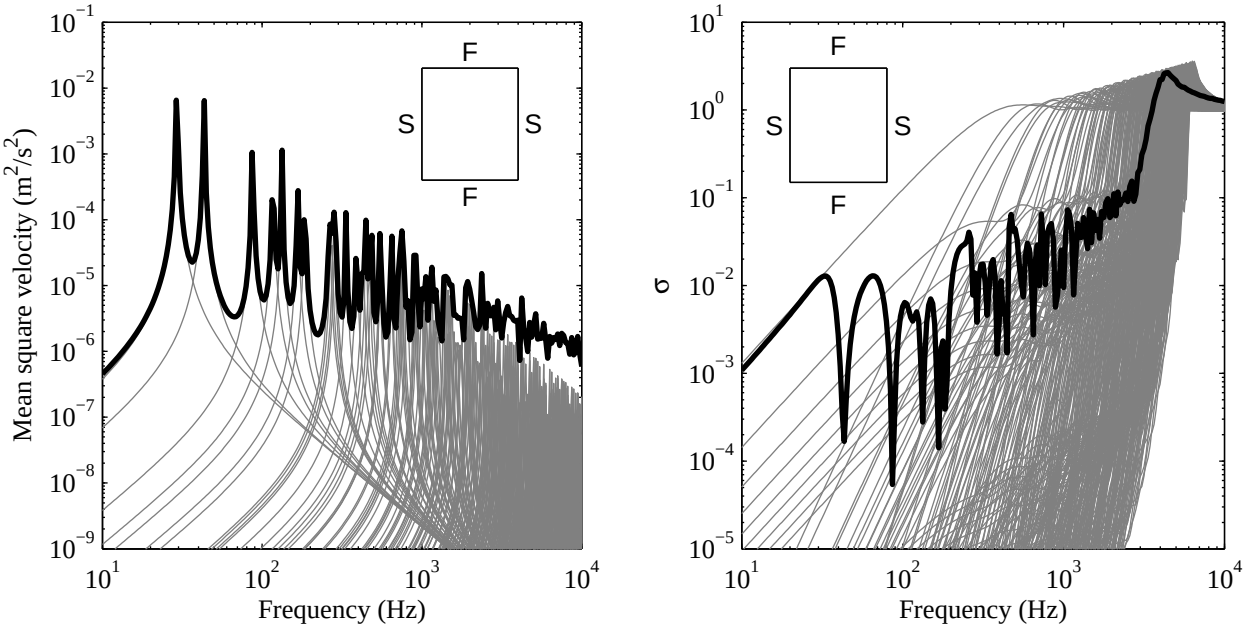

(a) *velocity* (b) *sigma*

Figure 3.22: Velocity and radiation efficiency for a plate SS-SS-F-F.

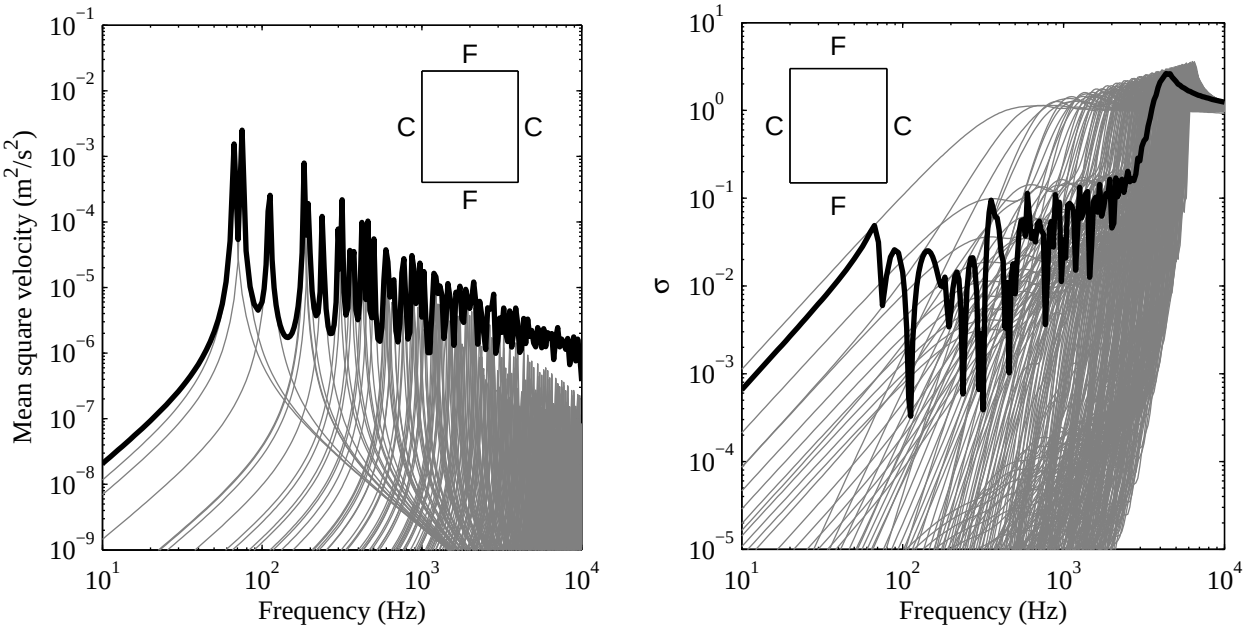

(a) *velocity* (b) *sigma*

Figure 3.23: Velocity and radiation efficiency for a plate C-C-F-F.

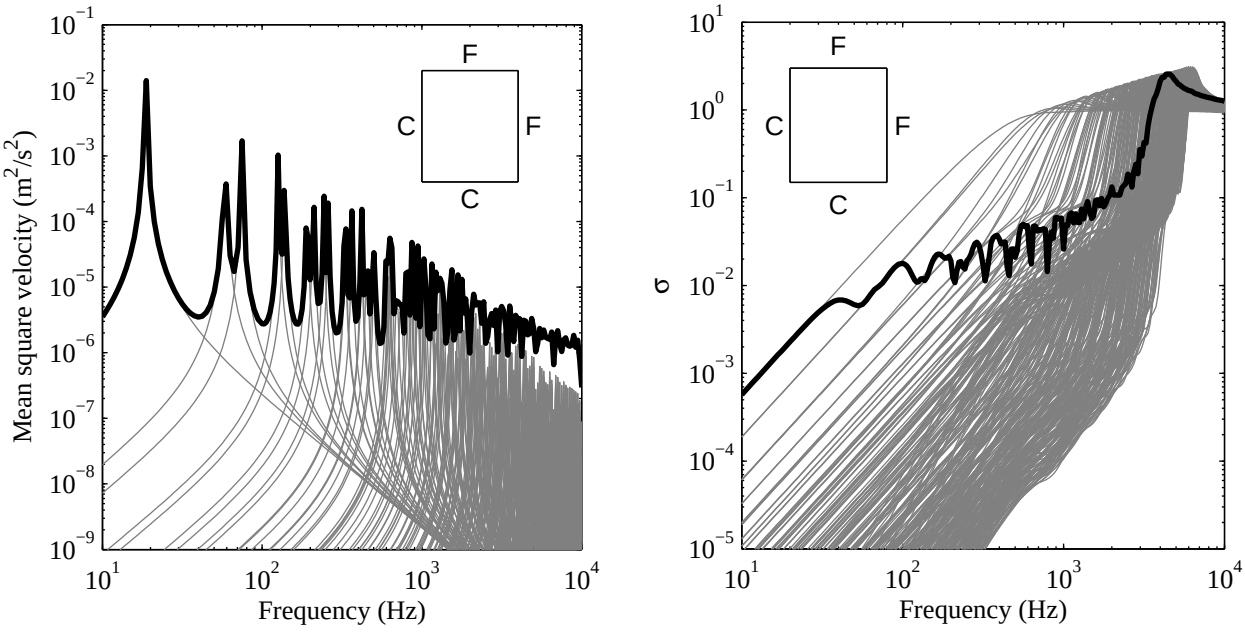

(a) *velocity* (b) *sigma*

Figure 3.24: Velocity and radiation efficiency for a plate C-F-C-F.

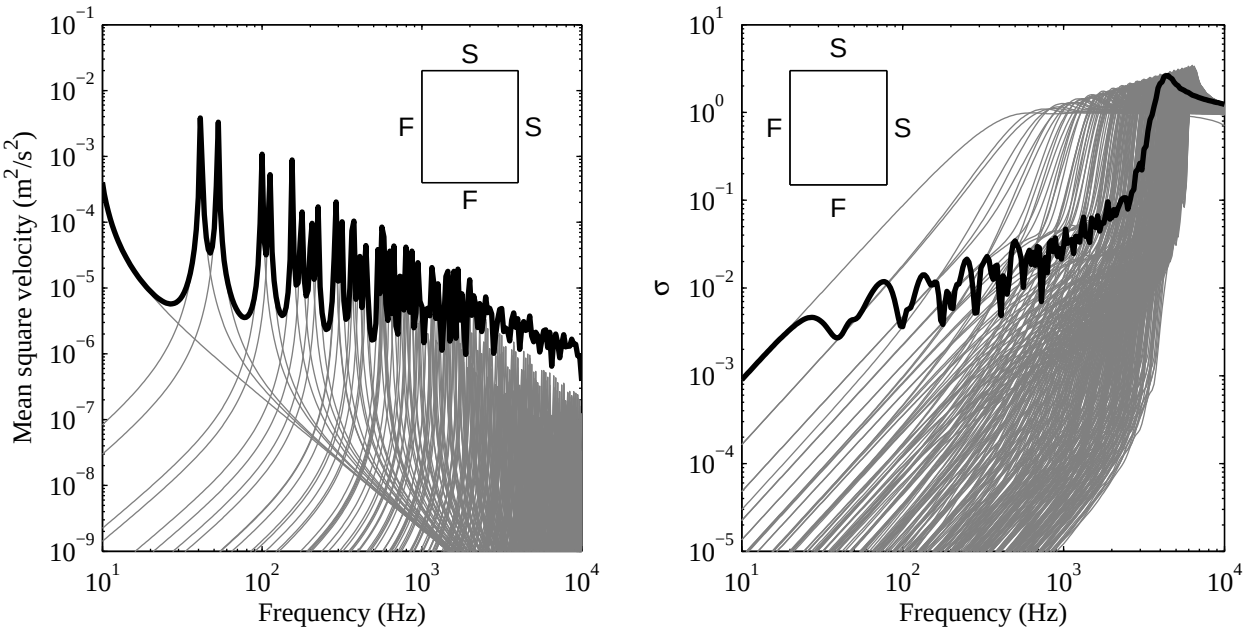

(a) *velocity* (b) *sigma*

Figure 3.25: Velocity and radiation efficiency for a plate F-SS-F-SS.

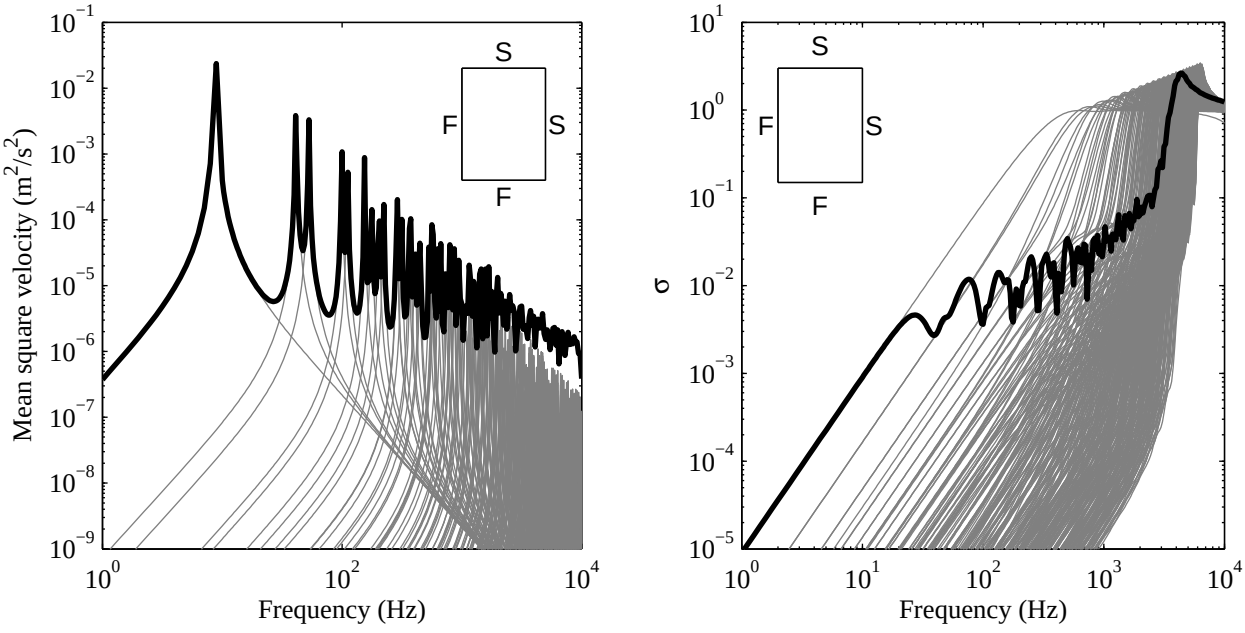

(a) *velocity* (b) *sigma*

Figure 3.26: Velocity and radiation efficiency for a plate F-SS-F-SS. The range of frequency considered is 1 Hz-10 KHz.

$$\sigma = \begin{cases} \frac{4S}{c^2} f^2 (monopole) & for f < f_{1,1} & f_{1,1} = \frac{\pi}{2}\left(\frac{1}{a^2} + \frac{1}{b^2}\right)\sqrt{\frac{D}{m''}} \\ \frac{4\pi^2}{c^2 S}\frac{D}{m''} & for f_{1,1} < f < f_e & f_e = \frac{3c}{P} \\ \frac{P_c}{4\pi^2 S f_c}\frac{(1-\alpha^2) ln\left(\frac{1+\alpha}{1-\alpha}\right)+2\alpha}{(1-\alpha^2)^{3/2}} & for f_e < f < f_c & \alpha = \sqrt{\frac{f}{f_c}} \\ 0.45\sqrt{\frac{P f_c}{c}} & Limit for f \approx f_c & f_c = \frac{c^2}{2\pi}\sqrt{\frac{m''}{D}} \\ (1 - f_c/f)^{-1/2} & for f > f_c & \end{cases} \tag{3.68}$$

where c is the speed of sound, m'' is the mass per unit area, $P = 2(a + b)$ is the perimeter of the plate, $S = ab$ is the area of the plate and D is the bending stiffness of the plate. Figure 3.27 shows a comparison between the results obtained in this works and the results obtained in Maidanik [3] and Xie [5]. The plate is considered simply supported. The subfigure above shows the comparison in the narrow band and the figure below shows the comparison in terms of third octave band. It can be seen that a good agreement between the results presented by Xie [5] and the results obtained in this work. Maidanik's formulae seems to be poor in the mid-frequency range.

In Figures 3.28 - 3.34, the subfigure above shows a comparison between the radiation efficiency of three different cases and the subfigure below represents the same comparison in terms of octave band.

As it can be seen in all Figures, the location of the first average radiation efficiency's peak is influenced by the value of the first natural frequency. The value of this peak increases as the value of the first natural frequency also does and it is located between the first and the second natural frequency value. For frequencies near and below the critical frequency, the value of the radiation efficiency is similar for all cases.

Figure 3.28 shows that for low frequencies (until 100 Hz approximately), the average radiation efficiency of a fully simply supported plate is slightly bigger than the fully clamped one, and much higher than the fully freely one. Clamped peak is the highest because of the value of its first natural frequency. In the mid-frequency range, clamped and simply supported radiation efficiency values are similar and higher than the freely case.

One can see easily the influence of different boundary conditions. A plate having two opposite clamped supported edges will have a higher radiation efficiency than the same plate having these edges simply supported. So does the frequency of the first peak. If these two opposite edges were freely supported, the radiation efficiency would be very low compared with the clamped and simply supported cases. The same results are obtained for a plate in which two adjacent edges have the same boundary condition. As it can be seen in Figures 3.28 and 3.34 the radiation efficiency of a plate in which two adjacent edges are clamped supported will always be higher than same plate having these edges simply or freely supported. When two adjacent edges are freely supported, the radiation efficiency decreases considerably.

Differences between cases are quantified in the next subsection.

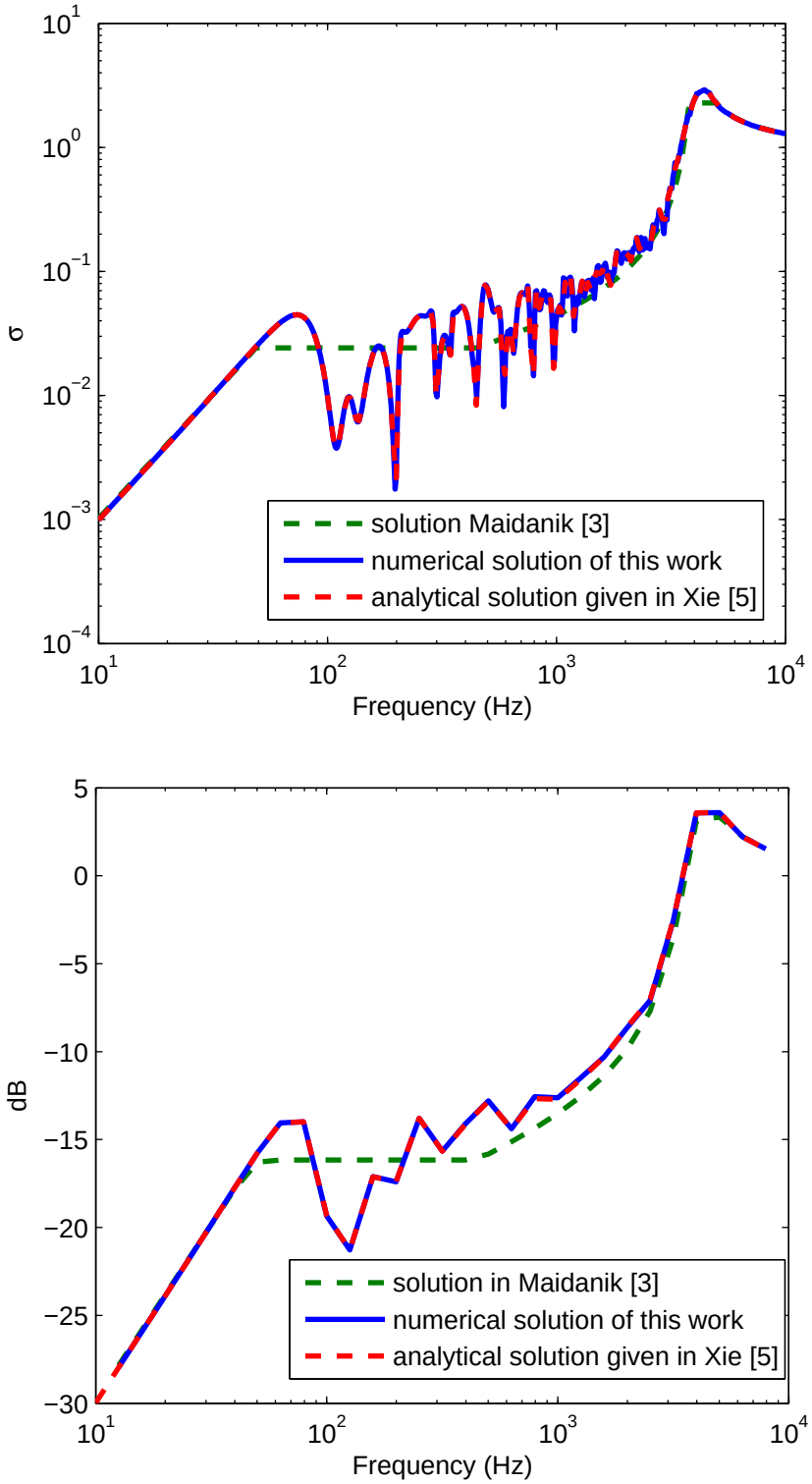

Figure 3.27: Comparison between Maidanik[5], Xie[1] and the numerical results in this work.

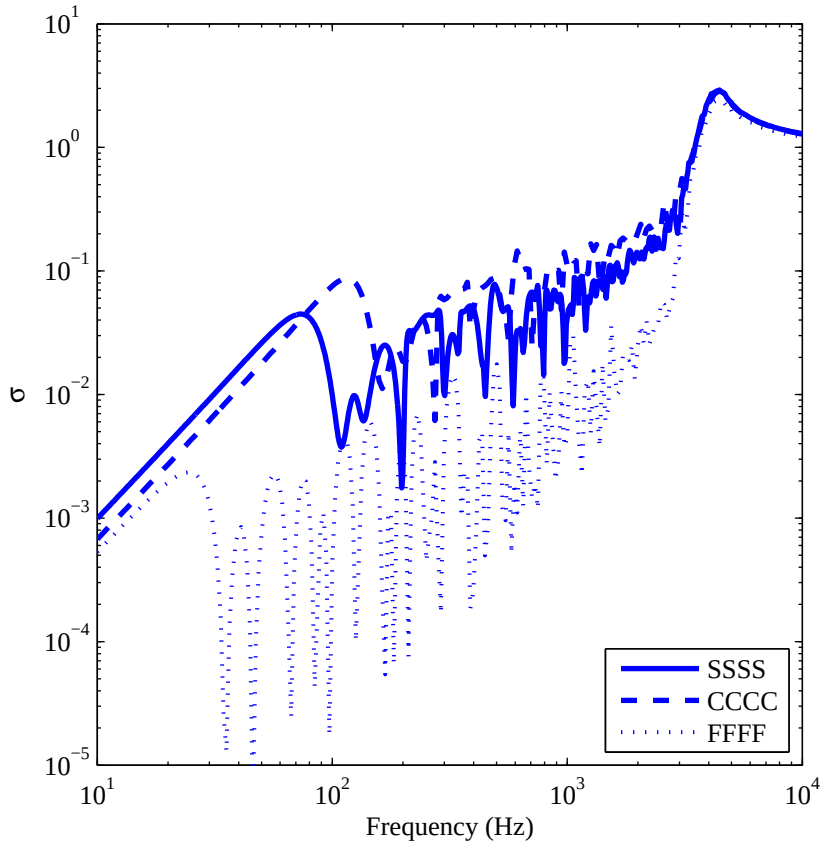

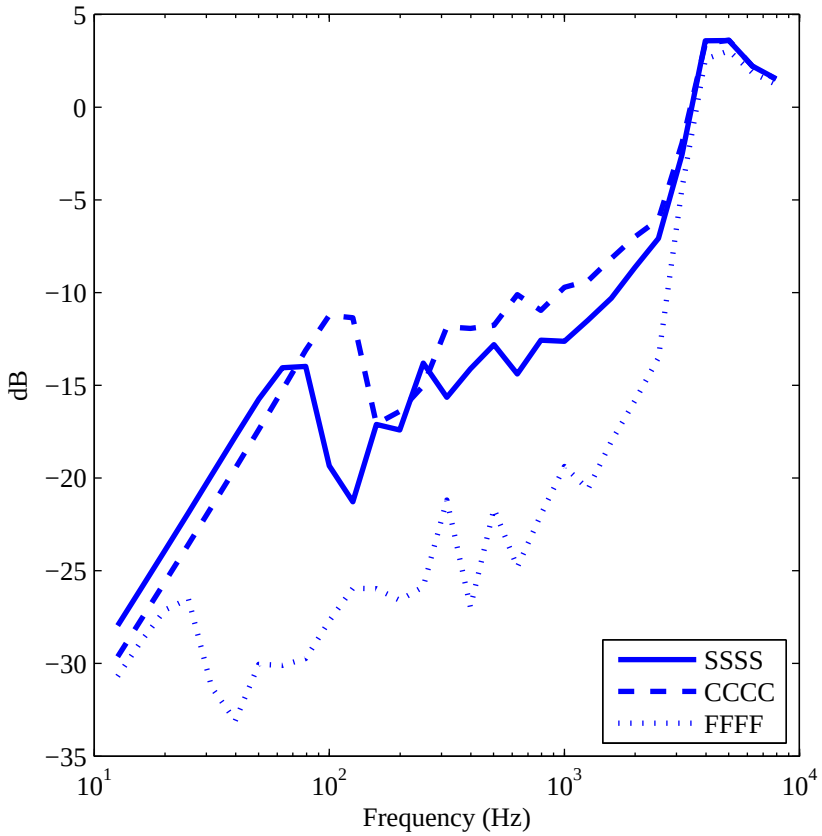

Figure 3.28: Radiation efficiency for SS-SS-SS-SS, CCCC and FFFF plate in third octave band.

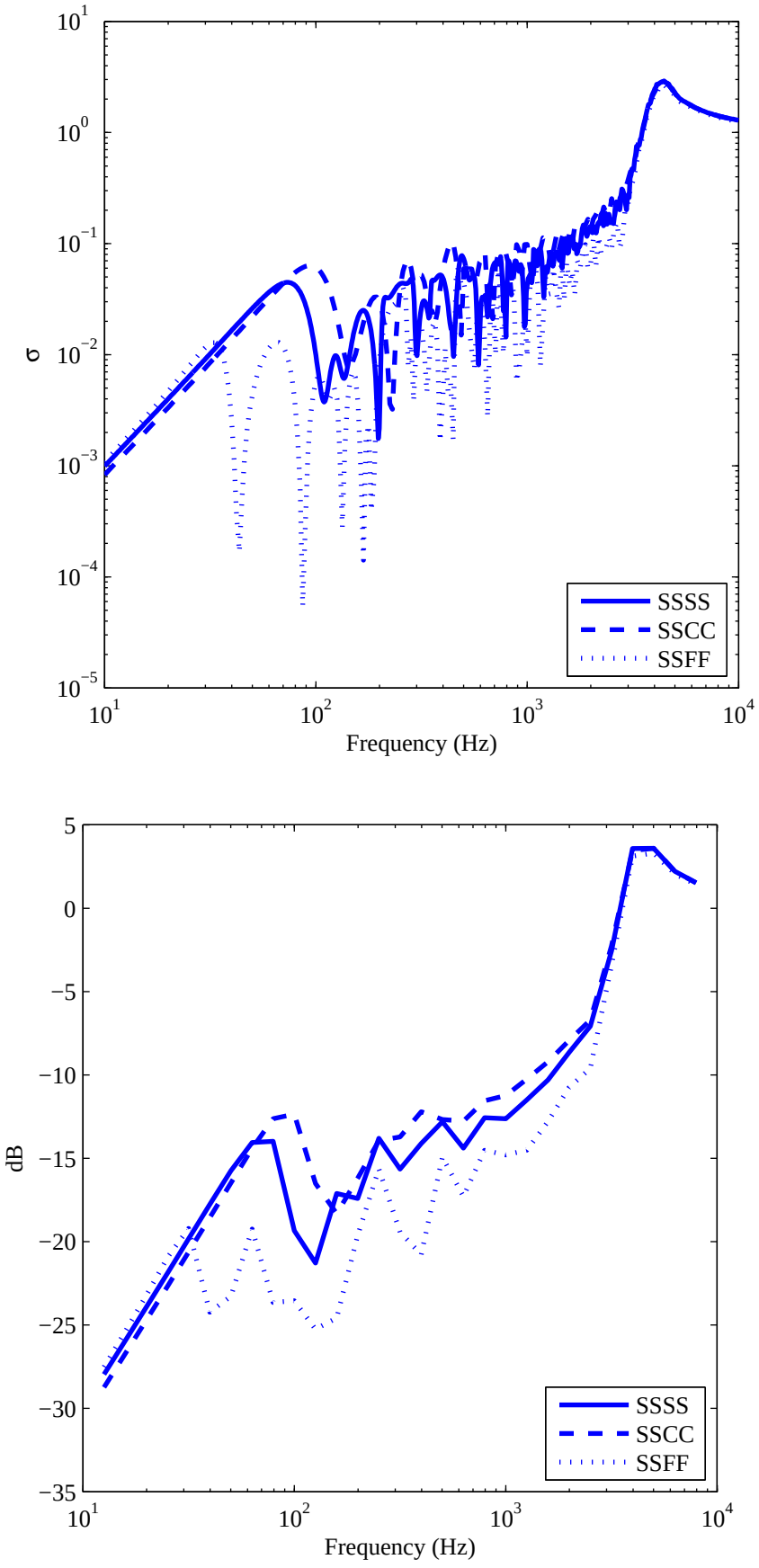

Figure 3.29: Radiation efficiency for SS-SS-SS-SS, SS-SS-C-C and SS-SS-F-F plate in third octave band.

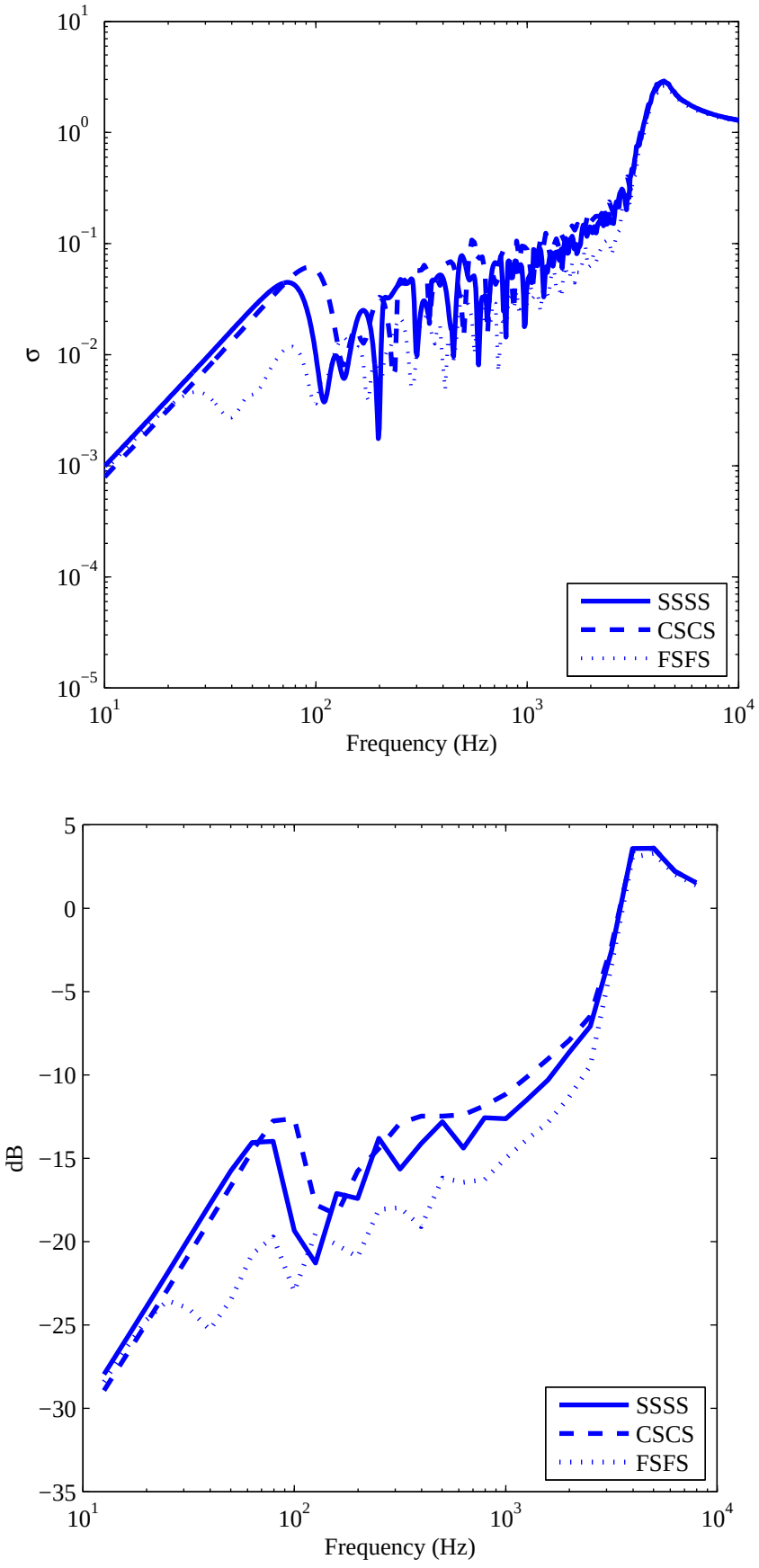

Figure 3.30: Radiation efficiency for SS-SS-SS-SS, C-SS-C-SS and F-SS-F-SS plate in third octave band.

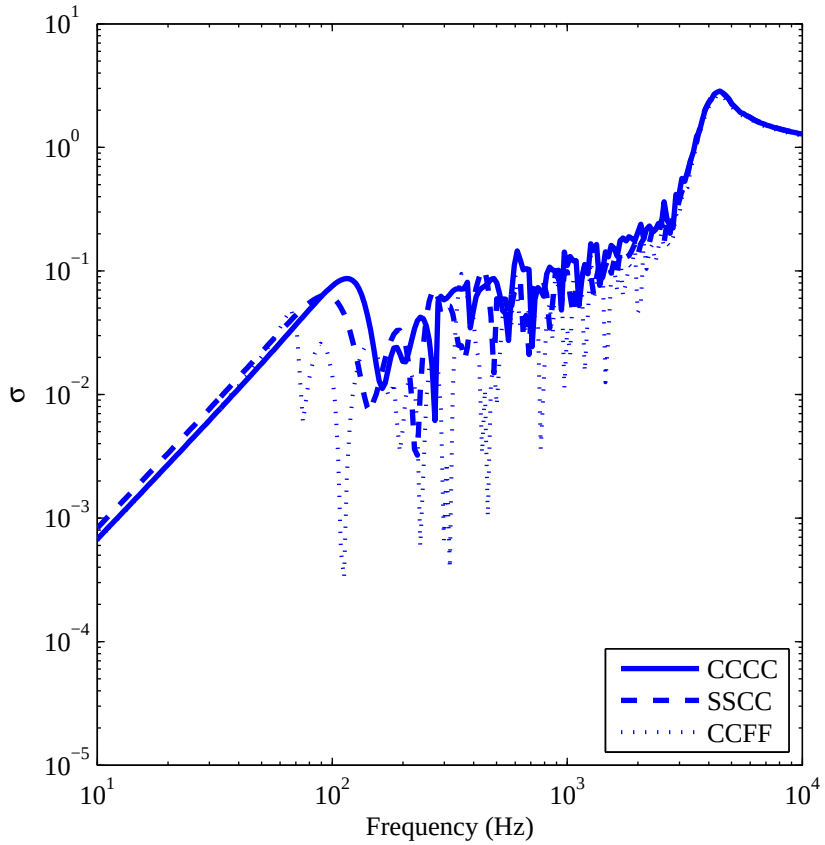

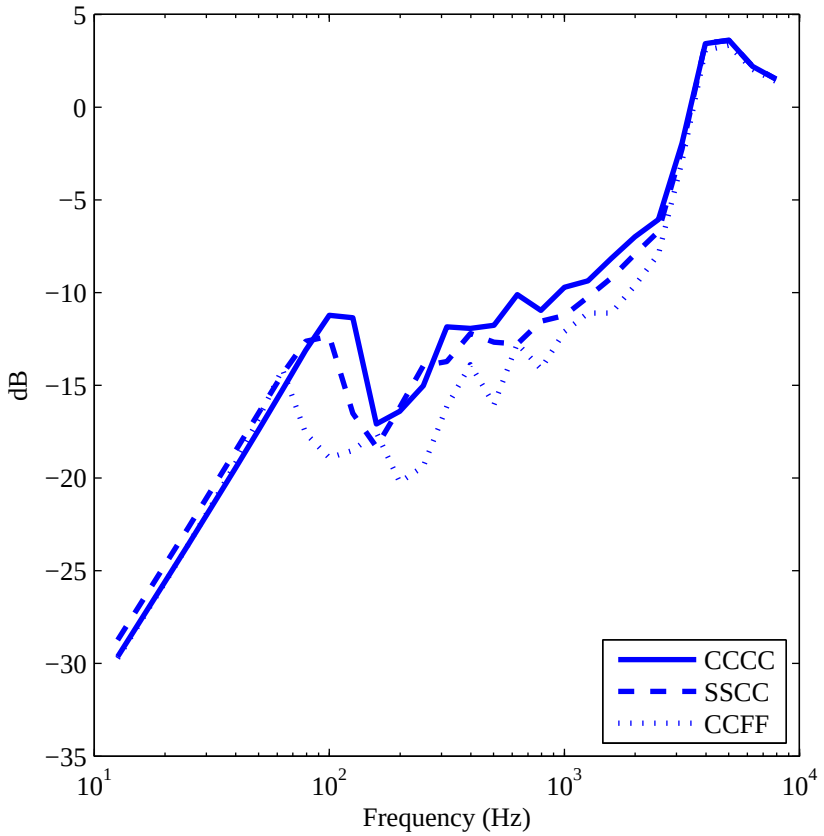

Figure 3.31: Radiation efficiency for C-C-C-C, SS-SS-C-C and C-C-F-F plate in third octave band.

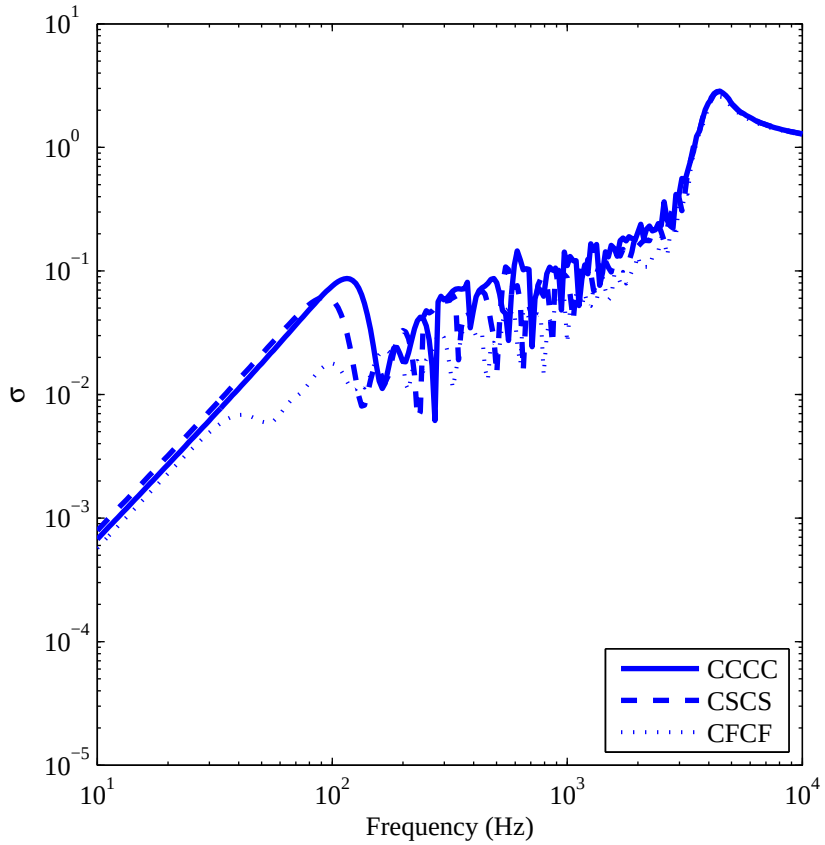

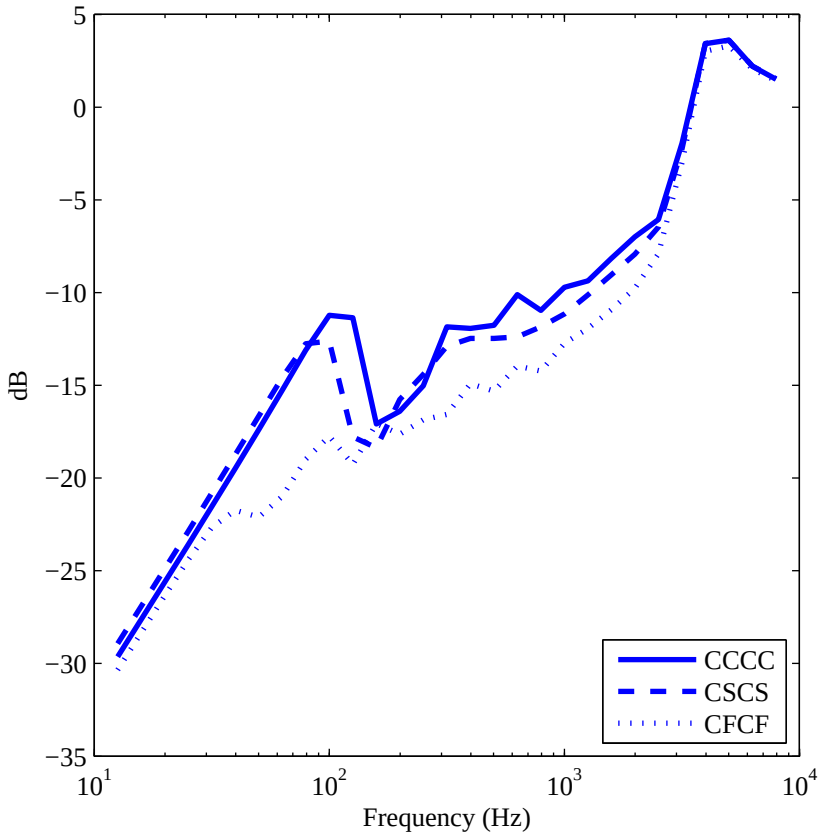

Figure 3.32: Radiation efficiency for C-C-C-C, C-SS-C-SS and C-F-C-F plate in third octave band.

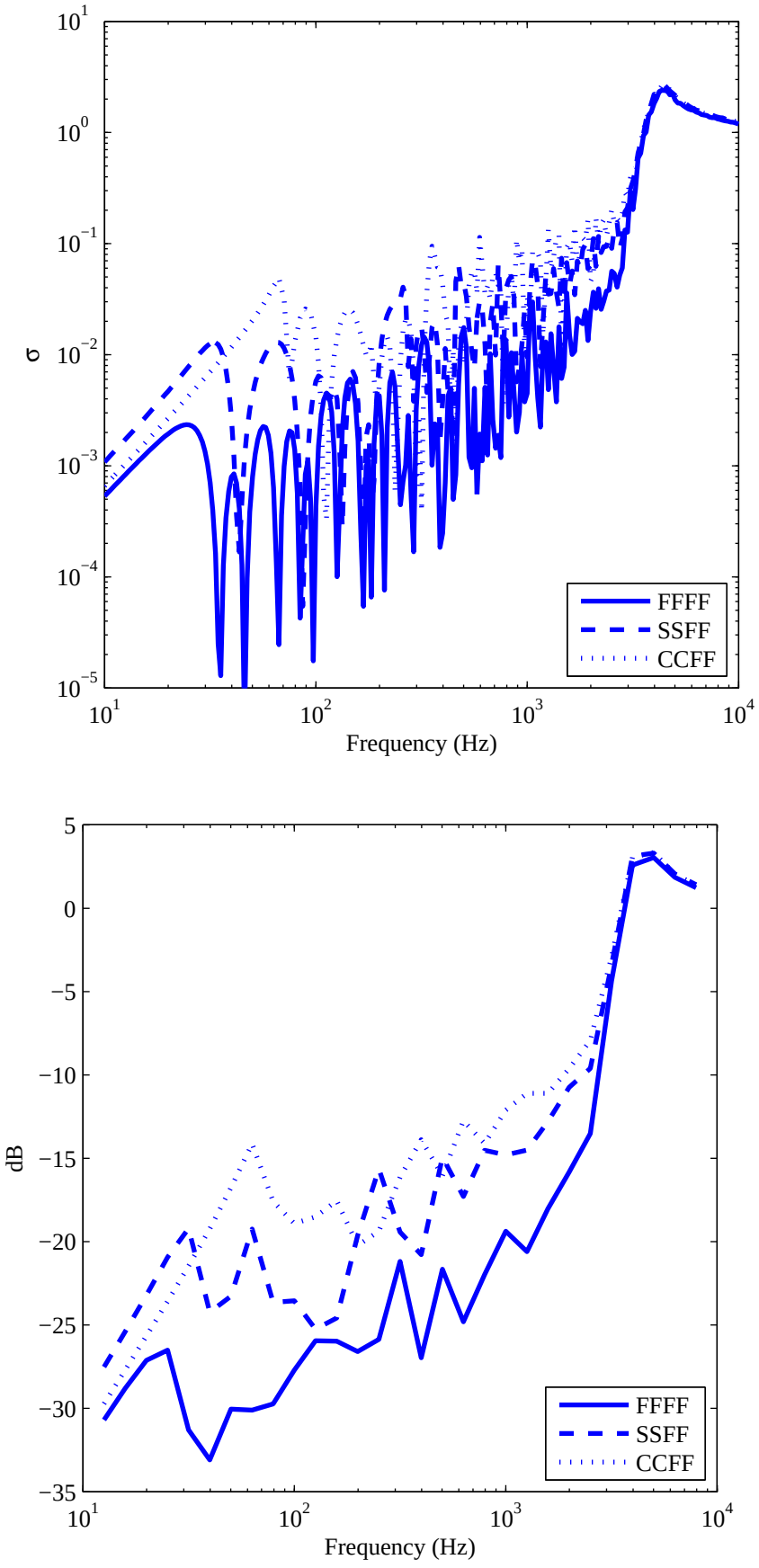

Figure 3.33: Radiation efficiency for F-F-F-F, SS-SS-F-F and C-C-F-F plate in third octave band.

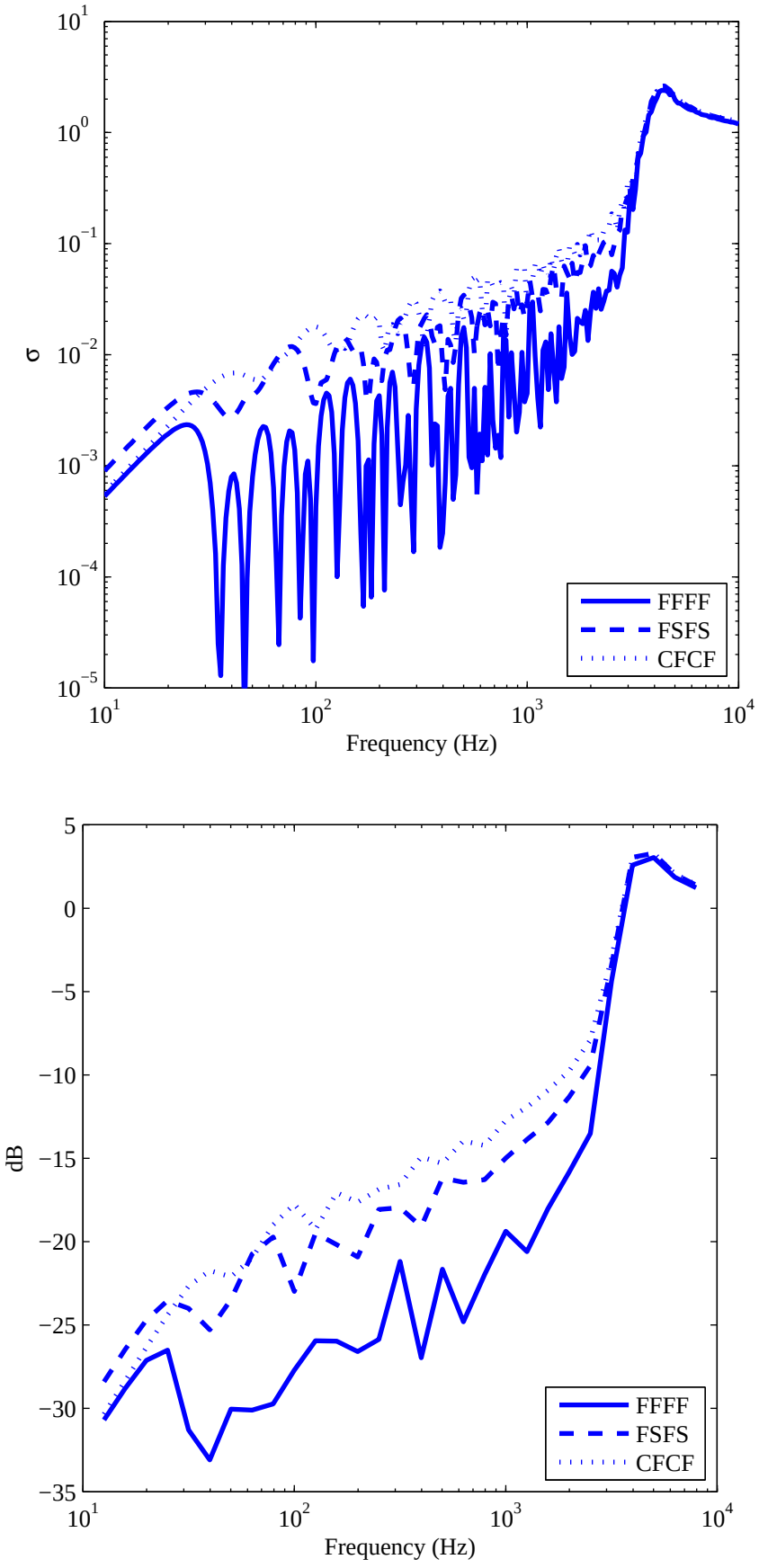

Figure 3.34: Radiation efficiency for F-F-F-F, F-SS-F-SS and C-F-C-F plate in third octave band.

Differences between cases

Figure 3.35 shows the difference in dB between for the cases in which the plate is fully simply, clamped and freely supported. Figure 3.36 shows the same quantity for other combination of boundary conditions.

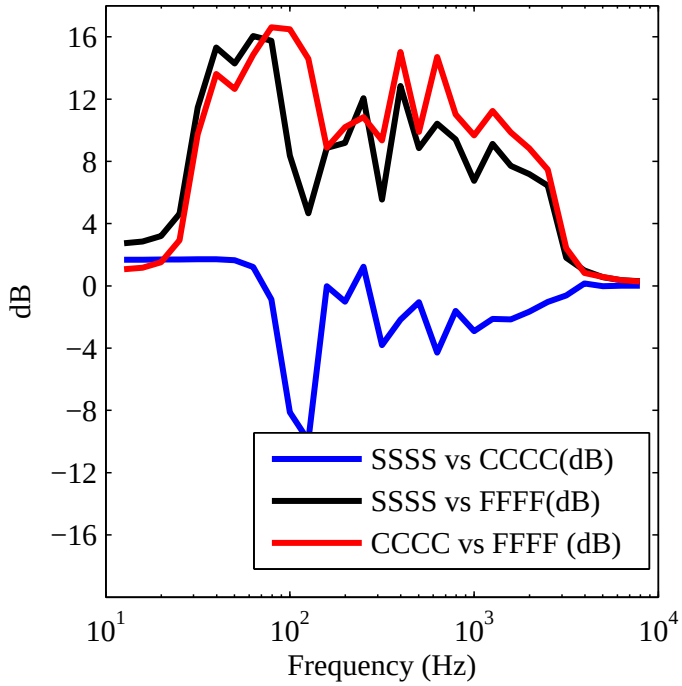

Figure 3.35: Differences in terms of octave third band of SSSS, CCCC and FFFF plates.

In this manner it is possible to verify what Leppington supposed about the difference of 3 dB in terms of radiation efficiency between the simply and fully clamped supported cases. As shown in Figure 3.35, the difference between the fully clamped and simply supported cases depends on the frequency of interest and oscillates between the values of 2 dB and -8 dB. In the same subfigure one can see that the difference between a fully clamped and fully freely supported plate is also variable and it reaches a maximum of 16 dB around 100 Hz.

In Figure fig:Differences in terms of octave third band, the effect on radiation efficiency's calculation of changing the boundary condition in a couple of edges (opposite or adjacent) is shown. As said before, a fully clamped plate is, in average, the most efficient. The introduction of a couple of clamped edges in a plate will always increase the radiation efficiency. In particular, it can introduce until 16 dB at 60 Hz in case of passing from a F-F-F-F to a C-C-F-F plate. The difference in average of introducing them in two opposite edges or in two adjacent edges is not relevant in terms of radiation efficiency.

Thus, the insertion in the same manner of a couple of two free supported boundary conditions will always make the radiation efficiency decrease. In particular, at low frequencies, the introduction of a couple of free edges makes the radiation efficiency decrease $4 - 8$ dB, while in the mid-frequency range the decrement is around 4 dB. As in the clamped case, the difference in average of introducing them in two opposite edges or in two adjacent edges is not relevant in terms of radiation efficiency.

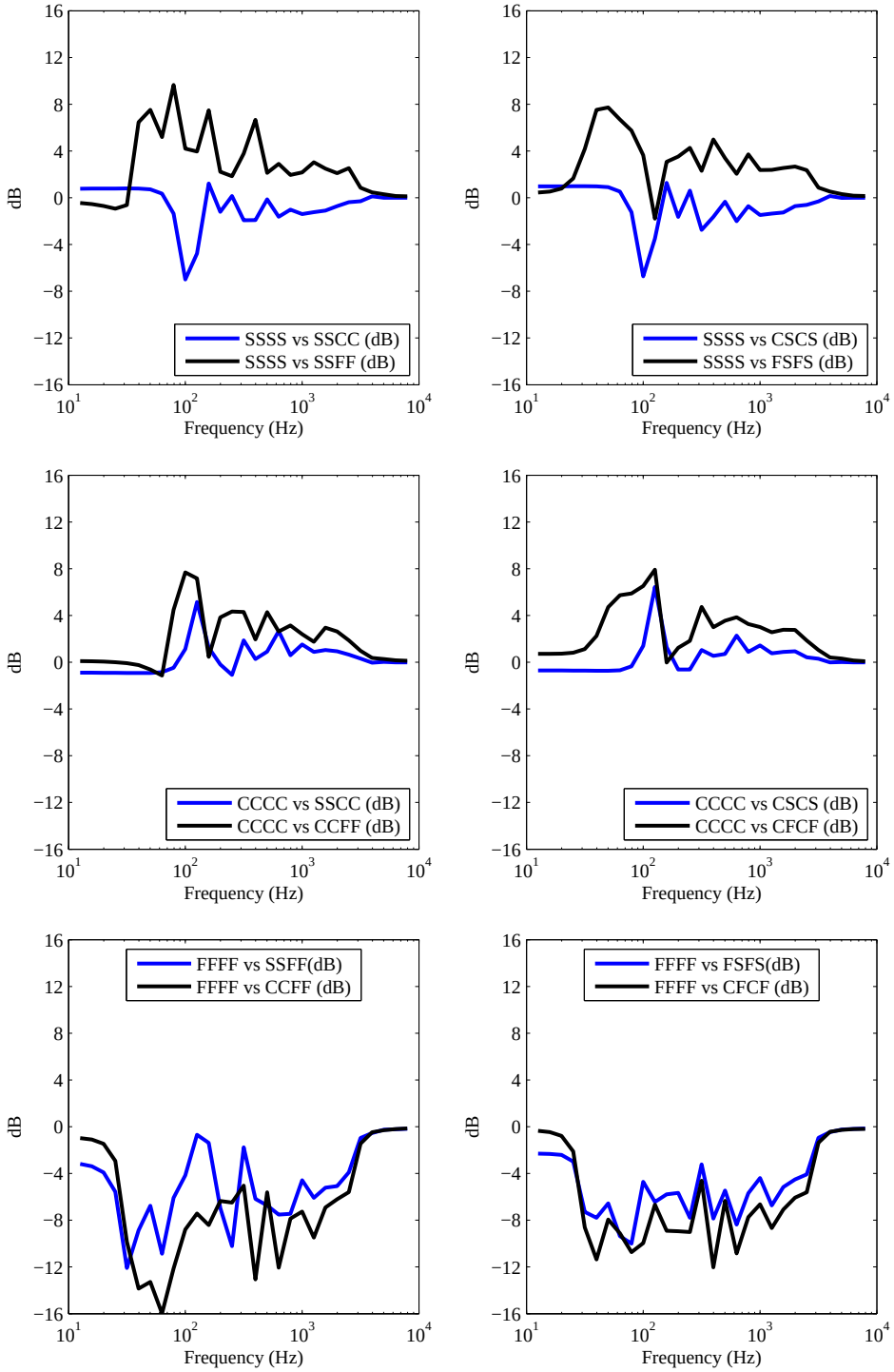

Figure 3.36: Differences in terms of octave third band for some different combinations of boundary conditions.

3.3.4 Response to point force

A Matlab code has been developed in order to reproduce the formulae (given in the first part of this chapter) for the calculation of the radiation efficiency when the plate is excited by a force in a single point of its surface. Figure 3.37 shows a comparison between the average radiation efficiency, that is when the plate is excited in all points of its surface, and the radiation efficiency when only one point is excited for a simply supported plate. Figure 3.38 shows the same quantities for a freely supported plate. The value of the mode shapes evaluated in the point where the force is applied determines the values of the modal amplitude velocities. The fact that a simply supported plate behaves as a monopole in a wider range of frequency when it is forced in the centre is explained as follows: the value of the first mode shape reaches its maximum in the centre. In the second, third and fourth mode the centre is a node. That means that these modes do not contribute to the acoustic emission. In Figure 3.38 it can be observed a big difference between the average radiation efficiency and the radiation efficiency when forcing the centre of a freely supported plate. The fact that the initial value of both curves is different is due to the three rigid modes. The first rigid mode corresponds to a vertical displacement, while the second and the third correspond to a rotation, that means that the second and the third rigid modes do not contribute to the acoustic emission. Taking in account the expression of the radiation efficiency given in equation (3.18), that means the radiation efficiency of a free plate when only forcing the centre is three times higher than the radiation efficiency when forcing all points of the plate. The considerations made for the case in which the plate is simply supported are valid for any other boundary combination. For example, in a freely supported plate, the first elastic mode in which the centre of the plate is not a node is the second elastic mode, which corresponds, considering the three rigid modes, to the fifth mode shape, while in the fourth mode, the centre is a node. Both of them are shown in Figure 3.39. For this reason, when the plate is forced in the centre the deep due to the fourth mode contribution is not present in the radiation efficiency curve, while it appears in the case of the average radiation efficiency.

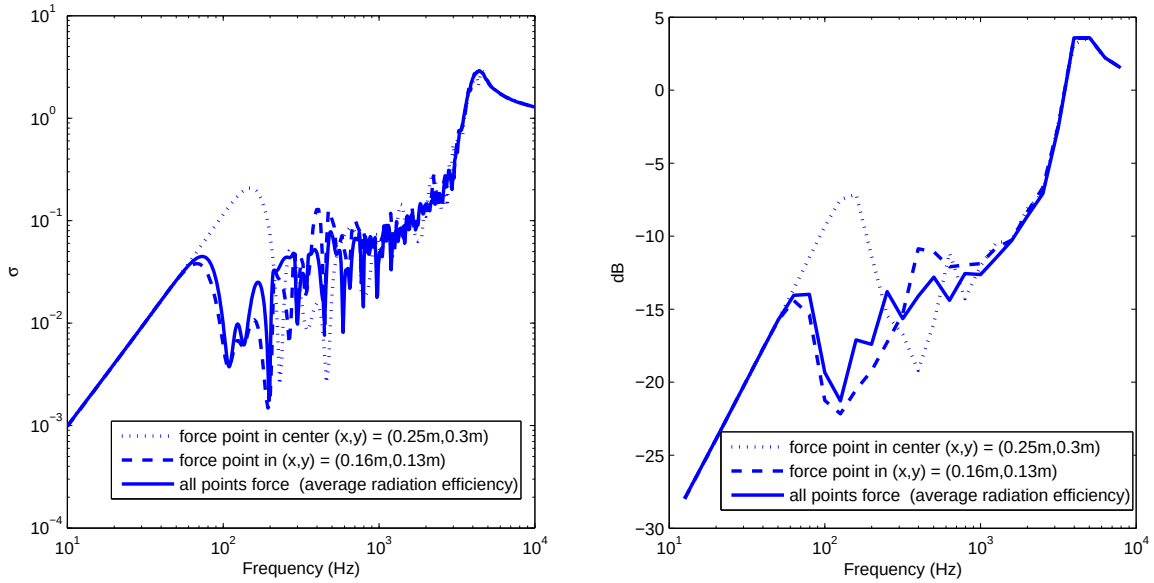

(a) *Radiation efficiency in narrow band.*

(b) *Radiation efficiency in terms of third octave band.*

Figure 3.37: Comparison between average radiation efficiency and radiation efficiency for different point forces. The plate is considered simply supported.

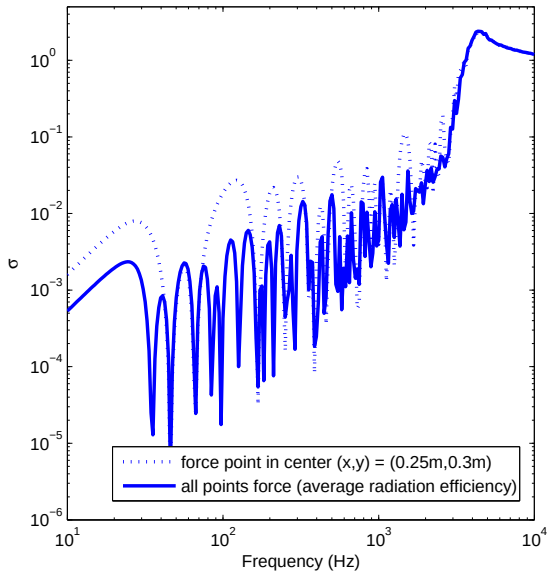

(a) *Radiation efficiency in narrow band.*

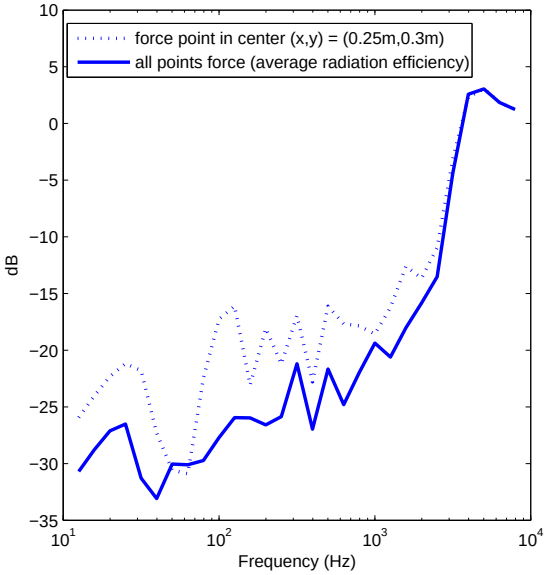

(b) *Radiation efficiency in terms of third octave band.*

Figure 3.38: Comparison between average radiation efficiency and radiation efficiency for different point forces. The plate is considered freely supported.

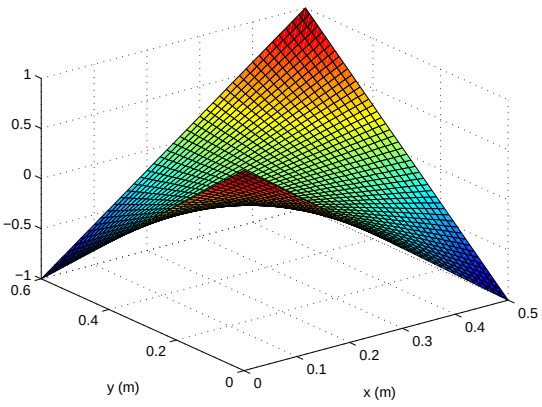

(a) *Fourth mode shape of a free supported plate.*

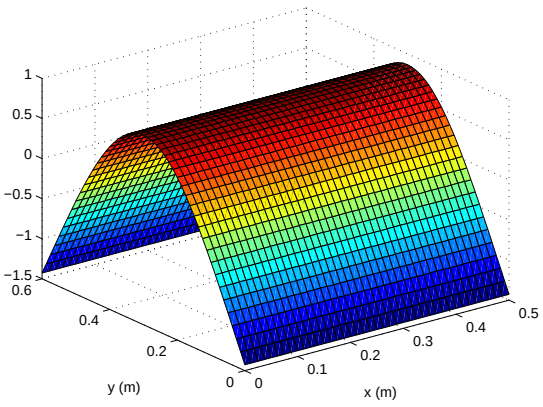

(b) *Fifth mode shape of a free supported plate.*

Figure 3.39: Fourth and fifth mode shapes of a F-F-F-F plate.

3.3.5 BEM analysis

Analytical and numerical results have been compared with numerical results given by the program LMS Virtual Lab. In Virtual Lab, there are many ways to calculate the radiation efficiency. One of them is the one explained in the second part of this chapter. A good equipment is required since the calculation times are quite long. In order to proceed to the acoustic calculation, Virtual Lab needs in input a structural mesh and an acoustic mesh. With the objective of reproducing accurately the acoustic behaviour of the baffled rectangular plate as in Figure 3.1, the structural mesh consists on a large rigid plane in which the plate is inserted. On the other hand, the acoustic mesh is simply the mesh of the plate. Both meshes were imported from Abaqus FEM and are equal in the region in which the plate lies. The field points, that is the points in which the results are given are equidistant to the plate and are the result of meshing a hemisphere of radius equal to 10 m. In this way, the assumption of far field can be taken. Structural, acoustic and hemisphere meshes are shown in Figure 3.40.

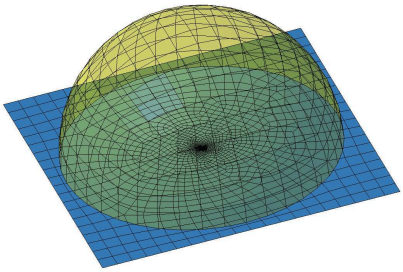

Figure 3.40: Structural, acoustic and hemisphere meshes.

Virtual Lab needs also in input the mode shapes associated to the input structural mesh in the frequency range under consideration. These have been imported from Abaqus and are normalized respect to the mass. In this way, Virtual Lab calculates the FRF in terms of velocity and transmits them to the acoustic mesh. In Figure 3.41 an example of this procedure is shown.

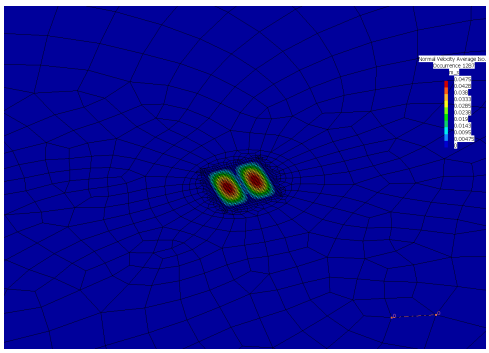

Figure 3.41: Velocity of the plate at frequency of 150 Hz.

Once the velocity of the plate is known, Virtual Lab can calculate the solution at field points in terms of pressure as well as the acoustic power and the radiation efficiency. In Figure 3.42 two examples of results are shown.

Some results obtained in this work are compared with the numerical results given by Virtual Lab. In Figure 3.43 due to the time of calculation of Virtual Lab, only few points of radiation's efficiency curve are calculated in BEM. At low frequencies the solution of BEM is slightly higher respect to the numerical solution. In the mid-frequency range results show a good agreement between both models. To avoid extremely large calculation time, the mesh adopted allows to obtain reliable results up to 1 or 4 KHz, depending on the case. In Figures 3.44 and 3.45 the radiation efficiency of a simply and freely supported plate forcing the center of the plate are shown. The numerical solution given in this work makes a good agreement with BEM, concluding that the models presented in this work are valid.

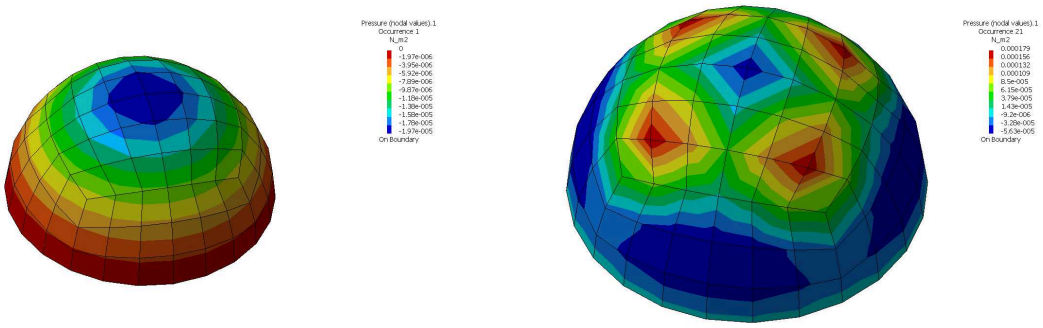

(a) *Pressure at 10 Hz.* (b) *Pressure at 31 Hz.*

Figure 3.42: Pressure values at field points for frequencies of 10 Hz and 31 Hz.

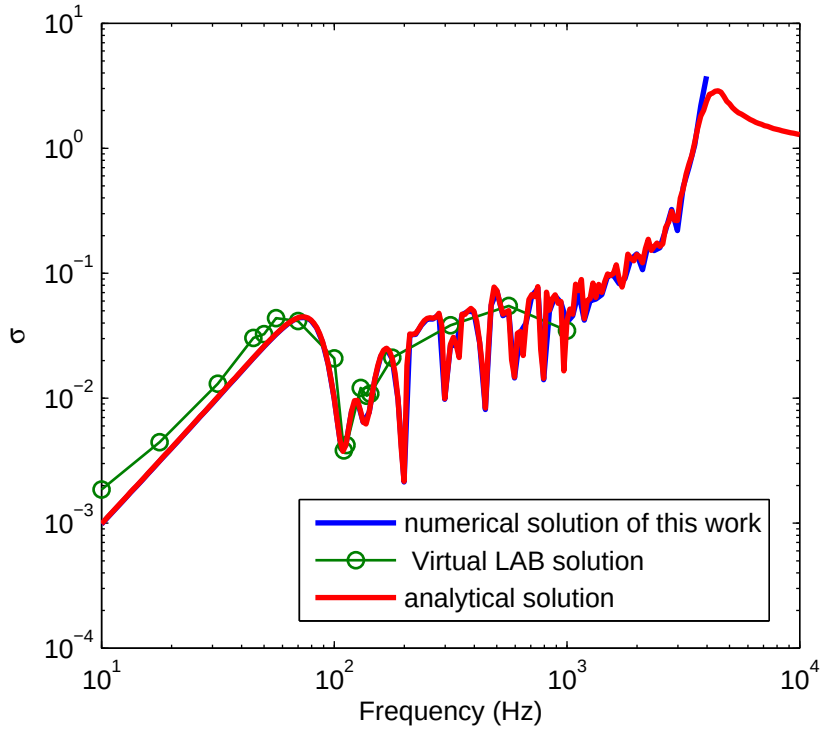

Figure 3.43: Average radiation efficiency of a simply supported plate. Comparison between numerical, BEM and analytical solution.

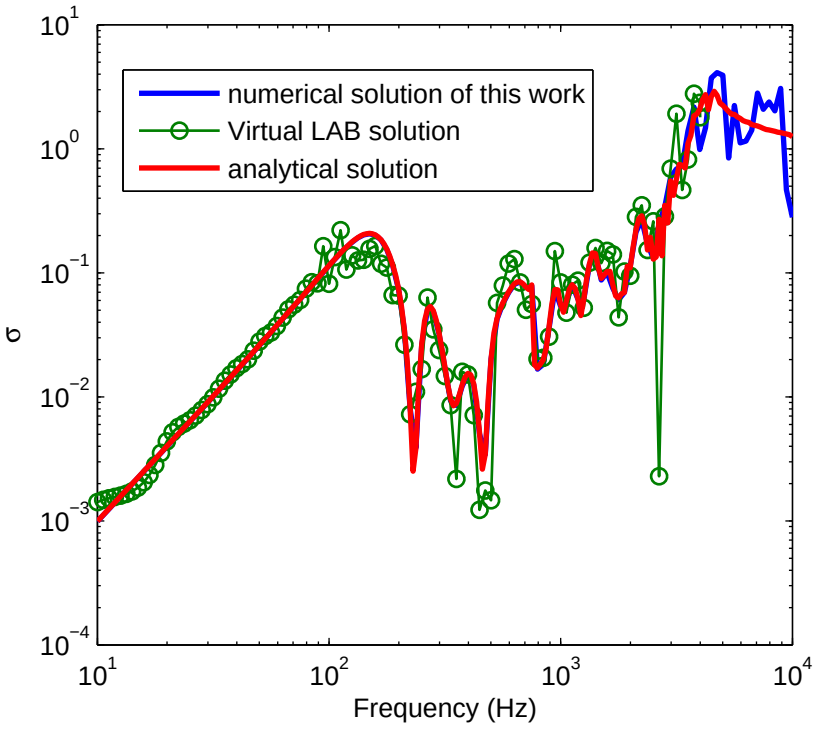

Figure 3.44: Radiation efficiency of a simply supported plate forcing the center of the plate. Comparison between numerical, BEM and analytical solution.

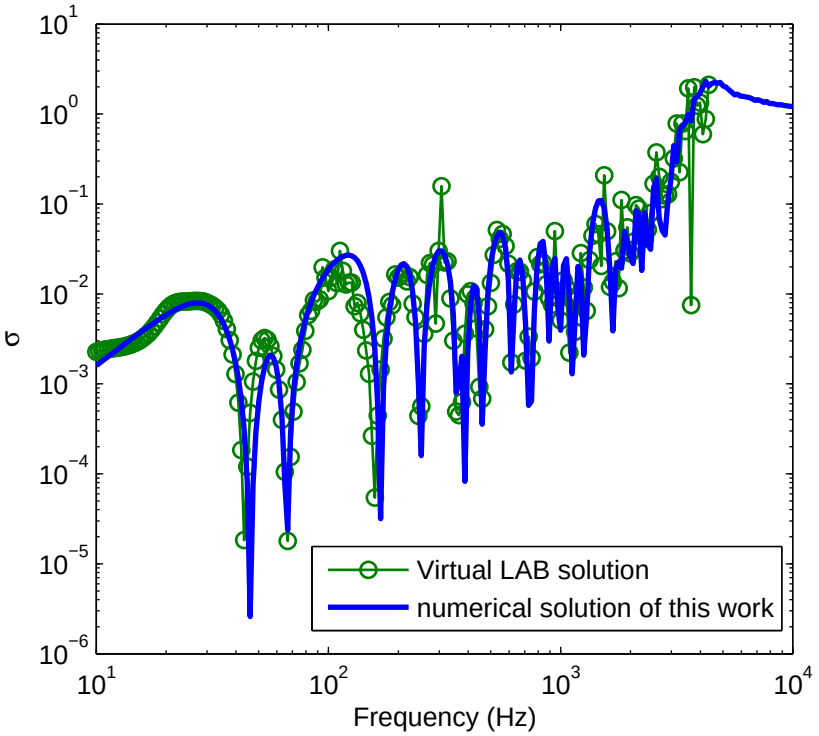

Figure 3.45: Radiation efficiency of a freely supported plate forcing the center of the plate. Comparison between numerical and BEM solution.

Chapter 4

Plates made of an orthotropic material

4.1 Introduction

Consider now a thin, flat rectangular plate of orthotropic and linearly elastic material with modulus of elasticity E_x in direction x, modulus of elasticity E_y in direction y, poisson ratio ν_x in direction x, poisson ratio ν_y in direction y and density ρ, having uniform thickness h and occuping the region in the *(x,y)*-plane $\Omega(x, Y) : 0 \leq x \leq a, 0 \leq y \leq b$. The strain-stress relationship is known and it is given by:

$$\begin{bmatrix} \epsilon_x \\ \epsilon_y \\ \gamma_{xy} \end{bmatrix} = \begin{bmatrix} 1/E_x & -\nu_{xy}/E & 0 \\ -\nu_{yx}/E_y & 1/E_y & 0 \\ 0 & 0 & 1/G \end{bmatrix} \begin{bmatrix} \sigma_x \\ \sigma_y \\ \tau_{xy} \end{bmatrix} \tag{4.1}$$

The inverse of equation (4.1) gives:

$$\begin{bmatrix} \sigma_x \\ \sigma_y \\ \tau_{xy} \end{bmatrix} = \begin{bmatrix} \frac{E_x}{1-\nu_{xy}\nu_{yx}} & \frac{\nu_{yx}E_x}{1-\nu_{xy}\nu_{yx}} & 0 \\ \frac{\nu_{xy}E_y}{1-\nu_{xy}\nu_{yx}} & \frac{E_y}{1-\nu_{xy}\nu_{yx}} & 0 \\ 0 & 0 & G \end{bmatrix} \begin{bmatrix} \epsilon_x \\ \epsilon_y \\ \gamma_{xy} \end{bmatrix} = [D]\,[\epsilon] \tag{4.2}$$

In this chapter a formulation for calculating the natural frequencies and mode shapes of a previously considered plate is presented. The plate will be assumed to be always fully simply supported.

4.2 Natural modes calculation of a thin orthotropic rectangular plate

The free vibrations of a plate having rectangular orthotropy are given by (see Leissa [14]):

$$D_x \frac{\partial^4 w}{\partial^4 x} + 2D_{xy} \frac{\partial^4 w}{\partial^2 x \partial^2 y} + D_y \frac{\partial^4 w}{\partial^4 y} + \rho \frac{\partial^2 w}{\partial^2 t} = 0 \tag{4.3}$$

where $w = w(x, y, t)$ is the vertical plate displacement and the bending stiffness D are related to the elastic constants by:

$$D_x = \frac{E_x h^3}{12(1 - \nu_{xy}\nu_{yx})} \tag{4.4}$$

$$D_y = \frac{E_y h^3}{12(1 - \nu_{xy}\nu_{yx})} \tag{4.5}$$

$$D_{xy} = D_x \nu_y + 2D_k \tag{4.6}$$

$$D_k = \frac{Gh^3}{12} \tag{4.7}$$

It can be noticed that these flexural terms can be obtained directly from a combination of the terms contained in the matrix $[D]$ of equation (4.2) provided it is multiplied by $h^3/12$. Assuming a time harmonic motion (as in equation (2.7)) and considering all sides simply supported a simple exact solution exists for the problem and it is given (see Leissa [14]) in terms of mode shapes by:

$$s_{mn}(x,y) = A_{mn} \sin\frac{m\pi x}{a} \sin\frac{n\pi y}{b} \tag{4.8}$$

and in terms of natural frequencies by:

$$\omega_{mn} = \sqrt{\frac{1}{\rho_s}\left(D_x M^4 + D_y N^4 + D_{xy} M^2 N^2\right)} \tag{4.9}$$

where $M = m\pi/a$ and $N = n\pi/b$.

Finally at the purpose of investigating the effect of the ratio between the stiffness along the two main directions x and y, the following problem can be set up:

$$\begin{array}{ll} E_s & = \sqrt{E_x E_y} \\ \frac{\nu_s}{E_s} & = \sqrt{\frac{\nu_{xy}}{E_x}\frac{\nu_{yx}}{E_y}} \\ \frac{E_x}{E_y} & = r \\ \frac{\nu_{xy}}{E_x} & = \frac{\nu_{yx}}{E_y} \end{array} \tag{4.10}$$

where the terms E_s and ν_s are representative for the Young's modulus and Poisson's coefficient of an equivalent isotropic plate. They are defined through a geometric mean operation whose terms are the elements defined in the matrix of equation (4.1). By varying the ortothropic ratio $r = E_x/E_y$ one can easily investigate the effect of the orthotropy on the natural modes of the plate and on the consequent sound radiation, having as a fixed referenced result the one obtained for the isotropic equivalent plate. It is important to underline that the equations presented in this section for rectangular plate with a rectangular orthotropy are valid only when the orthotropy directions coincide with the edge of the plate and in few other cases. In particular it has been shown that when the angle ϕ between the orthotropy axis x' and the plate axis x is a multiple of 22.5 *deg* equation 4.3 correctly describes the plate motion provided that the orthotropic constants are calculated as:

$$D_x = D'_x \cos^4\phi + D'_y \sin^4\phi + 2D'_{xy} \sin^2\phi \cos^2\phi \tag{4.11}$$

$$D_y = D'_x \sin^4\phi + D'_y \cos^4\phi + 2D'_{xy} \sin^2\phi \cos^2\phi \tag{4.12}$$

$$D_{xy} = \left(3D'_x + 3D'_y - 2D'_{xy}\right) \sin^2\phi \cos^2\phi + D_{xy}\left(\cos^2\phi - \sin^2\phi\right) \tag{4.13}$$

If the angle ϕ differs from 22.45 *deg* or from one of its multiples, the equation for the free vibrations assumes a different form.

4.3 Results

With the aim of evaluating the effect of introducing the orthotropy of the material, results of an orthotropic plate equivalent to an isotropic plate are presented. The geometry of the plate is the usual $(0.5x0.6x0.003m)$ and the density is fixed to $2700kg/m^3$. The elastic properties of the material must be defined. Remembering that for an orthotropic plate $r = \frac{E_x}{E_y} = \frac{\nu_{xy}}{\nu_{yx}}$, the elastic properties of the isotropic and its equivalent orthotropic plate follow the relations:

$$E_{al} = \sqrt{E_x E_y} \tag{4.14}$$

$$\nu_{al} = \sqrt{\nu_{xy}\nu_{yx}} \tag{4.15}$$

Since the value of E_{al} is set to $7.1e10$ and the value of ν_{al} is set to 0.3, the elastic parameters of the equivalent orthotropic plate can be calculated immediately for different values of r. Table 4.1 shows their values for three different ortothropic ratio.

r	$E_x(Mpa)$	$E_y(Mpa)$	ν_{xy}	ν_{yx}
10.40	2.29e11	2.20e10	0.97	0.093
20.97	3.25e11	1.55e10	1.37	0.065
28.39	3.78e11	1.33e10	1.59	0.0565

Table 4.1: Equivalent stiffness parameters of an orthotropic plate respect to an isotropic plate.

4.3.1 Free vibration

Using equation (4.2), natural frequencies of the orthotropic plate for different orthotropic ratio have been calculated. In Table 4.2. The effect of orthotropy can be explained as follows: if the orthotropy ratio increases, the value of the first natural frequency increases. For the rest of natural frequencies no trend can be found since the orthotropy results into mode condensations respect to the isotropic plate: depending on the mode number, some natural frequencies are higher and some others are lower.

A similar behaviour happens with mode shapes. The introducing of orthotropy makes the order of the modes change respect to the isotropic plate.

	Isotropic plate $r = 1$	Orthotropic plate $r = 10$	Orthotropic plate $r = 20$	Orthotropic plate $r = 30$
Mode	Frequency (Hz)	Frequency (Hz)	Frequency (Hz)	Frequency (Hz)
1	49.56	63.84	72.09	76.31
2	110.50	97.77	100.56	102.72
3	137.32	154.33	148.03	146.72
4	198.26	221.43	214.47	208.33
5	212.07	233.51	259.87	278.85
6	283.57	255.36	288.35	287.53
7	299.82	311.92	299.90	305.26
8	344.51	335.31	335.81	349.26
9	354.26	391.10	402.26	384.34
10	442.01	459.74	404.32	410.87

Table 4.2: First ten natural frequencies of an isotropic plate and his equivalent orthotropic plate for different values of r.

4.3.2 Radiation efficiency

The same Matlab code used for the calculation of the radiation efficiency of a plate made of an isotropic material is used to calculate the radiation efficiency of its equivalent orthotropic plate. Figures 4.1, 4.2 and 4.3 show a comparison between the isotropic plate and its equivalent orthotropic plate for different orthotropy ratio. At low frequencies the differences are not considerable. the mid-frequency range is divided in two zones: in the first zone the radiation efficiency of the orthotropic plate is higher, while in the second zone the opposite happens. At high-frequency range something similar happens: before the critical frequency of the isotropic plate, the radiation efficiency of the orthotropic plate is considerably higher, while after the critical frequency the isotropic plate's one is higher. The overall results are shown in Figure 4.4 and permit to compare the behaviour of the orthotropic plates when the orthotropy ratio varies. At low frequencies, the biggest the the ratio is, the lowest the radiation efficiency is, even though the differences are not important. On the other hand, at high frequencies, the radiation efficiency tends to increase as the orthotropy ratio increases.

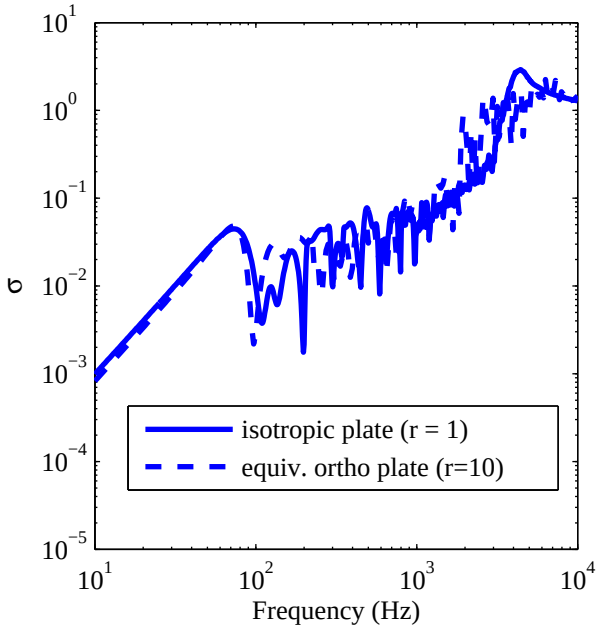

(a) *Radiation efficiency*

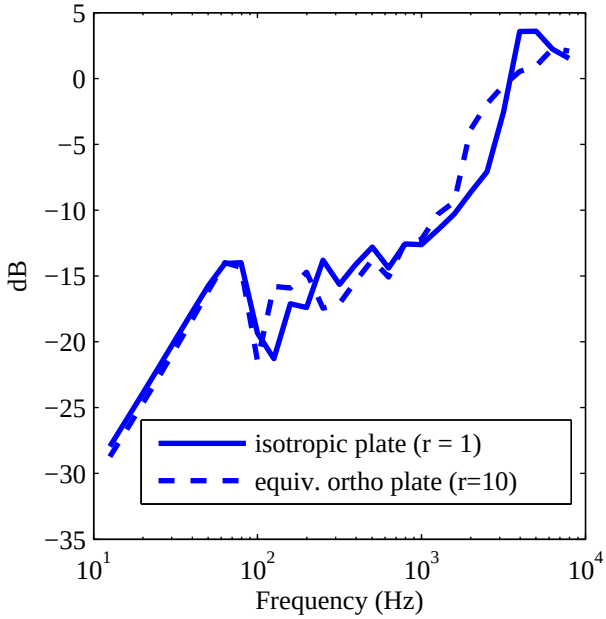

(b) *Radiation efficiency in terms of octave band*

Figure 4.1: Comparison between isotropic plate and its equivalent orthotropic plate for r=10.

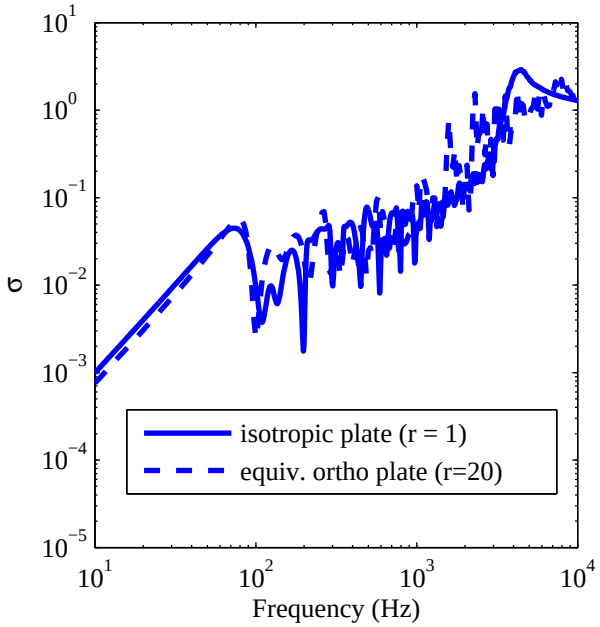

(a) *Radiation efficiency*

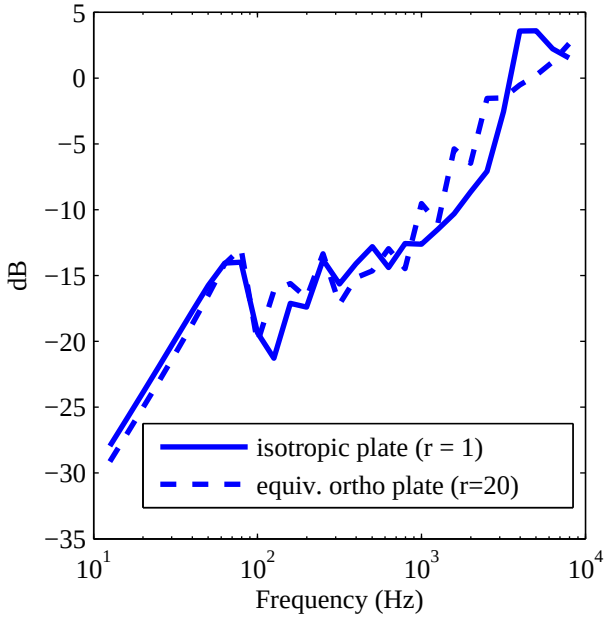

(b) *Radiation efficiency in terms of octave band*

Figure 4.2: Comparison between isotropic plate and its equivalent orthotropic plate for r=20.

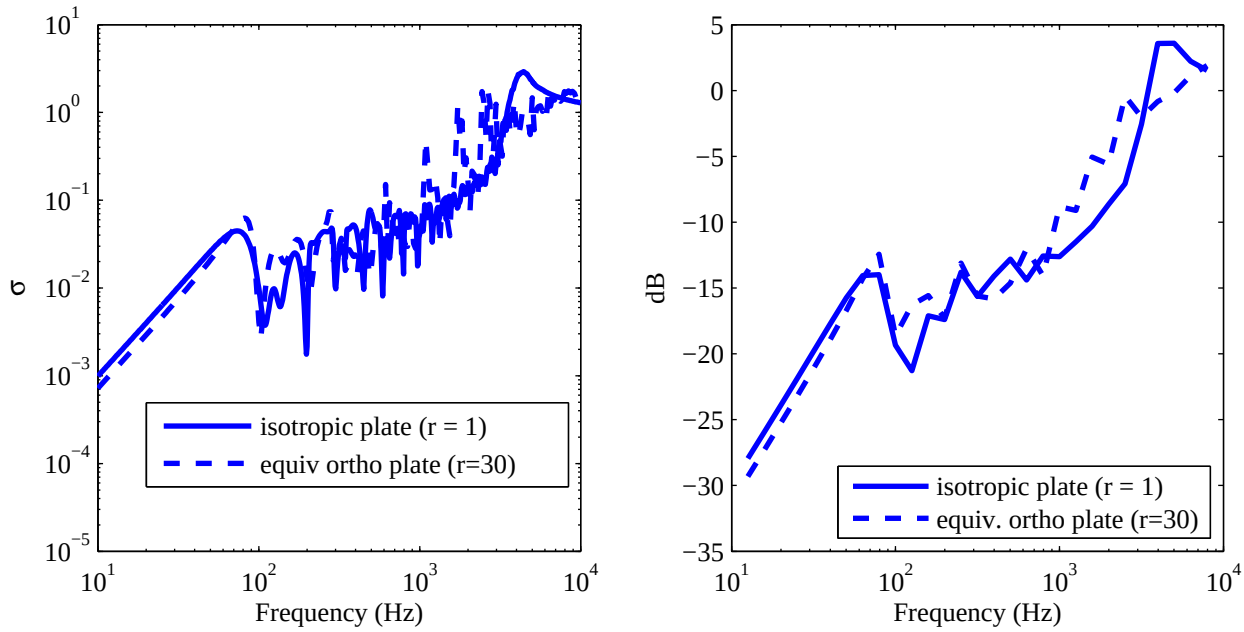

(a) *Radiation efficiency* (b) *Radiation efficiency in terms of octave band*

Figure 4.3: Comparison between isotropic plate and its equivalent orthotropic plate for r=30.

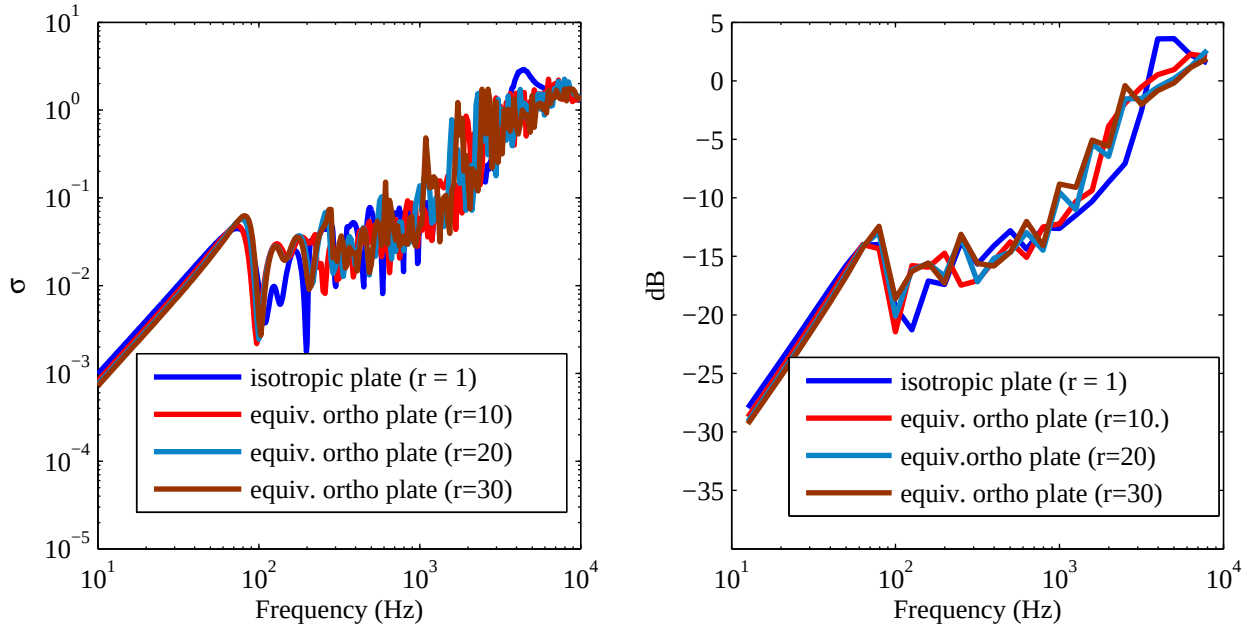

(a) *Radiation efficiency* (b) *Radiation efficiency in terms of octave band*

Figure 4.4: Comparison between isotropic plate and its equivalent orthotropic plate for different values of r.

Chapter 5

Ribbed plates

5.1 Introduction

The aim of the first part of this chapter is to present a model which will quantify easily the bending stiffness in both directions of the plate in the plane x-y when considering it reinforced by equidistant stiffeners in one direction, that is a plate reinforced symmetrically with respect to its middle plane as shown in Figure 5.1. Once the expressions for new stiffness are noted, one can calculate the geometry of the ribs. On the other hand, given a number and the geometry of the ribs, stiffness can be calculated immediately. The plate is always considered fully simply supported. The second part of this chapter shows a combined analytical-numerical method which allows one to calculate the free vibrations of a ribbed plate. Part three presents the results obtained applying the theory here after.

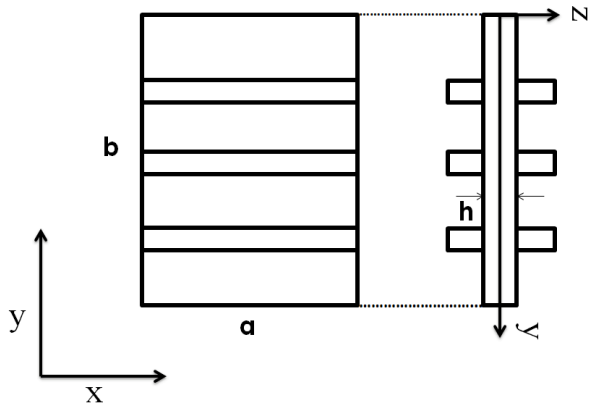

Figure 5.1: Plate reinforced by equidistant ribs in one direction.

5.2 Ribbed plates made of an isotropic material

5.2.1 PDE of the bending plate

In previous discussion it has been assumed that the elastic properties of the material of the plate are the same in all directions. There are, however, cases in which this assumption can not be made: this is the case of a ribbed plate. If someone wishes to bring the theory of plates into agreement with experiments, the anisotropy introduced by the insertion of ribs must be considered. Assuming that the material of the plate has three planes of symmetry with respect to its elastic properties, and taking them as the

coordinates planes, the relations between the stress and strain components for the case of plane stress in the x-y plane can be represented by the following equations:

$$\sigma_x = \frac{E_x}{1-\nu_{xy}\nu_{yx}}\epsilon_x + \frac{\nu_{yx}E_x}{1-\nu_{xy}\nu_{yx}}\epsilon_y \tag{5.1}$$

$$\sigma_y = \frac{\nu_{xy}E_y}{1-\nu_{xy}\nu_{yx}}\epsilon_y + \frac{E_y}{1-\nu_{xy}\nu_{yx}}\epsilon_x \tag{5.2}$$

$$\tau_{xy} = G\gamma_{xy} \tag{5.3}$$

It is assumed that the linear elements perpendicular to the middle plane of the plate before bending remain straight and normal to the deflection surface of the plate. Hence, previous expressions can be used for the components of strain:

$$\epsilon_x = -z\frac{\partial^2 w}{\partial x^2} \qquad \epsilon_y = -z\frac{\partial^2 w}{\partial y^2} \qquad \gamma_{xy} = -2z\frac{\partial^2 w}{\partial x \partial y} \tag{5.4}$$

The corresponding stress components, from equations (5.1), (5.2), and (5.3) are:

$$\sigma_x = -z\left(E_x\frac{\partial^2 w}{\partial x^2} + \nu_{yx}E_x\frac{\partial^2 w}{\partial y^2}\right) \tag{5.5}$$

$$\sigma_y = -z\left(E_y\frac{\partial^2 w}{\partial y^2} + \nu_{xy}E_y\frac{\partial^2 w}{\partial x^2}\right) \tag{5.6}$$

$$\tau_{xy} = -2Gz\frac{\partial^2 w}{\partial x \partial y} \tag{5.7}$$

With these the expressions for the stress components, the bending and twisting moments are:

$$M_x = \int_{-h/2}^{h/2}\sigma_x z\,dz = -\left(D_x\frac{\partial^2 w}{\partial x^2} + D_{xy}\frac{\partial^2 w}{\partial y^2}\right) \tag{5.8}$$

$$M_y = \int_{-h/2}^{h/2}\sigma_y z\,dz = -\left(D_y\frac{\partial^2 w}{\partial y^2} + D_{xy}\frac{\partial^2 w}{\partial x^2}\right) \tag{5.9}$$

$$M_{xy} = \int_{-h/2}^{h/2}\tau_{xy} z\,dz = 2D_{xy}\frac{\partial^2 w}{\partial x \partial y} \tag{5.10}$$

in which

$$D_x = \frac{E_x h^3}{12(1-\nu_{xy}\nu_{yx})} \qquad D_y = \frac{E_y h^3}{12(1-\nu_{xy}\nu_{yx})} \qquad D_k = \frac{Gh^3}{12} \qquad D_{xy} = \nu_{yx}D_x + D_k \tag{5.11}$$

substituing expressions (5.8), (5.9) and (5.10) in the differential equation of equilibrium of the plate (equation (2.6)) and considering the existence of a force q, we obtain the following equation for orthtropic plates:

$$D_x\frac{\partial^4 w}{\partial x^4} + 2D_{xy}\frac{\partial^4 w}{\partial x^2 \partial y^2} + D_y\frac{\partial^4 w}{\partial y^4} = q \tag{5.12}$$

5.2.2 Determination of the stiffness in the specific case

For a plate reinforced with ribs in one direction symmetrically with respect to its middle plane, one can take (see Timoshenko [19]):

$$D_x = \frac{Eh^3}{12\,(1-\nu^2)} + \frac{E^{'}I}{b_1} \qquad D_y = D_{xy} = \frac{Eh^3}{12\,(1-\nu^2)} \tag{5.13}$$

in which E and ν are the elastic constants of the material of the plating, $E^{'}$ the Young modulus, I the moment of inertia of a stiffener, taken with respect to the middle axis of the cross section of the plate and parameter b_1 is shown in Figure 5.2.

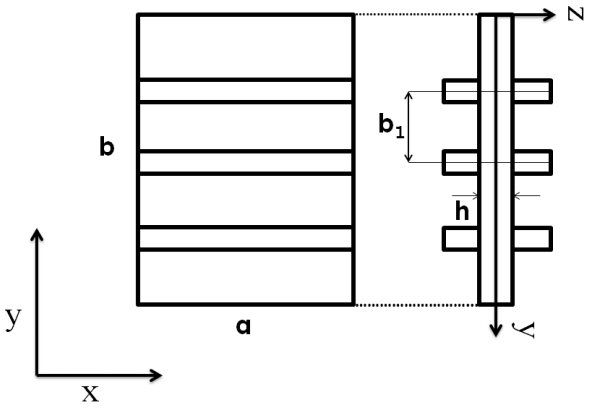

Figure 5.2: Plate reinforced by equidistant ribs in one direction. Parameter b_1.

5.2.3 Bending of rectangular plates

When the plate is simply supported on all sides, equation (5.12) can be solved applying the Navier method. Assuming that the plate is uniformly loaded, taking the coordinate axes as shown in Figure 5.1 and representing the load in the form of a double trigonometric series, the differential equation (5.12) becomes:

$$D_x \frac{\partial^4 w}{\partial x^4} + 2D_{xy} \frac{\partial^4 w}{\partial x^2 \partial y^2} + D_y \frac{\partial^4 w}{\partial y^4} = \frac{16 q_0}{\pi^2} \sum_{m=1,3,5\ldots}^{\infty} \sum_{n=1,3,5\ldots}^{\infty} \frac{1}{mn} \sin \frac{m\pi x}{a} \sin \frac{n\pi y}{b} \tag{5.14}$$

A solution of this equation that satisfies the boundary conditions can be taken in the form of double trigonometrical series:

$$w = \sum_{m=1,3,5\ldots}^{\infty} \sum_{n=1,3,5\ldots}^{\infty} a_{mn} \sin \frac{m\pi x}{a} \sin \frac{n\pi y}{b} \tag{5.15}$$

Substituting these series in equation (5.14), one finds the following expression for the coefficients a_{mn}:

$$a_{mn} = \frac{16 q_0}{\pi^2} \frac{1}{mn \left(\frac{m^4}{a^4} D_x + \frac{2m^2 n^2}{a^2 b^2} H + \frac{n^4}{b^4} D_y \right)} \tag{5.16}$$

Finally, the solution of equation (5.14) is:

$$w = \frac{16 q_0}{\pi^2} \sum_{m=1,3,5\ldots}^{\infty} \sum_{n=1,3,5\ldots}^{\infty} \frac{\sin \frac{m\pi x}{a} \sin \frac{n\pi y}{b}}{mn \left(\frac{m^4}{a^4} D_x + \frac{2m^2 n^2}{a^2 b^2} H + \frac{n^4}{b^4} D_y \right)} \tag{5.17}$$

5.3 Free vibration analysis of a ribbed plate by a combined analytical-numerical method

A combined analytical-numerical method for the calculation of the free vibrations of a ribbed plate is presented here after. The formulation is extracted from Dozio [20] and is extended also to the case in which the plate is made of an orthotropic material.

5.3.1 Problem statement

Plate made of an isotropic material

Consider a thin, flat rectangular plate of isotropic and linearly elastic material with modulus of elasticity E, Poison ratio ν and density ρ, having uniform thickness h and occupying the region in the x-y plane $\Omega(x, Y) : 0 \leq x \leq a, 0 \leq y \leq b$. The plate is orthogonally stiffened by a set of $j = 1, 2, ..., J$ prismatic ribs parallel to the x-axis. Ribs are made of an isotropic material, whose properties are E_r and ρ_r. Only bending motion is considered. As a result of plate bending, the ribs are subjected to bending and torsion deformation. Plate and ribs motion is described separately by using the assumed-modes method. The arising dynamic loads at the j th x-wise interface include a distribution of torsional line moment $m^j = m^j(x, t)$ and a transverse line force distribution $f^j = f^j(x, t)$.

Plate made of an orthotropic material

Consider a thin, flat rectangular plate of orthotropic and linearly elastic material with modulus of elasticity E_x in direction x, modulus of elasticity E_y in direction y, poisson ratio ν_x in direction x, poisson ratio ν_y in direction y and density ρ, having uniform thickness h and occupying the region in the x-y plane $\Omega(x, Y) : 0 \leq x \leq a, 0 \leq y \leq b$. The plate is orthogonally stiffened by a set of $j = 1, 2, ..., J$ prismatic ribs parallel to the x-axis. Ribs are made of an isotropic material, whose properties are E_r and ρ_r. Only bending motion is considered. As a result of plate bending, the ribs are subjected to bending and torsion deformation. Plate and ribs motion is described separately by using the assumed-modes method. The arising dynamic loads at the j th x-wise interface include a distribution of torsional line moment $m^j = m^j(x, t)$ and a transverse line force distribution $f^j = f^j(x, t)$.

5.3.2 Plate

Plate made of an isotropic material

According to the classical theory of thin plates, the equation motion of the forced plate is:

$$D\nabla^4 w + \rho h \frac{\partial w}{\partial t^2} = -\sum_{j=1}^{J} \left(f^j \delta_{yj} + m^j \delta_{yj}^{'} \right) \tag{5.18}$$

where $w = w(x, y, t)$ is the transverse displacement, $D = \frac{Eh^3}{12(1+\nu^2)}$ is the flexural stiffness of the plate, ∇^4 is the biharmonic operator, $\delta_{yj} = \delta(y - y_j)$ where δ is the Dirac delta function, y_j denotes the location of the jth x-wise rib. $\delta^{'}$ represents the first derivate of the Dirac delta function with respect to its argument. Plate deflection w can be expressed as the superposition of a finite number of mode shape s_{mn} as:

$$w = \sum_{m=1}^{M} \sum_{n=1}^{N} s_{mn}(x, y) w_{mn} e^{j\omega t} \tag{5.19}$$

where w_{mn} is the modal amplitude of the (m,n)-th mode of the plate and ω is the circular frequency. Mode shape functions can be written as the product of two independent rib functions:

$$s_{mn} = \phi_m(x)\psi_n(y) \tag{5.20}$$

Following Wartburton [21] function used is:

$$\phi_m(x) = A_m \cosh(\beta_m x) + B_m \cos(\beta_m x) + C_m \sinh(\beta_m x) + D_m \sin(\beta_m x) \tag{5.21}$$

where constants A_m, B_m, C_m, D_m and β_m are determined according to the specified edge boundary conditions of the plate at $x = 0$ and $x = a$. In case of study boundaries are simply supported.

After substituting equation (5.19) in equation (5.18), multiplying it with the (p,q)-th mode shape function, $s_{pq} = \phi_p(x)\psi_q(y)$ and integrating over the area of the plate, the solution must satisfy the following set of MxN coupled equations:

$$\sum_{m=1}^{M}\sum_{n=1}^{N} w_{mn}\int_0^a\int_0^b\left[D\left(\phi_m^{''''}\psi_n\phi_p\psi_q+2\phi_m^{''}\psi_n^{''}\phi_p\psi_q+\phi_m\psi_n^{''''}\phi_p\psi_q-\rho h\omega^2\phi_m\psi_n\phi_p\psi_q\right)\right]\,dxdy=$$
$$=-\sum_{j=1}^{J}\int_0^a\int_0^b\left[f^j\delta_{yj}\phi_p\psi_q+m^j\delta_{yj}^{'}\phi_p\psi_q\,dxdy\right] \tag{5.22}$$

where the prime denotes derivative of the shape function with respect of its argument. Using the dominant rib function for the (m,n)-th mode, equation (5.22) can be approximated as follows:

$$\left[D\left(I_{1m}I_{2n}+2I_{3m}I_{4n}+I_{6m}I_{5n}\right)-\rho h\omega^2 I_{6m}I_{2n}\right]w_{mn}=f_{mn}+m_{mn} \tag{5.23}$$

where f_{nm} and m_{mn} are the modal coupling line forces and moments given respectively by

$$f_{mn}=-\sum_{j=1}^{J}\psi_n^{y_j}\int_0^a f^j\phi_m dx \tag{5.24}$$

$$m_{mn}=-\sum_{j=1}^{J}\psi_n^{'y_j}\int_0^a m^j\phi_m dx \tag{5.25}$$

Equation (5.23) can be written in a compact notation as:

$$\left(k_{mn}-\omega^2\mu_{mn}\right)w_{mn}=f_{nm}+m_{mn} \tag{5.26}$$

where

$$k_{mn}=D\left(I_{1m}I_{2n}+2I_{3m}I_{4n}+I_{6m}I_{5n}\right) \tag{5.27}$$

is the modal stiffness of the (m,n)-th mode and

$$\mu_{mn}=\rho h I_{6m}I_{2n} \tag{5.28}$$

is the modal mass of the (m,n)-th mode.

Definite integrals I-VI in previous equations are:

$$\begin{aligned} I_{1m}&=\int_0^a\phi_m^{''''}\phi_m\,dx & I_{4n}&=\int_0^b\psi_n^{''}\psi_n\,dy\\ I_{2n}&=\int_0^b\psi_n^2\,dy & I_{5n}&=\int_0^b\psi_n^{''''}\psi_n\,dy\\ I_{3m}&=\int_0^a\phi_m^{''}\phi_m\,dx & I_{6m}&=\int_0^b\phi_m^2\,dx \end{aligned} \tag{5.29}$$

Finally the approximate natural frequency of the (m,n)-th mode is given by:

$$\omega_{mn}=\sqrt{\frac{D}{\rho h}\frac{I_{1m}I_{2n}+2I_{3m}I_{4n}+I_{6m}I_{5n}}{I_{6m}I_{2n}}} \tag{5.30}$$

Plate made of an orthotropic material

As presented in the previous chapter, the equation motion of the forced orthotropic plate is:

$$D_x\frac{\partial^4 w}{\partial^4 x}+2D_{xy}\frac{\partial^4 w}{\partial^2 x\partial^2 y}+D_y\frac{\partial^4 w}{\partial^4 y}+\rho\frac{\partial^2 w}{\partial^2 t}=-\sum_{j=1}^{J}\left(f^j\delta_{yj}+m^j\delta_{yj}^{'}\right) \tag{5.31}$$

where $w=w(x,y,t)$ is the transverse displacement, $\delta_{yj}=\delta(y-y_j)$ where δ is the Dirac delta function, y_j denotes the location of the jth x-wise rib. $\delta^{'}$ represents the first derivate of the Dirac delta function with respect to its argument. Plate deflection w can be expressed as the superposition of a finite number of mode shape s_{mn} as follows:

$$w = \sum_{m=1}^{M} \sum_{n=1}^{N} s_{mn}(x,y) w_{mn} e^{j\omega t} \tag{5.32}$$

Mode shape functions can be written as the product of two independent rib functions:

$$s_{mn}(x,y) = \phi_m(x)\psi_n(y) \tag{5.33}$$

For a fully simply-supported orthotropic plate, rib functions result to be (see equation (4.8)):

$$\phi_m(x) = \sin \frac{m\pi x}{a} \tag{5.34}$$

$$\psi_n(y) = \sin \frac{n\pi y}{b} \tag{5.35}$$

After substituting equation (5.32) in equation (5.31), multyplying it with the (p,q)-th mode shape function, $s_{pq} = \phi_p(x)\psi_q(y)$ and integrating over the area of the plate, the solution must satisfy the following set of *MxN* coupled equations:

$$\begin{aligned} \textstyle\sum_{m=1}^{M}\sum_{n=1}^{N} w_{mn} \int_0^a \int_0^b \left[\left(D_x \phi_m^{''''} \psi_n \phi_p \psi_q + 2D_{xy} \phi_m^{''} \psi_n^{''} \phi_p \psi_q + D_y \phi_m \psi_n^{''''} \phi_p \psi_q - \rho h \omega^2 \phi_m \psi_n \phi_p \psi_q \right) \right] dxdy = \\ = -\textstyle\sum_{j=1}^{J} \int_0^a \int_0^b \left[f^j \delta_{yj} \phi_p \psi_q + m^j \delta_{yj}^{'} \phi_p \psi_q \, dxdy \right] \end{aligned} \tag{5.36}$$

where the prime denotes derivative of the shape function with respect of its argument. Using the dominant rib function for the *(m,n)*-th mode, equation (5.36) can be approximated as follows:

$$\left[D_x I_{1m} I_{2n} + 2D_{xy} I_{3m} I_{4n} + D_y I_{6m} I_{5n} - \rho h \omega^2 I_{6m} I_{2n} \right] w_{mn} = f_{mn} + m_{mn} \tag{5.37}$$

where f_{nm} and m_{mn} are the modal coupling line forces and moments given respectively by:

$$f_{mn} = -\sum_{j=1}^{J} \psi_n^{y_j} \int_0^a f^j \phi_m dx \tag{5.38}$$

$$m_{mn} = -\sum_{j=1}^{J} \psi_n^{'y_j} \int_0^a m^j \phi_m dx \tag{5.39}$$

Equation (5.37) can be written in a compact notation as:

$$\left(k_{mn} - \omega^2 \mu_{mn} \right) w_{mn} = f_{nm} + m_{mn} \tag{5.40}$$

where

$$k_{mn} = D_x I_{1m} I_{2n} + 2D_{xy} I_{3m} I_{4n} + D_y I_{6m} I_{5n} \tag{5.41}$$

is the modal stiffness of the (m,n)-th mode and

$$\mu_{mn} = \rho h I_{6m} I_{2n} \tag{5.42}$$

is the modal mass of the (m,n)-th mode.

Definite integrals I-VI in previous equations are:

$$\begin{aligned} I_{1m} &= \int_0^a \phi_m^{''''} \phi_m \, dx \qquad I_{4n} = \int_0^b \psi_n^{''} \psi_n \, dy \\ I_{2n} &= \int_0^b \psi_n^2 \, dy \qquad I_{5n} = \int_0^b \psi_n^{''''} \psi_n \, dy \\ I_{3m} &= \int_0^a \phi_m^{''} \phi_m \, dx \qquad I_{6m} = \int_0^b \phi_m^2 \, dx \end{aligned} \tag{5.43}$$

If one substitutes equations (5.44) in equations (5.41) and (5.42), one obtains:

$$k_{mn} = D_x \frac{ab}{4} \frac{m^4\pi^4}{a^4} + 2D_{xy} \frac{ab}{4} \frac{m^2n^2\pi^2}{a^2b^2} + D_y \frac{ab}{4} \frac{n^4\pi^4}{b^4} \tag{5.44}$$

$$m_{mn} = \frac{ab}{4} \tag{5.45}$$

Finally the approximate natural frequency of the (m,n)-th mode is given by:

$$\omega_{mn} = \sqrt{\frac{D}{\rho h} \frac{I_{1m}I_{2n} + 2I_{3m}I_{4n} + I_{6m}I_{5n}}{I_{6m}I_{2n}}} = \sqrt{\frac{D_x \frac{ab}{4} \frac{m^4\pi^4}{a^4} + 2D_{xy} \frac{ab}{4} \frac{m^2n^2\pi^2}{a^2b^2} + D_y \frac{ab}{4} \frac{n^4\pi^4}{b^4}}{\rho h \frac{ab}{4}}} =$$

$$= \frac{\pi^2}{a^2\sqrt{\rho h}} \sqrt{D_x m^4 + 2D_{xy} m^2 n^2 \frac{a^2}{b^2} + D_y n^4 \frac{a^4}{b^4}} \tag{5.46}$$

which is the same expression given in equation (4.2).

5.3.3 Stiffening ribs

Forced bending and torsional motion of x-wise stiffening ribs can be written as:

$$E_r I^j \frac{\partial^4 w^j}{\partial x^4} + \rho_r A^j \frac{\partial^2 w^j}{\partial t^2} = f^j \tag{5.47}$$

$$E_r I_w^j \frac{\partial^4 \theta^j}{\partial x^4} - GJ^j \frac{\partial^2 w^j}{\partial x^2} + \rho_r I_0^j \frac{\partial^2 \theta^j}{\partial t^2} = m^j \tag{5.48}$$

where j=1...J, $w^j(x,t)$ and $\theta^j(x,t)$ are the transverse displacement and the angle of twist respectively, $E_r I^j$ is the is the bending stiffness, GJ^j refers to the Saint-Venant torsional stiffness for uniform torsion, $E_r I_w^j$ denotes the warping stiffness associated with non-uniform warping, $\rho_r A^j$ is the mass per unit length, $\rho_r I_o^j$ is the mass moment of inertia per unit length.

Assuming time-harmonic motion

$$w^j = \sum_{m=1}^{M} w_m^j \phi_m(x) e^{j\omega t} \qquad \theta^j = \sum_{m=1}^{M} \theta_m^j \phi_m(x) e^{j\omega t} \tag{5.49}$$

the solutions of the jth x-wise rib must satisfy the following modal equations:

$$\left(k_{Bm}^j - \omega^2 \mu_{Bm}^j\right) w_m^j = f_m^j \qquad (m = 1, 2, ...M) \tag{5.50}$$

$$\left(k_{Tm}^j - \omega^2 \mu_{Tm}^j\right) w_m^j = m_m^j \qquad (m = 1, 2, ...M) \tag{5.51}$$

where

$$k_{Bm}^j = E_r I^j I_{1m} \tag{5.52}$$

$$\mu_{Bm}^j = \rho_r A^j I_{6m} \tag{5.53}$$

are the modal stiffness and modal mass of the mth bending mode respectively and

$$k_{Tm}^j = E_r I_w^j I_{1m} - GJ^j I_{3m} \tag{5.54}$$

$$\mu_{Tm}^j = \rho_r I_o^j I_{6m} \tag{5.55}$$

are the modal stiffness and modal mass of the m-th torsional mode, respectively.

The modal coupling loads in equations (5.50) and (5.51) are given by the following expressions:

$$f_m^j = \int_0^a f^j \phi_m \, dx \qquad m_m^j = \int_0^a m^j \phi_m \, dx \tag{5.56}$$

5.3.4 Ribbed plate

By comparing equations (5.24), (5.25) and (5.56), one obtains the following relations between the modal coupling loads on the plate and those on the stiffening ribs:

$$f_{nm} = -\sum_{j=1}^{J} \psi_n^{y_j} f_m^j \tag{5.57}$$

$$m_{nm} = -\sum_{j=1}^{J} \psi_n^{'y_j} m_m^j \tag{5.58}$$

Then, using the equations (5.50) and (5.51), the harmonic motion of the plate can be written as follows:

$$\left(k_{mn} - \omega^2 \mu_{mn}\right) w_{mn} = -\sum_{j=1}^{J} \psi_n^{y_j} \left(k_{Bm}^j - \omega^2 \mu_{Bm}^j\right) w_m^j - \sum_{j=1}^{J} \psi_n^{'y_j} \left(k_{Tm}^j - \omega^2 \mu_{Tm}^j\right) \theta_m^j \tag{5.59}$$

Continuity conditions at the interface between plate and the ribs can be written, in terms of modal amplitudes as follows:

$$w_m^j = \sum_{n=1}^{N} \psi^{y_j} w_{mn} \qquad \theta_m^j = \sum_{n=1}^{N} \psi^{'y_j} w_{mn} \tag{5.60}$$

Substituting equation (5.60) in equation (5.59), the harmonic motion of the ribbed plate is described by the following set of coupled equations:

$$\left(k_{mn} - \omega^2 \mu_{mn}\right) w_{mn} + \sum_{j=1}^{J} \sum_{q=1}^{N} \left[\psi_n^{y_j} \left(k_{Bm}^j - \omega^2 \mu_{Bm}^j\right) \psi_q^{y_j} + psi_n^{'y_j} \left(k_{Tm}^j - \omega^2 \mu_{Tm}^j\right) \psi_q^{'y_j}\right] w_m^q = 0 \tag{5.61}$$

where p and q are the indexes which denote the coupling terms due to the presence of the stiffening ribs. Equation (5.61) can be expressed in a standard matrix form as:

$$\left(K - \omega^2 M\right) w = 0 \tag{5.62}$$

where the modal amplitudes are grouped into the column vector w as follows:

$$w = \left[w_{11}, w_{12}, ..., w_{1N}, w_{21}, ..., w_{2N}, ..., w_{mn}, ..., w_{MN}\right]^T \tag{5.63}$$

The mass matrix M is of the form:

$$\mathcal{M} = \begin{bmatrix} M_{1111} & M_{1112} & \cdots & M_{11pq} & \cdots & M_{11MN} \\ M_{1211} & M_{1212} & \cdots & & & \\ \vdots & & \ddots & & & \\ M_{mn11} & \cdots & & M_{mnpq} & & \\ \vdots & & & & \ddots & \\ M_{MN11} & & & & & M_{MNMN} \end{bmatrix} \tag{5.64}$$

whose elements are given by:

$$M_{mnpq} = \mu \delta_{mn} \delta_{mn} + \sum_{j=1}^{J} \left[\mu_{Bm}^j \psi_n^{y_j} \psi_q^{y_j} \delta_{mp} + \mu_{Tm}^j \psi_n^{'y_j} \psi_q^{'y_j} \delta_{mp}\right] \tag{5.65}$$

The stiffness matrix K is of the same size and form as M. The elements of the stiffness are given by:

$$K_{mnpq} = k_{mn}\delta_{mn}\delta_{mn} + \sum_{j=1}^{J}\left[k_{Bm}^{j}\psi_{n}^{y_j}\psi_{q}^{y_j}\delta_{mp} + k_{Tm}^{j}\psi_{n}^{'y_j}\psi_{q}^{'y_j}\delta_{mp}\right] \tag{5.66}$$

One observes that Mass and stiffness matrix are real, symmetric, positive defined and sparse. Then the resulting sparse eigenproblem can be solved numerically. Once the l-th numerical eigenvector w_l is known, the l-th natural mode shape of the ribbed plate may be recovered in the usual way as:

$$w_l(x, y) = s^T w_l \tag{5.67}$$

where

$$s = [\phi_1\psi_1, \phi_1\psi_2, ..., \phi_1\psi_N, \phi_2\psi_1, ..., \phi_2\psi_N, ..., \phi_m\psi_n, ..., \phi_M\psi_N] \tag{5.68}$$

5.4 Results

A MATLAB code has been written for the purpose of calculating the free-vibrations and mode shapes of a ribbed plate. Plate and ribs are considered to be made of aluminium. The resulting ribbed plate is considered fully simply-supported. In parallel, a Finite Element Model (FEM) of the plate has also been created in Abaqus in order to compare the numerical results with the analytical results. The geometry of the problem is always the same as in the previous chapter (see Figure 2.2). In this way, the effects of the introduction of the ribs is emphasized.

Finite Element Model

The procedure adopted in Abaqus is slightly different respect to the procedure adopted for the single plate. Then the mesh in ribs and plate is defined separately. The plate is composed of 0.01m shell elements with 6 degrees of freedom (DOF) per node. A rib is composed of 0.01m rib elements with 6 degrees of freedom per node. The final structure is formed of 3000 elements and 3111 nodes for the plate and 50 elements and 51 nodes for every x-rib. The size of rib elements is chosen equal to the plate elements in order to make the common nodes of plate and rib coincide. After meshing, ribs and plate are merged by nodes forming an unique structure in which common nodes have been highlighted. Figure 5.3 shows the structure obtained after the merge in the specific case in which the plate is reinforced with seven equidistant ribs.

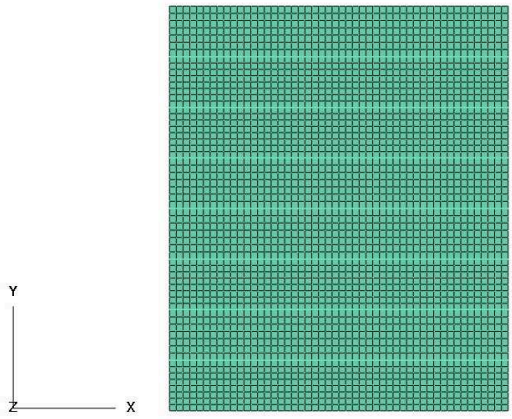

Figure 5.3: Plate reinforced with seven equidistant ribs. Final mesh.

In Abaqus, the orientation of the ribs is defined by specifying the co-ordinates of the normal vector respect to the rib's section. After that, the boundary conditions are specified in all nodes appertaining to the an edge. In all ribbed cases, the boundary condition considered is simply-supported. This constrain is inserted in Abaqus by preventing the three displacements (parallel to the axis) of nodes appertaining

to an edge. Finally, natural frequencies and mode shapes are calculated using a frequency step. Using the Lanczos eigensolver and defining the range of interest (until 10 KHz in case of study), Abaqus solves the eigenvalue problem. Eigenvectors have been normalized respect by displacement.

5.4.1 Plate made of isotropic material reinforced with ribs: stiffness parameters

The stiffness in both directions of the plate is calculated using the formulation presented in the second part of this chapter. To simplify the comprehension, the parameter r, which expresses the ratio between the stiffness in directions x (Dx) and y (Dx), can be kept as the resultant plate is orthotropic. This makes easier the comparison between a ribbed plate (where the single plate is made of an isotropic material) and a not reinforced plate made of an orthotropic material. Its expression is:

$$r = \frac{Dx}{Dy} \tag{5.69}$$

A plate having 5 ribs in direction x has been taken as the base case. The ribs section is considered as follows: the base of the ribs r_b is fixed to the value of 0.003 m (equal to the thickness of the plate) and the height of the ribs r_h are multiple of the base. Proceeding in this manner, different values of r are obtained. Results of this procedure are presented in Table 5.1.

$r_b(m)$	$r_h(m)$	r_h/r_b	Dx	Dy	r
0.003	0.009	3	305	175	1.74
0.003	0.015	5	775	175	4.43
0.003	0.021	7	1820	175	10.40
0.003	0.027	9	3670	175	20.97
0.003	0.030	10	4968	175	28.39
0.003	0.036	12	8457	175	48.33
0.003	0.042	14	13326	175	76.15
0.003	0.045	15	16350	175	93.43

Table 5.1: Ribs base cases.

For every value of r, five subcases are considered. Each subcase considers a different number of equidistant ribs. In particular, the number of ribs considered are one, three, five, seven and ten. Ribs are also considered equal and their base is fixed to 0.003 m (equal to the thickness of the plate) and their height is a calculated for the different values of r. Table 5.2 presents the geometry of the ribs:

				$r_h(m)$				
Dx	Dy	r	$r_b(m)$	1 rib	3 ribs	5 ribs	7 ribs	10 ribs
305	175	1.74	0.003	0.0130	0.0103	0.0090	0.0082	0.0074
775	175	4.43	0.003	0.0216	0.0172	0.0150	0.0136	0.0123
1820	175	10.40	0.003	0.0303	0.0240	0.0210	0.0191	0.0172
3670	175	20.97	0.003	0.0389	0.0309	0.0270	0.0245	0.0221
4968	175	28,39	0.003	0.0433	0.0343	0.0300	0.0273	0.0245
8457	175	48.33	0.003	0.0519	0.0412	0.0360	0.0327	0.0294
13326	175	76.15	0.003	0.0606	0.0481	0.0420	0.0382	0.0343
16350	175	93.43	0.003	0.0649	0.0515	0.0450	0.0409	0.0368

Table 5.2: Rib's geometry. Five subcases are considered for every value of r.

Deformed shapes of two different cases are shown as an example in Figures 5.4 and 5.5. For both Figures, the left subfigure shows the deformed shape of the semi-analytical model, calculated with equation (5.17). The right subfigure shows the deformed shape calculated with Abaqus, and plotted also using Matlab. Maximum displacement of both examples is in the center of the plate and is given in Table 5.3.

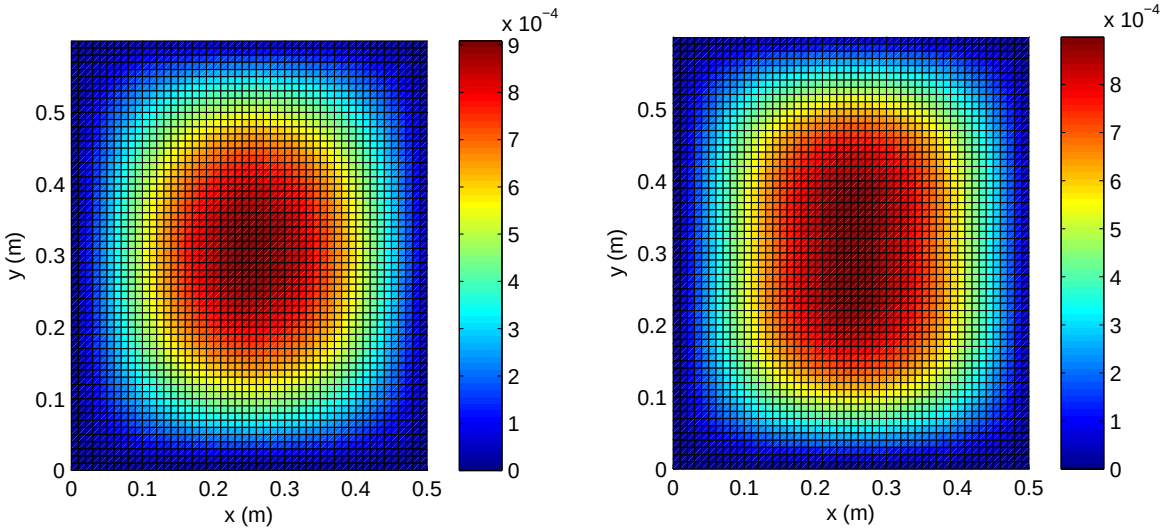

(a) *Semi-analytical model.* (b) *Numerical model.*

Figure 5.4: Deformed shape for case r = 4.43. Plate reinforced with one rib.

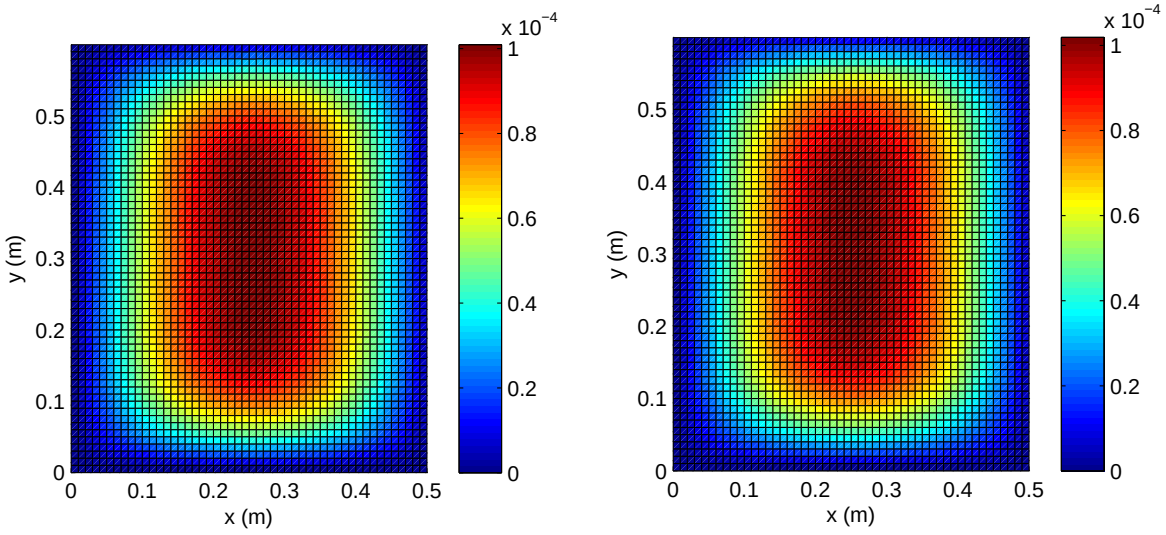

(a) *Semi-analytical model.* (b) *Numerical model.*

Figure 5.5: Deformed shape for case r = 28.39. Plate reinforced with seven ribs.

		maximum displacement (m)		
Number of ribs	r	analytical model	numerical model	*relative error*(%)
1	4.43	$9.0892 \cdot 10^{-4}$	$8.990 \cdot 10^{-4}$	1.09
7	48.33	$1.0094 \cdot 10^{-4}$	$1.019 \cdot 10^{-4}$	-0.95

Table 5.3: Maximum vertical displacement.

Table 5.3 reveals a good agreement between analytical and numerical cases. This is confirmed in Table 5.4, where the maximum displacement for different values of r, maintaining the number of ribs (seven in this case), is calculated.

	maximum displacement (m)		
r	analytical	numerical	*relative error*(%)
1.74	$1.60 \cdot 10^{-3}$	$1.60 \cdot 10^{-3}$	0.251
10.40	$4.52 \cdot 10^{-4}$	$4.48 \cdot 10^{-4}$	1.071
28.39	$1.73 \cdot 10^{-4}$	$1.73 \cdot 10^{-4}$	0.029
48.33	$1.01 \cdot 10^{-4}$	$1,02 \cdot 10^{-4}$	-0.942
93.43	$4.84 \cdot 10^{-5}$	$4.73 \cdot 10^{-5}$	2.451

Table 5.4: Maximum vertical displacement. Plate reinforced with seven ribs.

5.4.2 Plate made of isotropic material reinforced with ribs: free vibration

The model of the stiffness has been validated, natural frequencies and modal shapes can be calculated. As in the previous subsection, a validation of the semi-analytical model is required before proceeding to the radiation efficiency's calculation. Natural frequencies and mode shapes have been calculated using the theory presented third part of this chapter. The different parameters in equations (5.65) and (5.66) are calculated as follows:

- Flexural stiffness:

$$E_r I^j = E_r \tfrac{1}{12} r_b r_h^3$$

- Saint-Venant torsional stiffness (expression taken from [22]):

$$G_r J^j = G_r \tfrac{1}{3} r_b r_h^3 \left[1 - 0.63 \tfrac{r_h}{r_b} \left(1 - \tfrac{1}{12} \left(\tfrac{r_h}{r_b}\right)^4\right)\right]$$

- Mass moment of inertia per unit of length:

$$\rho_r I_0^j = \rho_r \left(\tfrac{1}{12} r_b r_h^3 + \tfrac{1}{12} r_h r_b^3\right) = \tfrac{1}{12} \rho_r r_h r_b \left(r_h^2 + r_b^2\right)$$

- Warping stiffness associated with non-uniform warping:

$$E_r I_w^j = E_r \cdot 0 = 0$$

- Kronecker delta:

$$\delta_{ij} = \begin{cases} 1 & \text{if } i = j \\ 0 & \text{if } i \neq j \end{cases}$$

I_w^j is considered equal to zero for simplicity, after observing that its effect is neglectable. Figures 5.6, 5.7, 5.8, 5.9 and 5.10 show the MAC function and the scatter-plot for five different values of r. The plate is considered to be reinforced (i.e) by seven ribs. Results show a good agreement between the analytical and numerical models at low frequencies. It can be observed that for all cases, as the frequency increases, the difference between the models so does. In addition, as the value of r increases, the range in which the both models make a good agreement is shorter. The model is not accurate when the orthotropy ratio is high and that is the reason why from now the considered values of r will be smaller than thirty.

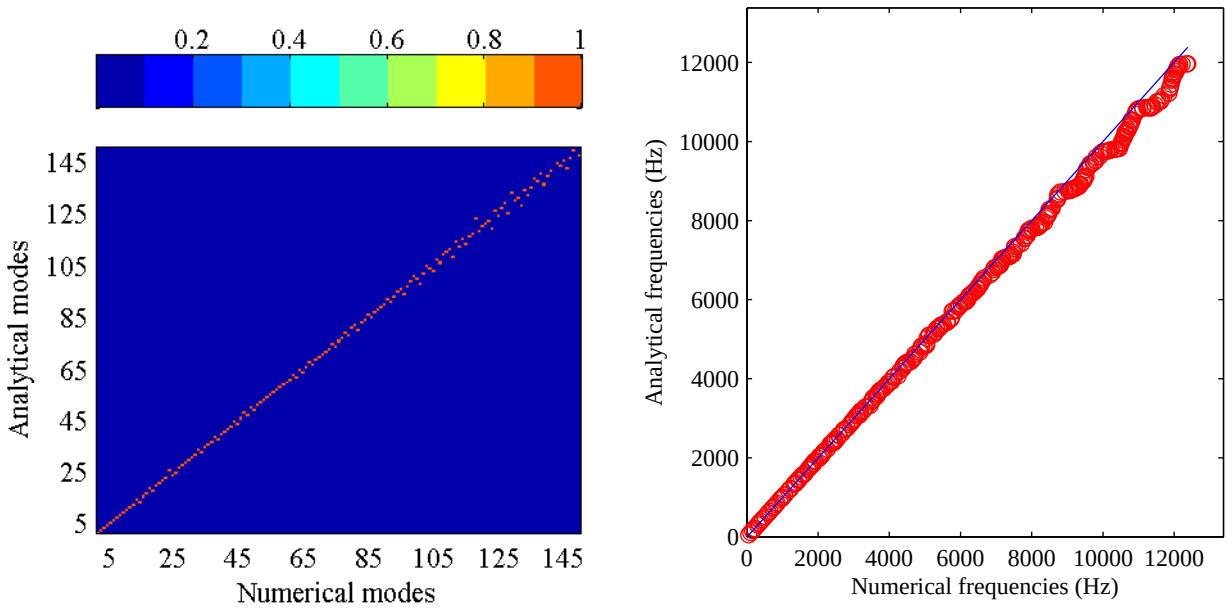

(a) *MAC* (b) *scatter plot*

Figure 5.6: MAC and scatterplot for r = 1.74. Plate reinforced with seven ribs.

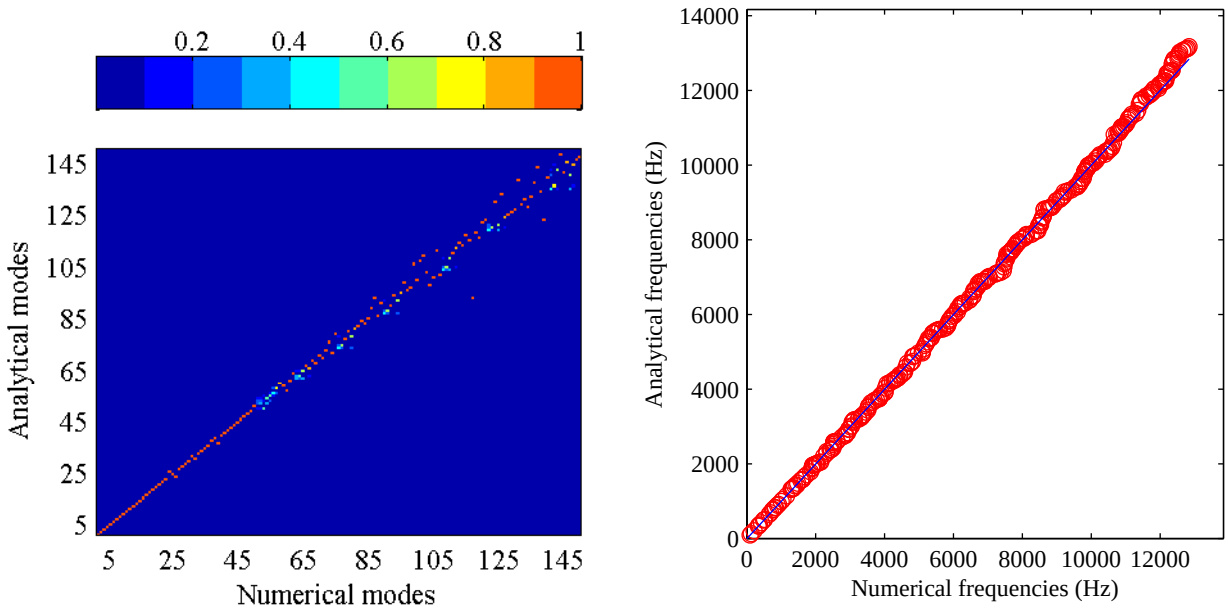

(a) *MAC* (b) *scatter plot*

Figure 5.7: MAC and scatterplot for r = 10.40. Plate reinforced with seven ribs.

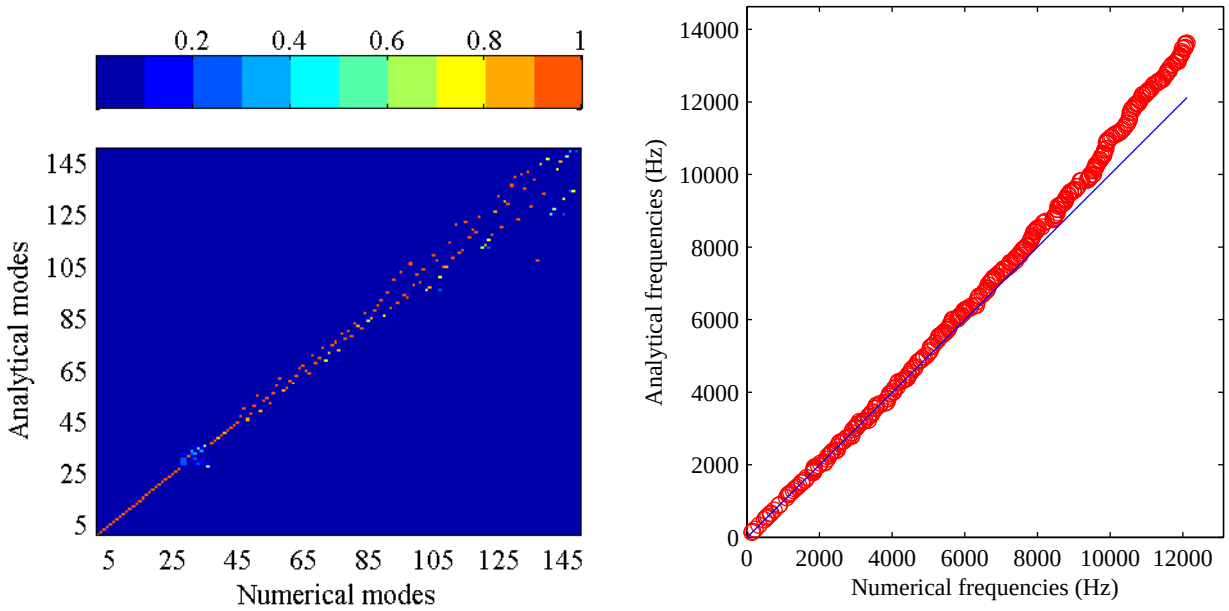

(a) *MAC* (b) *scatter plot*

Figure 5.8: MAC and scatterplot for r = 28.39. Plate reinforced with seven ribs.

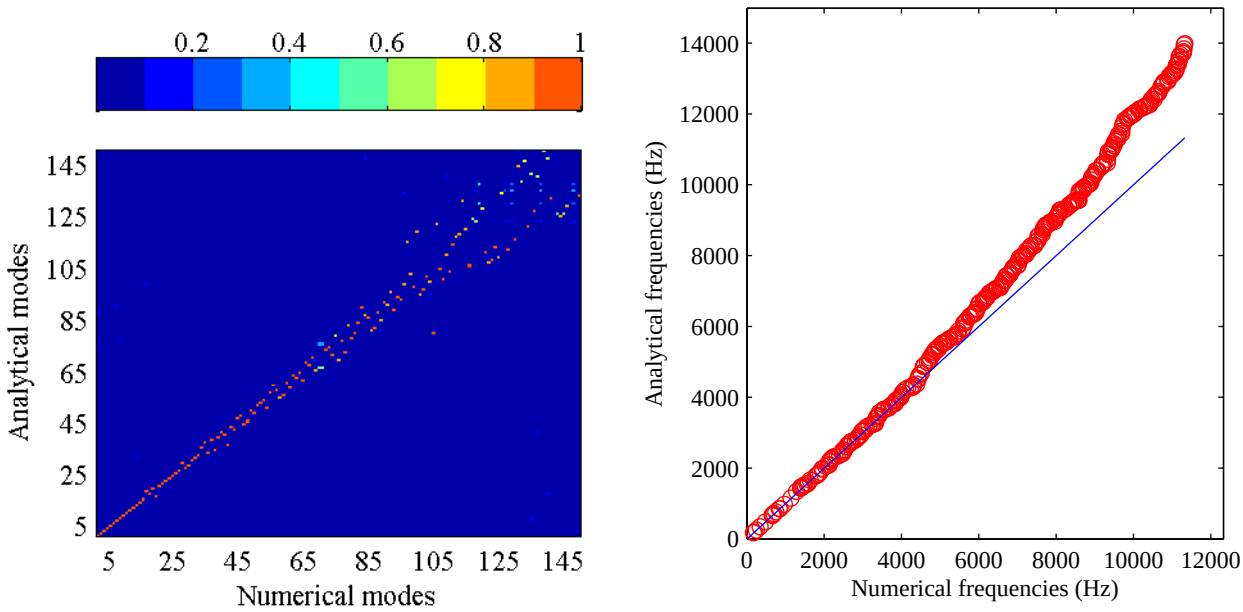

(a) *MAC* (b) *scatter plot*

Figure 5.9: MAC and scatterplot for r = 48.33. Plate reinforced with seven ribs.

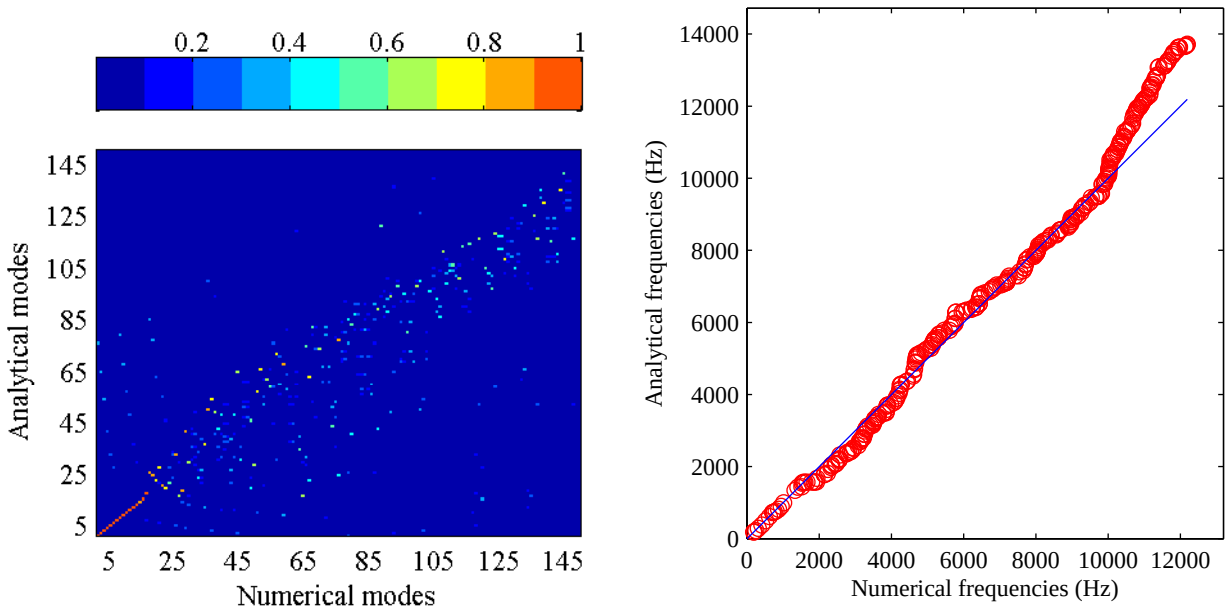

(a) *MAC* (b) *scatter plot*

Figure 5.10: MAC and scatterplot for r = 93.43. Plate reinforced with seven ribs.

It is known that the introduction of ribs into a structure makes its stiffness higher. What one expects is that the natural frequencies for a ribbed plate are higher. In Table 5.5 the first natural frequency for different cases are shown. Taking into account that the first natural frequency for the unribbed fully simply-supported plate is 49.56 Hz the affirmation is confirmed. Observing the first column (plate reinforced with one rib), it can be noticed another limitation of the model: for high values of r, if the plate is reinforced with only one rib, the geometry of the rib is very large compared with the plate and its motion becomes dominant and so happens for any number of ribs if their geometry is large compared with the palte. It can be concluded that the model presented in this chapter is valid when the dimensions of the ribs are not very large compared with the dimensions of the plate.

	1 rib	3 ribs	5 ribs	7 ribs	10 ribs
r=Dx/Dy	Freq (Hz)	Freq (Hz)	Freq (Hz)	Freq (Hz)	Freq (Hz)
4.43	70.03	70.01	68.87	67.95	66.75
10.40	91.68	95.42	93.66	92.02	89.90
20.97	111.33	127.15	124.65	122.04	118.66
28.39	111.33	144.64	141.75	138.57	134.44
48.33	111.33	181.65	178.31	173.79	167.91
93.43	111.33	240.45	237.34	230.92	222.19

Table 5.5: First natural frequencies of ribbed plates for different values of r.

Some examples of mode shapes are shown in Figures 5.11 and 5.12. The thick black line denotes the position of the ribs. The nomenclature (m,n) used for the isotropic plate to refer a mode number loses its sense for a ribbed plate since for a ribbed plate a mode is formed by a combination of mode shapes given by the autovector of the eigenvalue associated to the mode. It is noted that the ribs have an important effect on the mode shape. At low frequencies, the form of the modes of the unribbed plate are dominant. However, it has been noticed that at high frequencies the ribs impose nodal lines to the mode shape, as it can be seen in Figure 5.12. The effects on the radiation efficiency are studied in next

subsection.

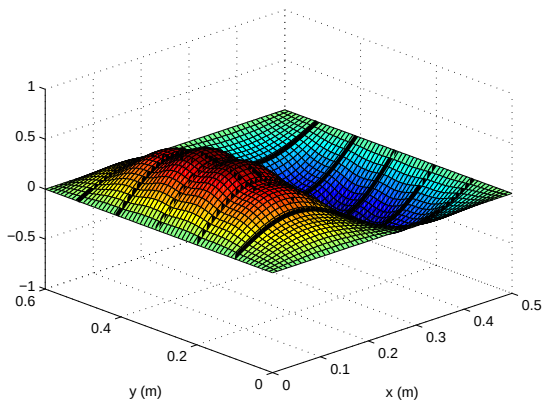

(a) *6th mode shape* ($539Hz$)

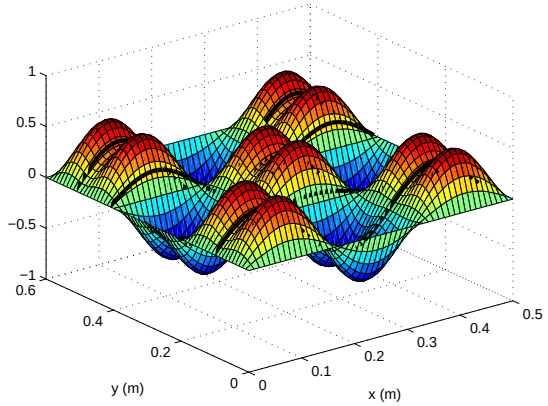

(b) *17th mode shape* ($1.06KHz$)

Figure 5.11: 6th and 17th mode shapes. Ribs are plotted in black. r = 28.39.

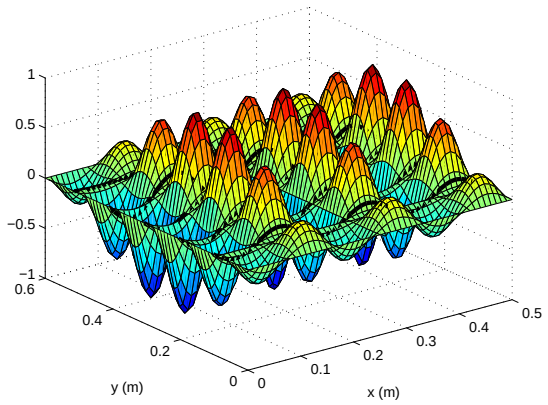

(a) *50th mode shape* ($2.28KHz$)

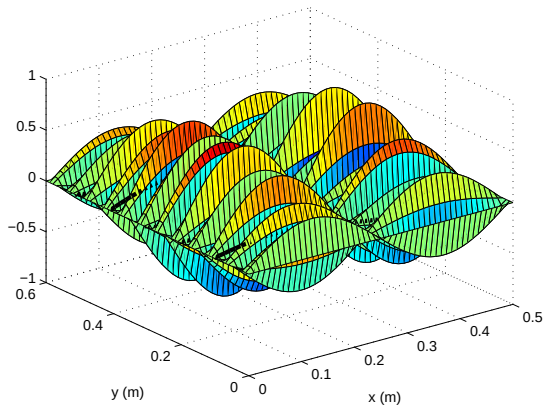

(b) *265th mode shape* ($10KHz$)

Figure 5.12: 50th and 265th mode shapes. Ribs are plotted in black. r = 28.39.

5.4.3 Plate made of isotropic material reinforced with ribs: radiation efficiency

The theory presented in the third chapter is also applicable for a ribbed plate: the radiation efficiency can be calculated by using a modal summation method based on the far field sound intensity. However some considerations must be done before. The most important is to note that the introduction of the ribs introduces mass to the final structure. The total mass is calculated as follows:

$$M = M_p + M_r \tag{5.70}$$

where M_p is the mass of the single plate and M_r is the mass of the ribs calculated as:

$$M_r = n_r(r_h - h)r_b a\rho_r \tag{5.71}$$

In expression (5.71), n_r is the number of the ribs, r_h is the heigth of the ribs, h is the plate's thickness, r_b is the rib's base, a is the rib's length and ρ_r is the rib's density.

An equivalent thickness of the ribbed plate is considered. Its expression is, using equation (5.70):

$$h_{eq} = \frac{M}{\rho a b} \tag{5.72}$$

h_{eq} calculated in equation (5.72) is the thickness considered in equation (3.9) in order to calculate the modal mass.

Figures 5.13 - 5.17 show a comparison between the radiation efficiency of an unribbed plate and the same plate reinforced with ribs for different values of the orthotropy ratio r. The effects of the introduction of the ribs in terms of radiation efficiency are the next: the region in which the plate behaves as a monopole is larger since the value of the first natural frequency of a ribbed plate is higher than the value of the first natural frequency of the unribbed plate. In this zone the radiation efficiency of the ribbed plate is slightly lower than the unribbed. In the mid-frequency range, the radiation efficiency of the ribbed plate is definitely higher and after the critical frequency both radiation efficiencies are equal. In Figure 5.18 all results are summarized and permits one to compare the effect of increasing the orthotropy ratio for a ribbed plate: at low frequencies (i.e. when the plate behaves as a monopole), the highest r is, the lowest the radiation efficiency of the plate is. The opposite happens when the frequency increases: the radiation efficiency of a ribbed plate is higher. In the mid-frequency range, the difference between a ribbed plate having an orthotropy ratio r and the unribbed plate seems to be approximately constant. For example, the difference between the radiation efficiency of a ribbed plate and the unribbed plate with $r = 30$ is near from 5 dB.

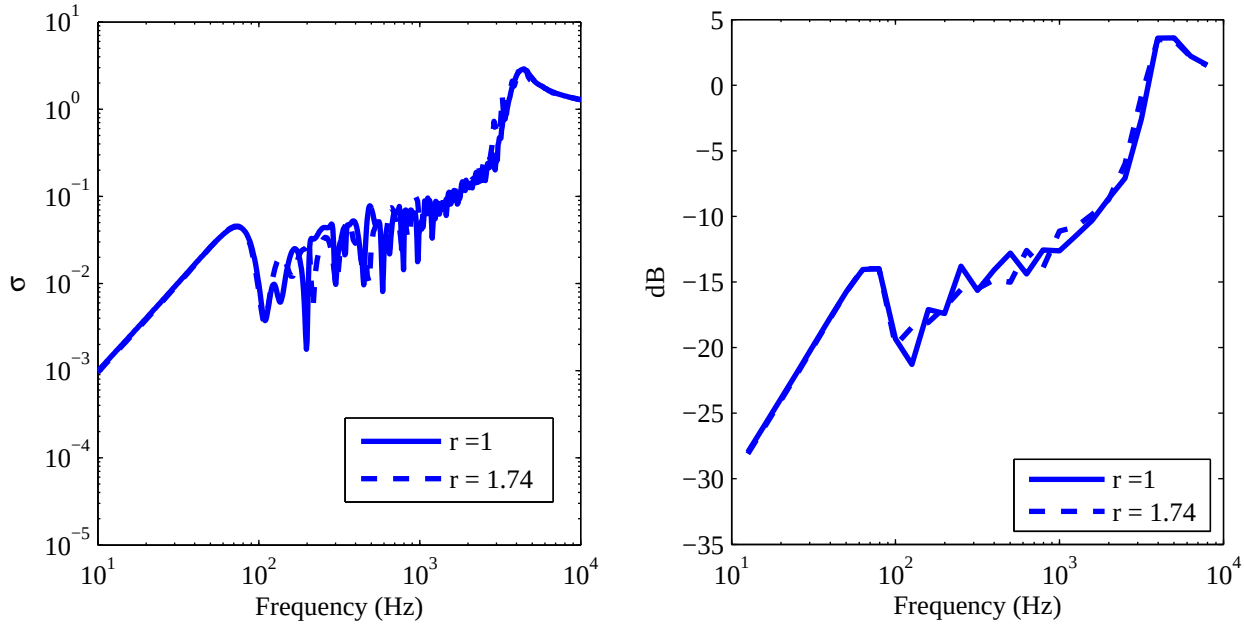

(a) *Radiation efficiency* (b) *Radiation efficiency in terms of octave band*

Figure 5.13: Comparison between isotropic plate and ribbed plate (5 ribs) for r=1.74.

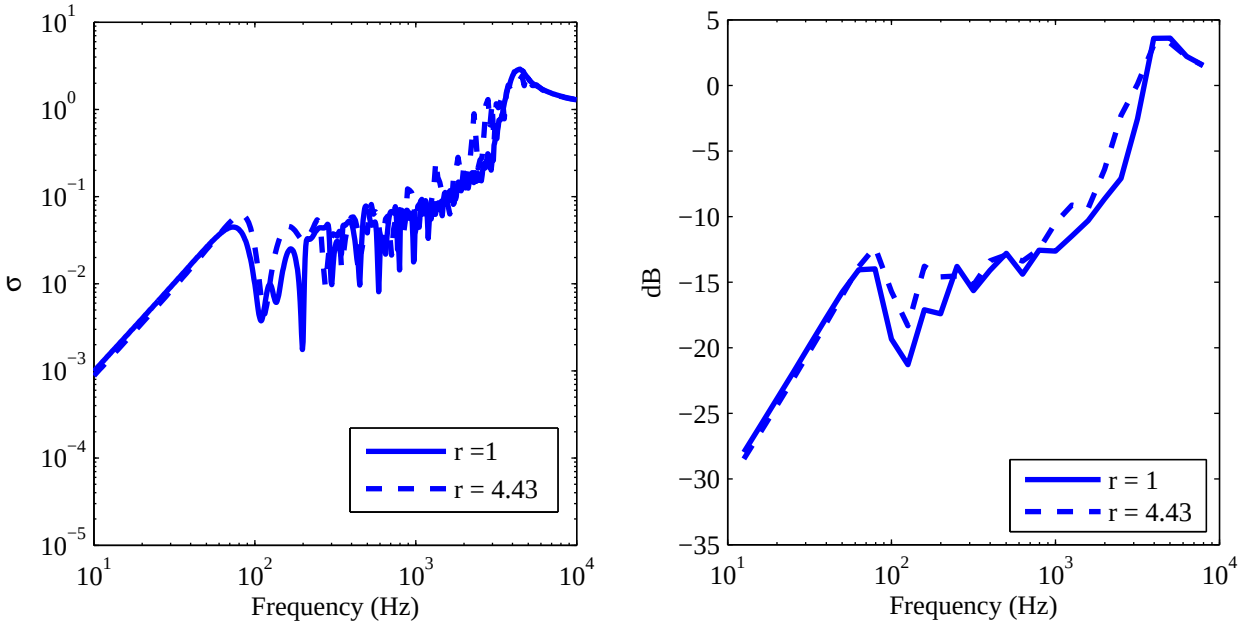

(a) *Radiation efficiency* (b) *Radiation efficiency in terms of octave band*

Figure 5.14: Comparison between isotropic plate and ribbed plate (5 ribs) for r=4.43.

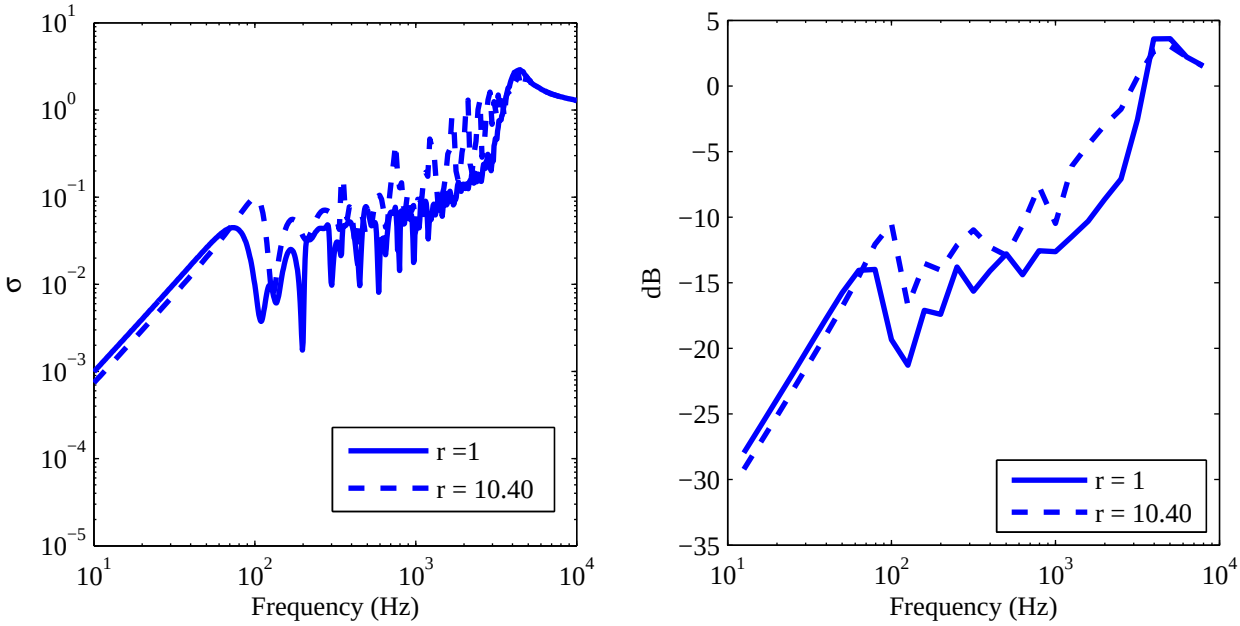

(a) *Radiation efficiency* (b) *Radiation efficiency in terms of octave band*

Figure 5.15: Comparison between isotropic plate and ribbed plate (5 ribs) for r=10.40.

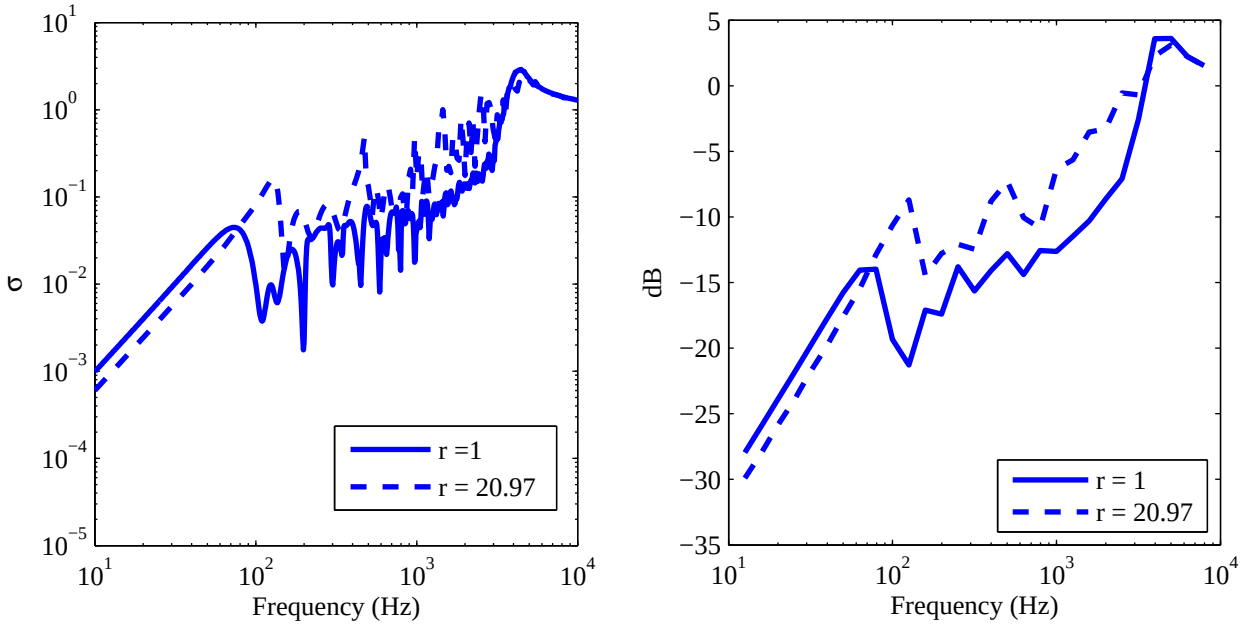

(a) *Radiation efficiency* (b) *Radiation efficiency in terms of octave band*

Figure 5.16: Comparison between isotropic plate and ribbed plate (5 ribs) for r=20.97.

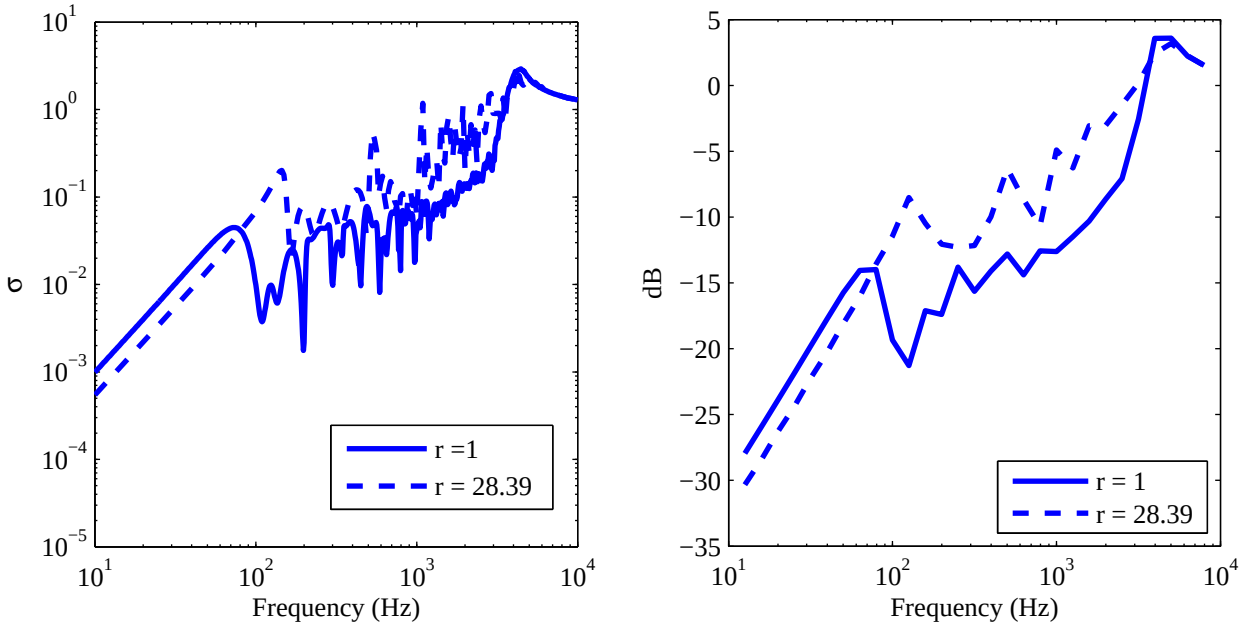

(a) *Radiation efficiency* (b) *Radiation efficiency in terms of octave band*

Figure 5.17: Comparison between isotropic plate and ribbed plate (5 ribs) for r=28.39.

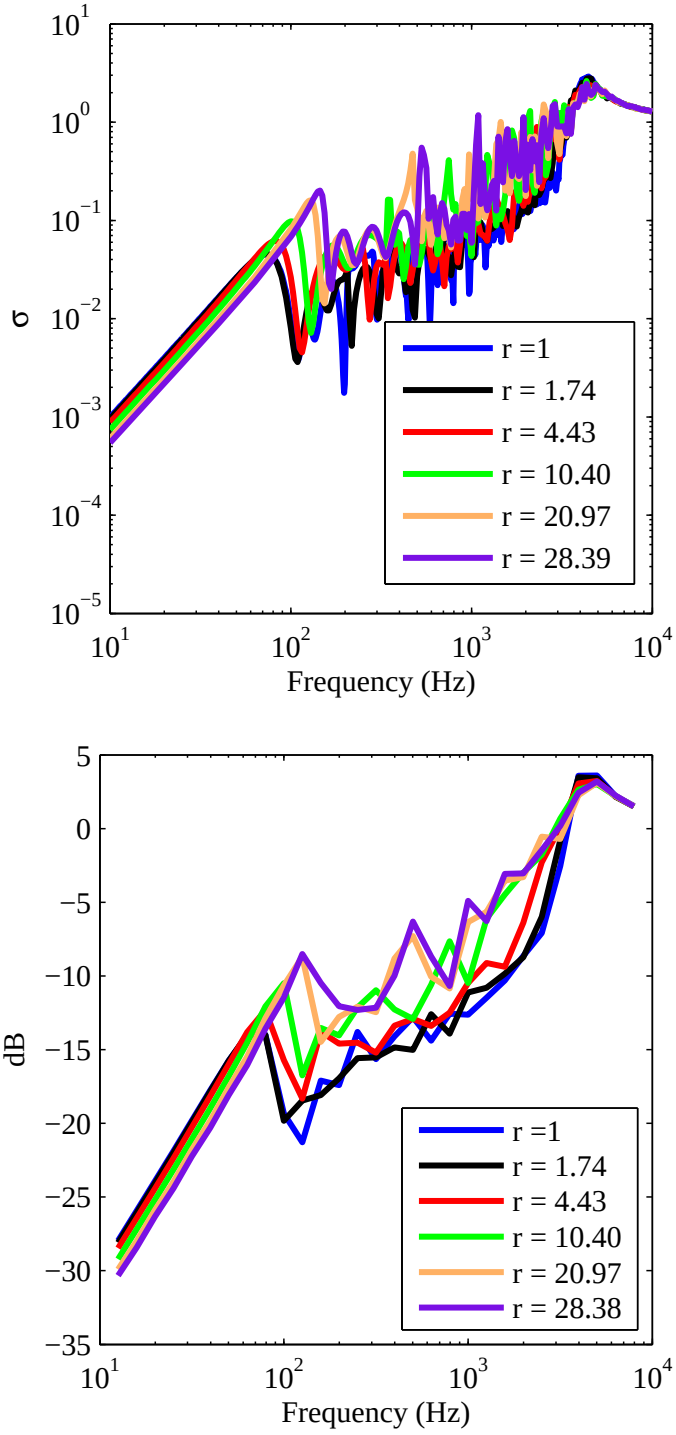

Figure 5.18: Comparison between isotropic plate and ribbed plate (5 ribs) for different values of r.

5.4.4 Orthotropic plate equivalent to a ribbed plate with the same stiffness ratio

After calculating the radiation efficiency of a ribbed plate, one may wonder which the relation between the radiation efficiencies of the ribbed plate and its equivalent plate made of an orthotropic material is. The first attempt is to consider an orthotropic plate which has the same geometry as the original plate (0.5x0.6x0.003m) conserving also its density (2700 Kg/m^3). The first subsection shows how to calculate the parameters of stiffness of the equivalent orthotropic plate. The second subsection shows the correspondence of both plates in terms of free vibrations. The third part compares the radiation efficiency of both models.

Parameters of the orthotropic plate

Remembering that

$$r = \frac{D_x}{D_y} = \frac{E_x}{E_y} = \frac{\nu_{xy}}{\nu_{yx}} \tag{5.73}$$

one may try to equal the stiffness in both directions obtaining the expressions:

$$D_y^o = D_y^r \quad \Rightarrow \quad \frac{E_y\ h^3}{12(1 - r\nu_{yx}^2)} = \frac{E_{al}\ h^3}{12(1 - \nu_{al}^2)} \tag{5.74}$$

$$D_x^o = D_x^r \quad = rD_y^o \tag{5.75}$$

in which superindexes o and r refer to the orthotropic and ribbed homogeneous plate respectively and νal is the possion coefficient of the aluminium. Using the previous equations one arrives to the following equaliance:

$$r\nu_{yx}^2 = \nu_{al}^2 \tag{5.76}$$

The value of the parameter ν_{yx} does not have a relevant influence on the values of E_x and E_y due to its low value respect to ν_{xy}. That is the reason why, in order work with reasonable values, it is assumed that $\nu_{xy} = 0.3$. Table (5.6) shows the elastic parameters of the orthotropic plate equivalent to the ribbed plate.

r	E_y	E_x	ν_{yx}	ν_{xy}
10.40	7.70e10	8.01e11	0.0288	0.3
20.97	7.74e10	1.62e12	0.0143	0.3
28.39	7.75e10	2.20e12	0.0106	0.3

Table 5.6: Stiffness of the orthotropic plate equivalent to the ribbed plate for different values of r.

Free vibration

Using the same Matlab code as in chapter 4 the free vibrations of the orthotropic plate have been calculated analytically. In parallel a FEM model of the orthotropic plate has been accomplished with Abaqus. Since the geometry of the plate is always the same, in Abaqus one just need to introduce the orthotropy by specifying the material properties in the different directions. In this way, the plate is formed of the usual 3000 elements and 3111 nodes, and the boundary conditions are simply supported. Figure 5.19 shows the MAC and the scatter-plot for the case in which $r = 28.38$. The scatter-plot and MAC function show a good agreement between analytical and numerical results.

Ribbed plate and his equivalent orthotropic plate are compared in terms of values of natural frequencies. In Table 5.7 first eight natural frequencies of the ribbed plate and its equivalent orthotropic plate are shown for different values of r. For the ribbed plate it is taken the base case, that is a plate with five ribs in direction x. The natural frequencies of the orthotropic plate are higher. This is due to the fact that the mass of the ribbed plate is higher.

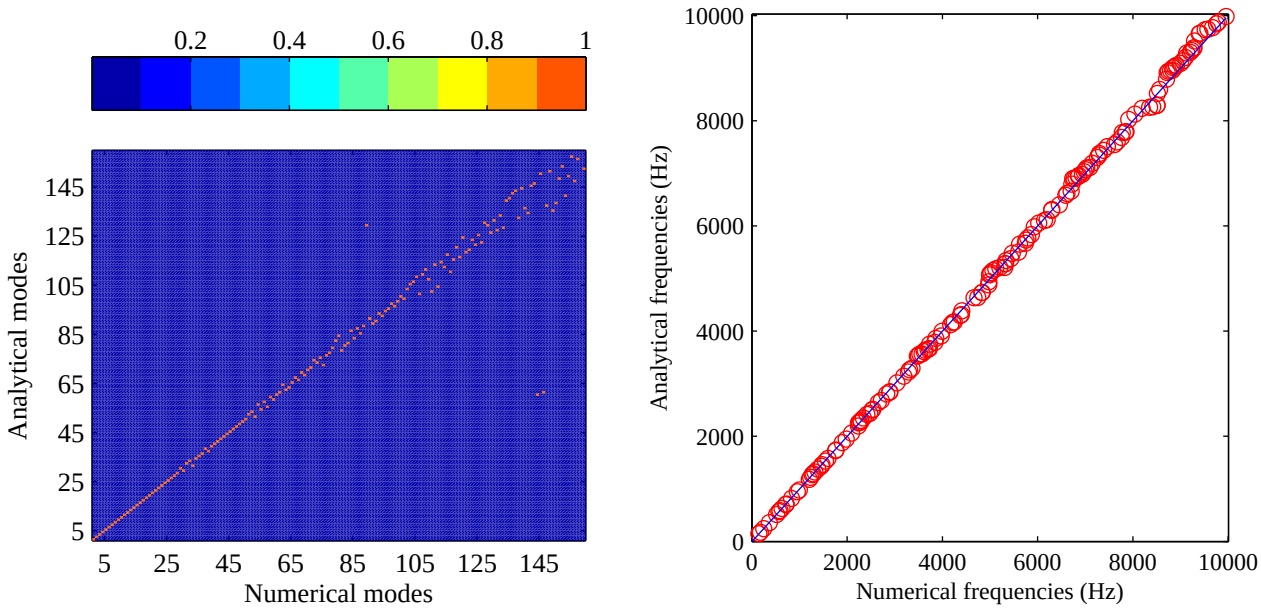

(a) *MAC* (b) *scatter plot*

Figure 5.19: MAC and scatterplot of the equivalent orthtotropic plate for r=28.39.

	r=10 Frequency (Hz)		r=20 Frequency (Hz)		r=30 Frequency (Hz)	
Mode	Ribbed plate	Orthotropic plate	Ribbed plate	Orthotropic plate	Ribbed plate	Orthotropic plate
1	93.67	97.61	124.65	129.04	141.76	146.75
2	130.23	138.73	152.77	160.99	166.48	175.44
3	210.82	223.08	222.60	234.73	230.94	244.21
4	334.47	350.09	337.37	353.28	340.83	358.20
5	348.13	360.12	473.48	494.78	490.94	514.84
6	371.66	390.45	489.25	513.71	539.69	568.12
7	424.58	452.46	491.65	516.15	552.27	587.01
8	496.57	517.41	526.89	562.28	583.15	628.03

Table 5.7: Comparison between the first 8 natural frequencies of a ribbed plate and its equivalent orthotropic plate conserving the stiffness ratio.

Radiation efficiency

Figures 5.20 - 5.22 show the radiation efficiency of the ribbed plate and its equivalent orthotopic plate for different orthotropy ratios. At low frequencies the radiation efficiency of both plates is equal, while as the frequency increases the radiation efficiency of the orthtropic plate is in average higher.

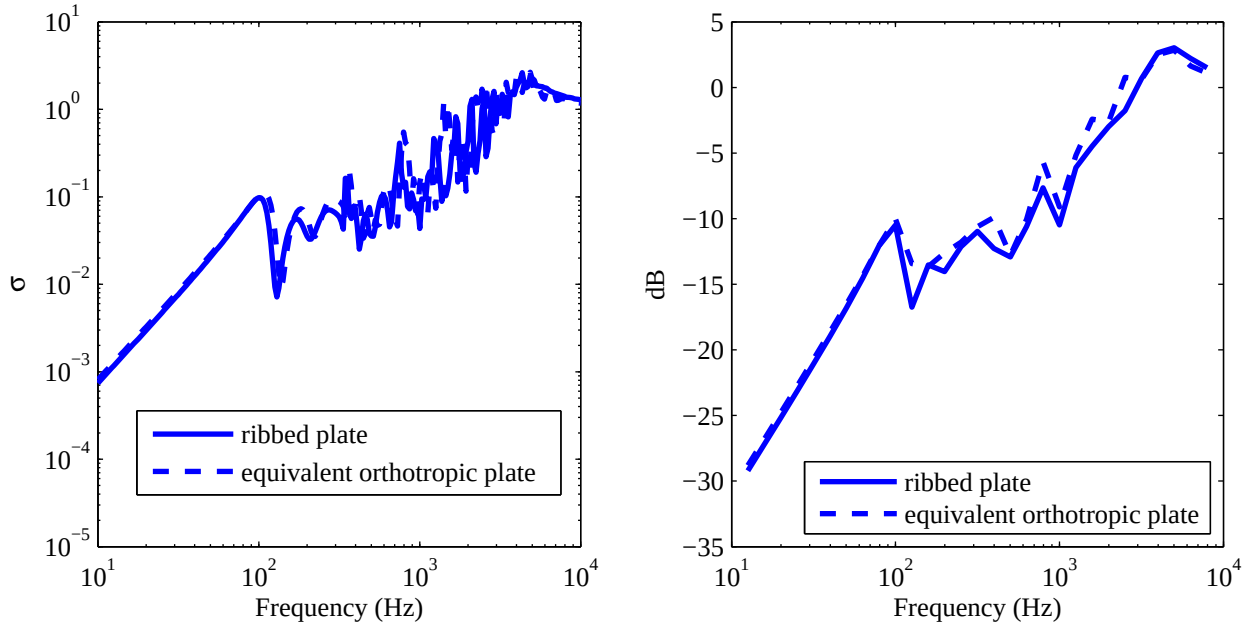

(a) *Radiation efficiency* (b) *Radiation efficiency in terms of third octave band*

Figure 5.20: Comparison between a ribbed plate and its equivalent orthotropic plate having the same stiffness for r = 10.40.

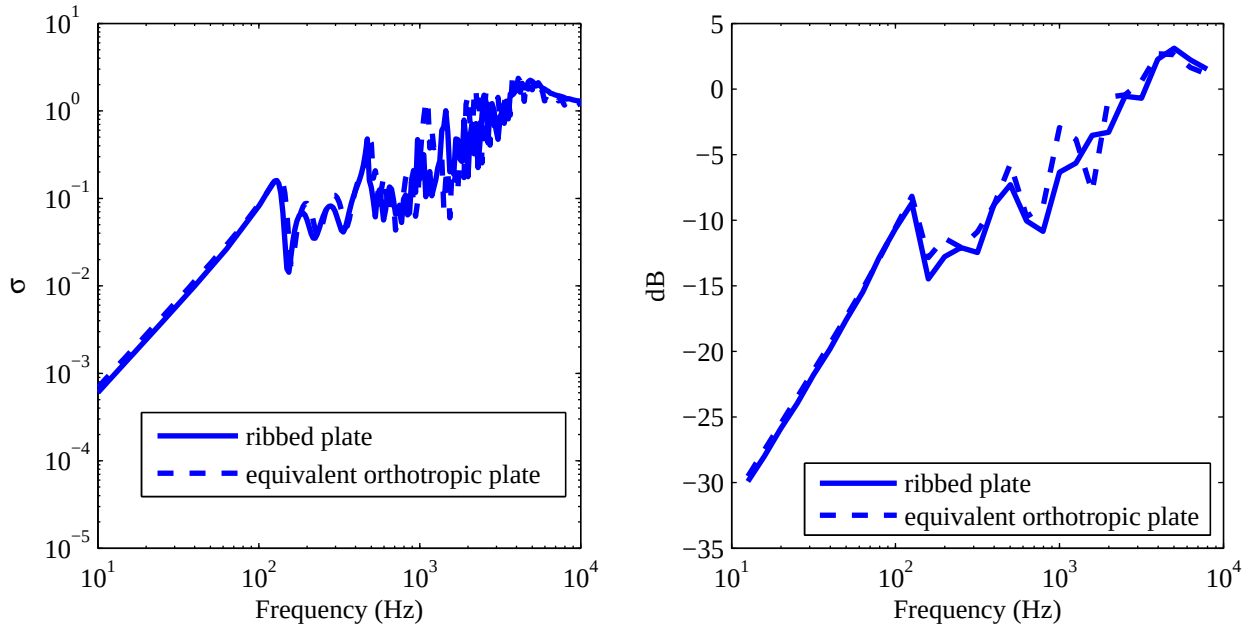

(a) *Radiation efficiency* (b) *Radiation efficiency in terms of third octave band*

Figure 5.21: Comparison between a ribbed plate and its equivalent orthotropic plate having the same stiffness for r = 20.97.

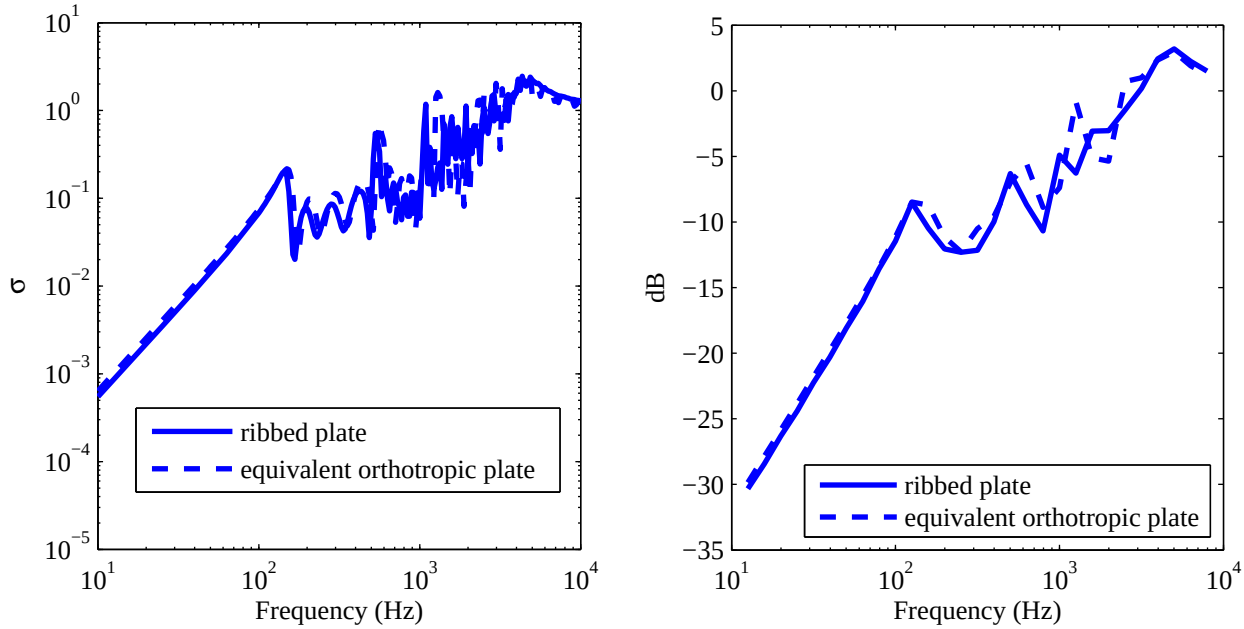

(a) *Radiation efficiency* (b) *Radiation efficiency in terms of third octave band*

Figure 5.22: Comparison between a ribbed plate and its equivalent orthotropic plate having the same stiffness for r = 28.39.

5.4.5 Orthotropic plate equivalent to a ribbed plate with the same stiffness ratio and mass

Parameters of the orthotropic plate

In this case, the equivalent orthotropic plate has the same stiffness and the same mass of the ribbed plate. The stiffness in both directions are the same as in the previous section. In order to make the orthotropic plate have the same mass of the ribbed plate, a different density of material must be considered for every value of r and number of ribs. Different cases have been calculated, but in this paragraph the orthotropy ratio is fixed to 28.38 in order to make the understanding easier. Table 5.8 shows the values of the density of the orthtropic plate material for different number of ribs when $r = 28.39$.

Number of ribs	Mass (Kg)	Density of orthotropic plate (Kg/m^3)
3	2.81	3116
5	2.97	3298
7	3.11	3452
10	3.29	3653
20	3.77	4189

Table 5.8: Density of equivalent orthotropic plate for different number of ribs and having the same mass of the ribbed plate. $r = 28.39$.

Radiation efficiency

The radiation efficiency of both plates has been calculated. In Figure 5.23 the difference between the orthotropic plate and the ribbed plate for different number of ribs and for $r = 28.38$ is shown. The results are similar to the results obtained in the previous section. It can be pointed out that at low frequencies the difference does not depend on the number of ribs. Until 800 Hz increasing the number of

ribs makes the difference between the ribbed plate and the orthotropic plate decrease: it seems that in terms of radiation efficiency, as the number of ribs increases, the difference between a ribbed plate and its equivalent orthotropic plate (with the same orthotropy ratio and mass) is constant and low (less than 1 dB in this case). At high frequencies the difference turns into several peaks and no conclusion can be made.

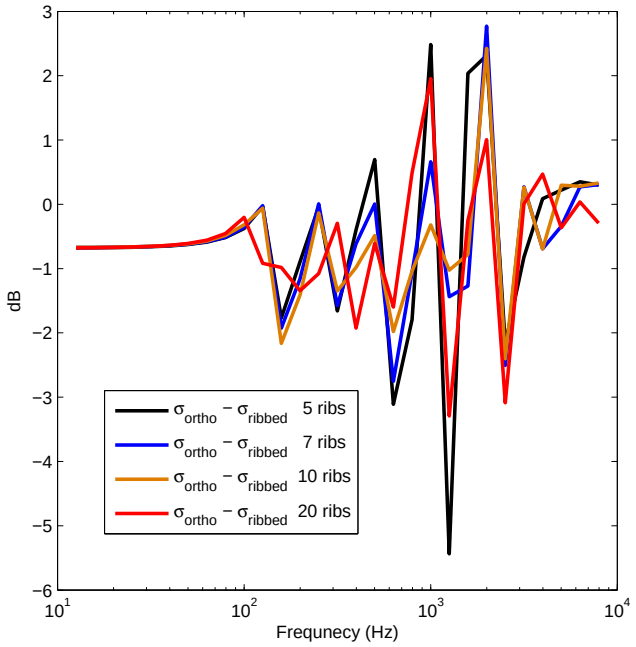

Figure 5.23: Differences between ribbed and orthotropic plate in terms of third octave bands. $r = 28.39$.

5.4.6 Plate made of an orthotropic material reinforced with ribs: test case

The aim of this paragraph is to present an example of applicability of the methodology applied in this work. In particular it is presented a simplified model of the soundboard of a grand piano which consists of a rectangular plate made of wood and reinforced with with 5 equidistant ribs. The orthotropy is introduced by the material and by the ribs. Real data from a grand piano is considered for the material and for the geometry of the plate. In Figure 5.24 it is shown the plate data. In this case, the plate is not reinforced symmetrically respect to its middle plate and in the expression of the mass moment of inertia per unit of length it is added an extra-term which takes in account the mass transport of the ribs. In equation (5.77) it is shown its expression:

$$\rho_r I_0^j = \rho_r \left(\frac{1}{12} r_b r_h^3 + \frac{1}{12} r_h r_b^3 + r_b r_h \left(r_h/2 + h/2 \right)^2 \right) = \frac{1}{12} \rho_r r_h r_b \left(r_h^2 + r_b^2 + \left(r_h/2 + h/2 \right)^2 \right) \tag{5.77}$$

The radiation efficiency is shown in Figure 5.25. The number of modes at low frequencies is very high compared with the plate studied in this work and that is the reason why natural frequencies until 3 KHz are considered. The values of the radiation efficiency are above the unit in a wide range of frequency. A sensitivity analysis when varying the number and the location of the ribs would be very useful for a craftsman[1]. In this way, the effect on the radiation efficiency of introducing or removing ribs in arbitrary locations would be noted and the structure of the piano could be modified in order to improve its performance.

[1]The person who builds grand pianos

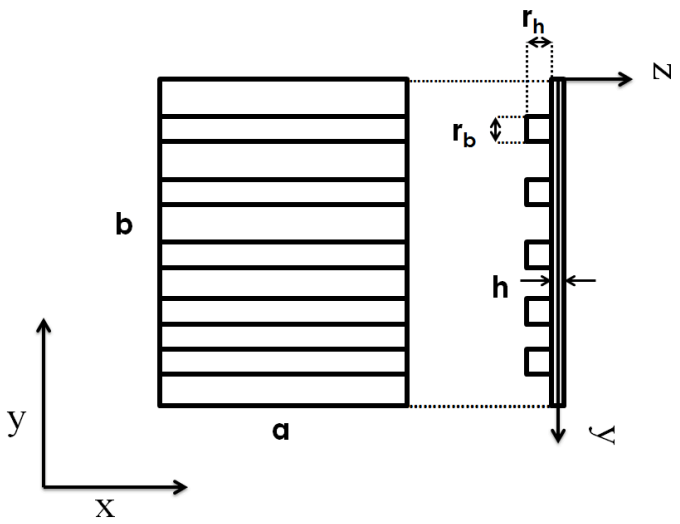

(a) *Geometry of the ribbed plate.*

Parameter	Value
a	0.9 (m)
b	1.4 (m)
h	0.007 (m)
r_b	0.02 (m)
r_h	0.02 (m)
E_y	1.28e10 (MPa)
E_x	6.25e8 (MPa)
G	6.17e8 (Mpa)
ν_{xy}	0.36
ν_{yx}	0.02
ρ	437 (Kg/m^3)
E_r	1.33e10 (MPa)
ν_r	0.37
ρ_r	505.5 (Kg/m^3)

(b) *Parameters of the ribbed plate.*

Figure 5.24: Geometry and parameters of the ribbed plate.

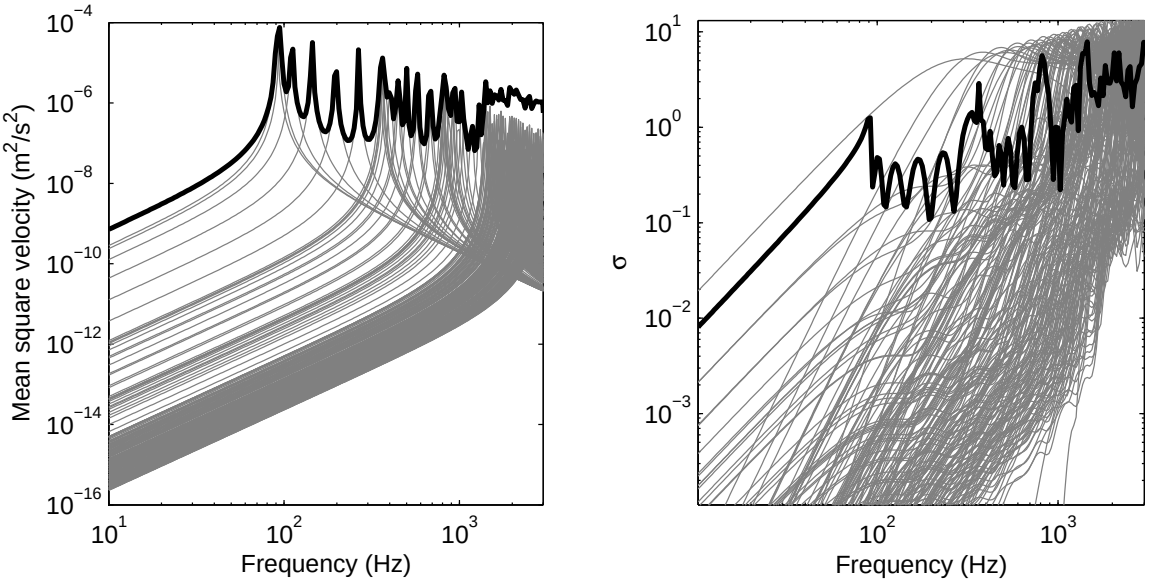

(a) *Velocity*

(b) *Radation efficiency.*

Figure 5.25: Velocity and radiation efficiency of the model of the soundboard of the piano.

Chapter 6

Conclusions

This work presents a methodology for calculating the radiation efficiency of rectangular thin plates. This methodology is applicable to common complex structures used in real applications. The radiation efficiency of rectangular plates is calculated by summing the effect of all modes that contribute to the acoustic emission in the frequency range under consideration. Structural models, validated with a FE model, are taken from literature and have been extended, in order to calculate the natural frequencies and mode shapes for different configurations of the plate. The results of the radiation efficiency obtained are compared with a BEM model and make a good agreement.

This work starts considering a plate made of an isotropic material and its radiation efficiency is calculated for different boundary conditions. Results reveal that a clamped supported plate has the highest radiation efficiency while a freely supported plate has the lowest. It is shown in terms of third octave bands the difference between two plates having the same geometry and material properties but different boundary conditions. In particular, it is found that the difference between a clamped supported and a simply supported plate in the mid-frequency range is not 3 dB as stated by Leppington, but it is variable and can reach up a value of 10 dB.

In the second part of this work, the orthotropy is introduced to the plate by considering its material orthotropic or by introducing a number of equidistant ribs parallel to an edge. The plate is considered always simply supported and the radiation efficiency is calculated for different stiffness ratio r. Results show that the radiation efficiency of a ribbed plate is always higher than the same plate unribbed and that the difference between them, in average, increases as the radiation ratio increases. A relation between a ribbed plate and its equivalent orthotropic with the same stiffness and mass is found. Results show that at low frequencies the difference between them is constant and low, and decreases when the number of ribs of the ribbed plate increases. Finally, it is shown a reduced model of the soundboard of a grand piano and its radiation efficiency is calculated.

The models obtained in this work have been compared with a numerical model and make a good agreement. In terms of modellistics, it is noted that in this work the ribs are always parallel to an edge. A model for a plate reinforced with ribs in arbitrary locations would approximate better some real cases as the soundboard of the piano. All the models presented in this work may be validated experimentally.

Appendix A

Acoustic emission of a vibrating surface

Consider a flat, thin plate lying in the plane $x - y$. When in the plate a bending wave propagates in direction x with a velocity c_B, a pression wave inthe air volume above the plate propagates with a velocity $c(c = 343m/s)$. The direction (shown in Figure A.1)[1] of propagation depends on the ratio between the wave length that propagates along the plate λ_B and the wave length that propagates in the air λ.

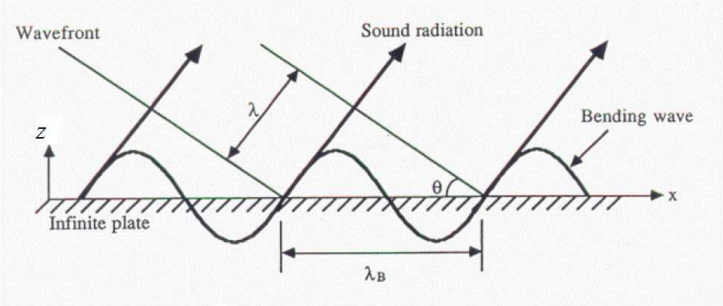

Figure A.1: sound radiation from an infinte plate.

where

$$c_B = \lambda_B f \qquad c = \lambda f \qquad \theta = arcsin\left(\frac{\lambda}{\lambda_B}\right) \tag{A.1}$$

In the interface surface-fluid, the vibration velocity of the air particles is equal to the velocity of vibration of the plate in the normal direction of it. If $\lambda_B > \lambda$ the acoustic is efficient. Otherwise, if $\lambda_B < \lambda$, the acoustic emission is inefficient. That is, if the flexural wave of the plate propagates with a velicity which is higher than the velocity of the sound in the air ($c_B > c$), the acoustic emission is efficient (supersonic regime). In the other hand, if the flexural wave of the plate propagates with a velicity which is lower than the velocity of the sound in the air ($c_B < c$), the acoustic emission is inefficient (subsonic regime).

The limit case corresponds to the case in which $\lambda_B = \lambda$. This condition is verified when the frequency of vibration of the plate is equal to a certain value of frequency of vibration , known as critical frequency. It's expression is:

$$f_c = \frac{c^2}{2\pi}\sqrt{\frac{\rho_0 h}{D}} \tag{A.2}$$

[1]Figure extracted from Norton [17]

In equation (A.2), ρ is the air density, h is the plate's thickness and D is the flexural stiffness of the plate.

Consider a mode of vibration (m, n). A propagating waves exist in both direction x and y. Their wave lenghts are:

$$\lambda_{xm} = \frac{m}{2L_x} \qquad \lambda_{yn} = \frac{n}{2L_y} \tag{A.3}$$

where λ_{xm} and λ_{yn} are the length of the edges in x and y direction.

The velocity of propagation of the flexural waves is:

$$c_B(\omega) = \sqrt[4]{\frac{D}{\rho h}}\sqrt{\omega} \tag{A.4}$$

where ρ is the density of the material of the plate.

Thus,

$$\lambda_B(\omega) = \frac{c_B}{f} = \frac{2\pi}{\sqrt{\omega}}\sqrt{\frac{D}{\rho h}} \tag{A.5}$$

Corner modes, edge modes and surface modes

When the plate is finite, it exists an acoustic emission. As explained before, two cases can be distinguished, depending on the value of the frequency of the vibration of the structural mode of the plate.

- If the frequency of vibration of the plate is lower than the value of the critical frequency f_c, the acoustic emission is limited to the corners and the edgesof the plate. For a given mode, if only the vibration of the corners contribute to the acoustic emission, the mode is called *corner mode*. On the other hand, if only the vibration of the edges contribute to the acoustic emission, the mode is called *edge mode*. In both cases, $f_{mn} < f_c$, $c_B < c$ and $\lambda_B < \lambda$ and the radiation efficiency is not maximum.

  Corner modes

  In this case, $\lambda_{xm}, \lambda_{yn} < \lambda$ and in the plate take place dipole and quadripole cancellations. As a result of it. only the corners contribute to the acoustic emission. Figure (A.2) shows this behaviour.

  Edge modes

  In this case, there are two possible subcases, the first is the subcase in which $\lambda_{xm} < \lambda$ and $\lambda_{yn} > \lambda$ and the second is the subcase in which $\lambda_{xm} > \lambda$ and $\lambda_{yn} < \lambda$. When the wave lenght in one direction is higher than λ, the vibration of the edges of that direction contribure to the acoustic emission. Figure A.2 shows this behaviour [2].

- If the frequency of vibration of the plate is higher than the value of the critical frequency f_c, the vibration of the whole plate contributes to the acoustic emission and the radiation efficiency is maximum. In this case, for a given mode of vibration of the plate $f_{mn} > f_c$, $c_B > c$ and $\lambda_B > \lambda$ and the mode is called *surface mode*. In every surface mode, $\lambda_{xm}, \lambda_{yn} > \lambda$ and the effects of the cancellations disappear.

[2] Figures extracted from Norton [17]

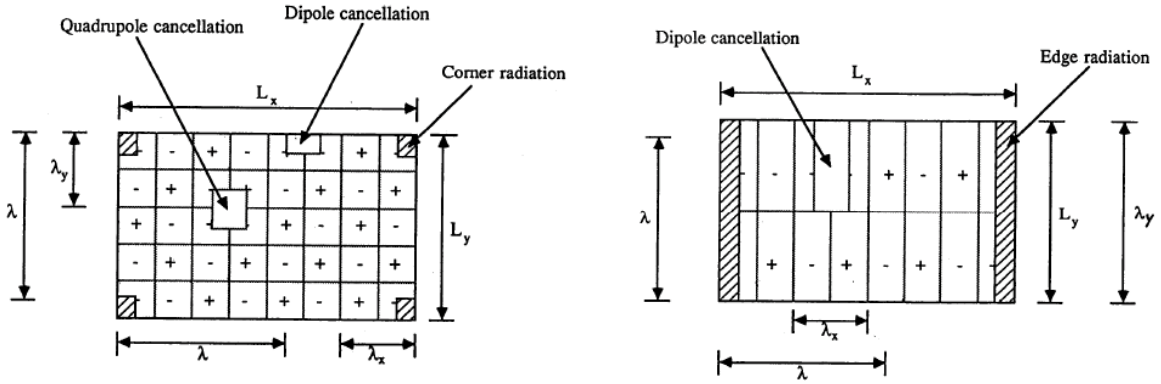

(a) *Corner mode.*

(b) *Edge mode.*

Figure A.2: Schematic illustration corner and edge radiation for a finite plate.

Bibliography

[1] F. G. Leppington, E. G. Broadbent, and K. H. Heron. The Acoustic Radiation Efficiency of Rectangular Panels. *Proceedings of the Royal Society of London. A. Mathematical and Physical Sciences*, 382(1783):245–271, August 1982.

[2] John W. Rayleigh. *The theory of sound*. Dover, 2nd edition, 1945.

[3] Gideon Maidanik. Response of Ribbed Panels to Reverberant Acoustic Fields. 34(6):809+, June 1962.

[4] C. E. Wallace. Radiation Resistance of a Rectangular Panel. *The Journal of the Acoustical Society of America*, 51(3B):946–952, 1972.

[5] G. Xie, D. Thompson, and C. Jones. The radiation efficiency of baffled plates and strips. *Journal of Sound and Vibration*, 280(1-2):181–209, February 2005.

[6] M. C. Gomperts. Radiation from rigid baffled, rectangualr plates with general boundary conditions. *Acustica*, 30, 1974.

[7] M. C. Gomperts. Sound radiation from thin rectangular plates. *Acustica*, 37:93–102, 1977.

[8] Alain Berry. A general formulation for the sound radiation from rectangular, baffled plates with arbitrary boundary conditions. *The Journal of the Acoustical Society of America*, 88(6):2792+, 1990.

[9] J. Park. Influence of support properties on the sound radiated from the vibrations of rectangular plates. *Journal of Sound and Vibration*, 264(4):775–794, July 2003.

[10] Scott D. Snyder and Nobuo Tanaka. Calculating total acoustic power output using modal radiation efficiencies. 97(3):1702+, March 1995.

[11] Manfred Heckl. Wave Propagation on BeamPlate Systems. 33(5):640+, May 1961.

[12] Andreas Rousounelos, Stephen J. Walsh, and Victor V. Krylov. Effects of beam-stiffening on the sound power radiated by finite plates. *Proceedings of the Institute of Acoustics*, 29(5):42–49, 2007.

[13] Singiresu S. Rao. *Vibration of Continuous Systems*. Wiley, 1 edition, February 2007.

[14] A.W. Leissa. *Vibration of plates*. NASA SP. Scientific and Technical Information Division, National Aeronautics and Space Administration, 1969.

[15] A. W. Leissa. The free vibration of rectangular plates. *Journal of Sound and Vibration*, 31(3):257–293, December 1973.

[16] F. Fahy and J. Walker. *Advanced Applications in Acoustics, Noise and Vibration*. Spon Press, 1 edition, September 2004.

[17] Michael P. Norton. *Fundamentals of Noise and Vibration Analysis for Engineers*. Cambridge University Press, January 1990.

[18] L.L. Beranek. I.L. Ver, C.I. Holmer. *Noise and Vibration Control*. McGraw-Hill, 1971.

[19] S. Timoshenko and S. Woinowsky-Krieger. *Theory of Plates and Shells*. 1959.

[20] Lorenzo Dozio and Massimo Ricciardi. Free vibration analysis of ribbed plates by a combined analyticalnumerical method. *Journal of Sound and Vibration*, 319(1-2):681–697, January 2009.

[21] G. B. Warburton. The vibration of rectangular plates. *ARCHIVE: Proceedings of the Institution of Mechanical Engineers 1847-1982 (vols 1-196)*, 168(1954):371–384.

[22] J.I. Craig O.A. Bauchau. *Structural Analysis: with applications to aerospace structures*. Spinger-Verlag, 2009.